Fire Simulator (Prototype 2)

Contents

Revision History

Version	Datetime	Description
0.1	01-02-2020	Commencement of thesis chapter 1
0.2	11-01-2022	ROS calculation on buttongrass fire model has been updated
0.3	10-07-2022	ROS bias has been updated. Figure for confusion matrix is added. Bug fix for Heathland model
0.4	22-07-2022	Site productivity has been updated for Buttongrass moorland model
1.0	01-01-2023	Fire models: Grassland, Spinifex, Forest, and Pine, have been update in accordance with product version of AFDRS
1.1	01-02-2023	Raster keys have been modified. Mask function for fire isochrone is added. Lateral fire channel is added in the prediction. Satellite, Himawari, is added as hotspot.
1.2	23-03-2023	Fire severity has been addressed. Goodness of Fit (GoF) has been added in confusion matrix as verification

Glossary

Table 1: Terminology

Term	Description
Prototype 1	The prototype for the fire simulation in the prior study (Ozaki, Aryal and Fox-Hughes, 2019)
Prototype 2	Enhancement of Prototype 1
FDRS	New Australian fire danger rating system to be debuted in near future public (The Australasian Fire and Emergency Service Authorities Council (AFAC), 2020)
Research Prototype	Prototype for FDRS

1 Introduction

1.1 Aim/Vision

This document is a guidance of Prototype 2, which is the second fire simulator. In previous study, the first prototype, Prototype 1, was implemented with three fire models, which are widely used in Australia (Ozaki, Aryal and Fox-Hughes, 2019). On the other hand, new fire danger rating system (FDRS) for Australia is being developed and expected to be released in a few years. At this stage, documentations regarding to the prototype of FDRS (Research Prototype) are in public (The Australasian Fire and Emergency Service Authorities Council (AFAC), 2020). The prototype for FDRS is called **Research Prototype** in this study to avoid ambiguity. Prototype 2 inherits legacy functionalities by replacing these old fire models with new models from Research Prototype.

1.2 Scope and purposes

This document describes system architecture, database entities, process of data, fire models, verification methods and configuration files. However, differences among regions are out of scope. Instead, they are described main document in each study case.

2 Software Architecture and Concepts in Prototype 2

Specification of Prototype 2 is addressed in this section.

2.1 Software Architecture

This prototype runs on the python flamework, GeoDjango similar to the Prototype 1 (see below).
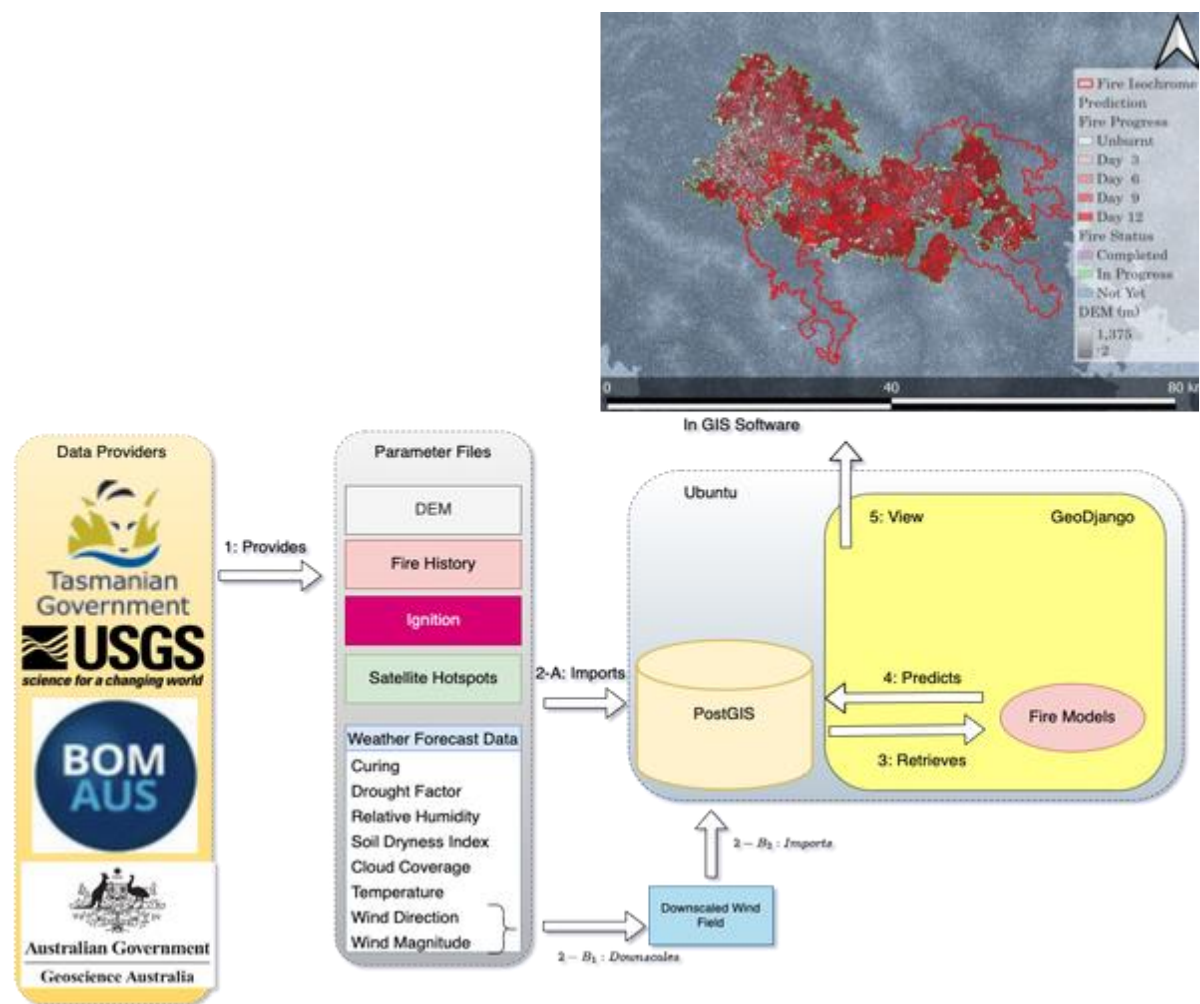
Figure 1: System architecture of Prototype 2 running on GeoDjango

Operation system is Ubuntu and Database management system (DBMS) is PostgreSQL with spatial database extension functions, PostGIS. Both input and output data are processed by Quantum GIS (QGIS) and WindNinja (seen below). Windninja is a diagnostic tool and resamples and downsizes wind data so that the wind magnitude and direction become more topographically sensitive (Firelab, 2020).

Table 2: OS and software employed for development of Prototype 2

Type	Software/System	Version
Operating System	Ubuntu	20.04
Programming Language	Python	3.7.5
Python framework	GeoDjango	3.1
Database Management System	PostgreSQL	11
Spatial Database Extension	PostGIS	3.0
Software	WindNinja	3.6.0
Software	QGIS	3.12.3

There are some feature improvements. For instance, the number of fire models increases from three to eight. The number of geometries also rises from three to five. A type of wind can be still configured in

Prototype 2 for simulation. Concretely, either crude wind from BARRA (coarse) or the resampling wind field (fine) is configurable. There was only a slope distance coefficient using McArthur's Fire Index in Prototype 1 while there are two types of downslope coefficients for calculating rate of fire spreading (ROS) in Prototype 2. In terms of verification methods, there was Confusion Matrix only in Prototype 1 while Prototype 2 employed two more verification methods: Cohen's Kappa static and Fractions Skill Score as below.

Table 3: Feature comparison between prototype 1 and 2

Fire Simulator	Prototype 1	Prototype 2
Fire models	Forest Fire Danger Index (FFDI), Grassland Forest Danger Fire Index (GFDI), Buttongrass Moorlands model	CSIRO Grassland fire spread model (Grassland), CSIRO Grassland for northern Australia model (Savanna), Desert spinifex model (Spinifex), Buttongrass moorlands model (Buttongrass), Dry Eucalypt Forest Fire Model (DEFFM or "Vesta"), Mallee heath model (Mallee heath), Heathland model (Shrubland), Adjusted Pine model (Pine)
Prediction Geometries	Delaunay, Square, Voronoi	Delaunay, Diamond, Hexagon, Square, Voronoi
Resolution of wind	Coarse, Fine	Coarse, Fine
Slope coefficient of ROS	McArthur's FDI	McArthur's FDI with Plan/projected (2D) or Linear/ground (3D)
Verification methods	Confusion Matrix	Confusion Matrix, Cohen's Kappa statistic, Fractions Skill Score (FSK)

2.2 Software concepts

Software concepts of Prototype 2, such as Object Oriented Programming (OOP), Object Relation Mapping (ORM), regional difference and time-zone format are addressed in this section.

2.2.1 Object Oriented Programming (OOP) and Object Relation Mapper (ORM)

Two main concepts of the architecture of the fire simulations are object-oriented programming (OOP) and Object Relational Mapper (ORM). There are a few pillars in OOP, such as (1) encapsulation, (2) polymorphism and (3) inheritance in the class, which is a structured container with properties and methods (Snyder, 1986; Wegner, 1990). Prototype 2 is capable of following OOP because the script language, Python, follows this concept. In terms of (1) encapsulation, class attributes can be controlled with different degrees: private, protected and public. Private data in the class cannot be gained an access from any external classes. Protected properties are also prohibited. However, ascendant classes or descendant classes can get an access to these protected properties. Public properties can be accessible from any classes. There are many more concepts such as namespace in OOP, however, these are omitted here because they are not the foci in this study. With regard to (2) polymorphism, the class methods can have various interfaces. For example, method A can have one or more parameters for flexibility. (3) inheritance is also important in this study to absorb regional difference. For instance, there can be various fire histories in each state or territory of Australia, however, a structure of fire history class might not be uniform among states and territories. Therefore, an abstract class of fire history is necessary to contain common features of the fire history throughout the states so as to communicate with other classes, such as vegetation, as a representative. Then a concrete fire history class in each state, inherits this abstract fire history class and implements its regional function. Further, the abstract fire history class inherits a vector class because its ascendant class is indeed a vector class and shares

common features of vector data. The below diagram shows the class hierarchy using Unified Modelling Language (UML).
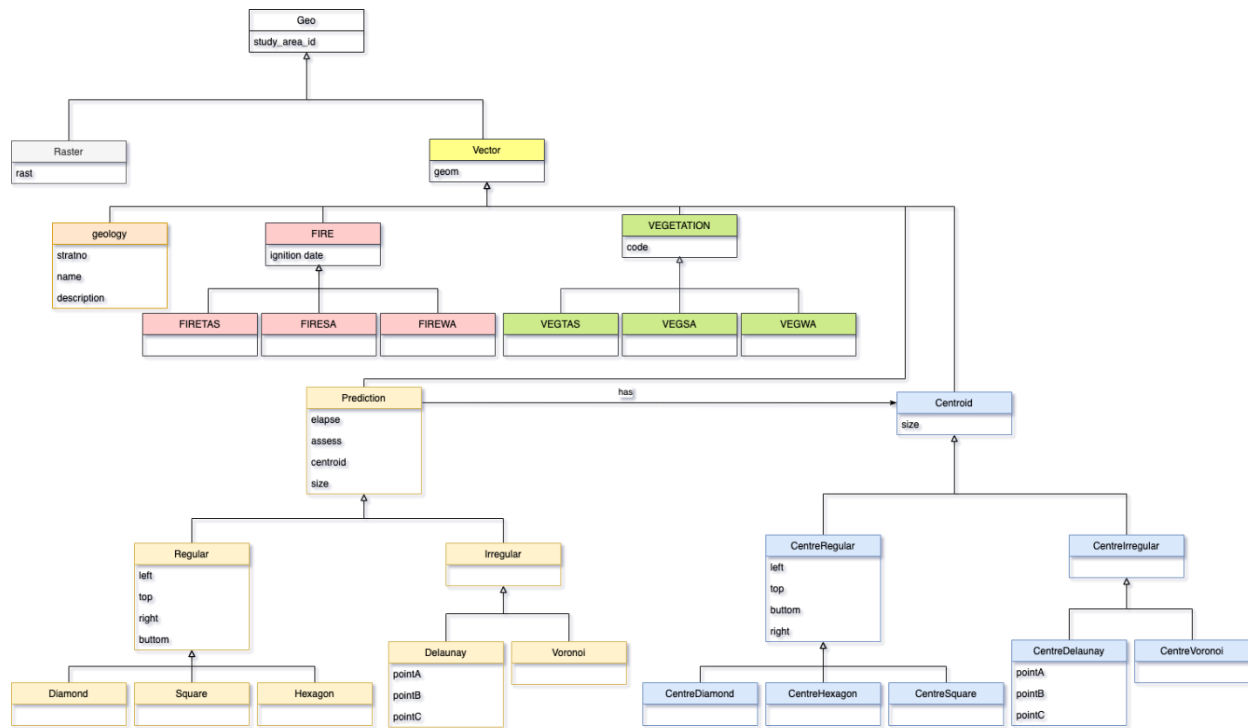
Figure 2: UML class diagram for geodata

Another concept is ORM, which is capable of manipulating database table through the counterpart class by mapping data without issuing Structure Query Language (SQL) statements (Plekhanova, 2009). Concretely, database tables such as wildfire_tas_veg are seamlessly handled using counterpart classes, such as VEGETATION class which is locally inherited by TASVEG in Tasmania.

2.2.2   Regional difference in the system

Each spatial table contains coordinate system and time-zone so that a state or territory can possess different time-zone and spatial reference identifier (SRID). A mapping of coordinate system and time zone is configured in another table or storage (see below).

Table 4: Study fire, Time zones and coordinate systems

#	Fire name	Time zone	Coordinate system (SRID)
1	Riveaux Road Fire	Hobart	GDA 94 zone 55 (28355)
2	Gembrook and Thomson Dam Fires	Melbourne	GDA 94 zone 55 (28355)
3	TBA		
4	TBA		

2.2.3   Time zone format

There is a difference in conversion between datetime and date fields. Datetime is one of the common types of the database column. Any datetime is stored as Coordinate Universal Time (UTC) format in the

database of this prototype while the datetime is converted to local time using time zone information when corresponding data are displayed. For instance, the datetime is displayed as 10:00 am on the 1st of January in 2020 in Hobart time if it is 23:00 pm on the 31st of December 2019 UTC. On the other hand, date is not converted If there is date part only without time in an original file because the maximum temporal gap is 11 hours in Australia from UTC and this gap is still less than half a day and can be rounded out (see below). For example, date is the 1st of January in 2020 in the date field if the UTC date is the same in Australia.
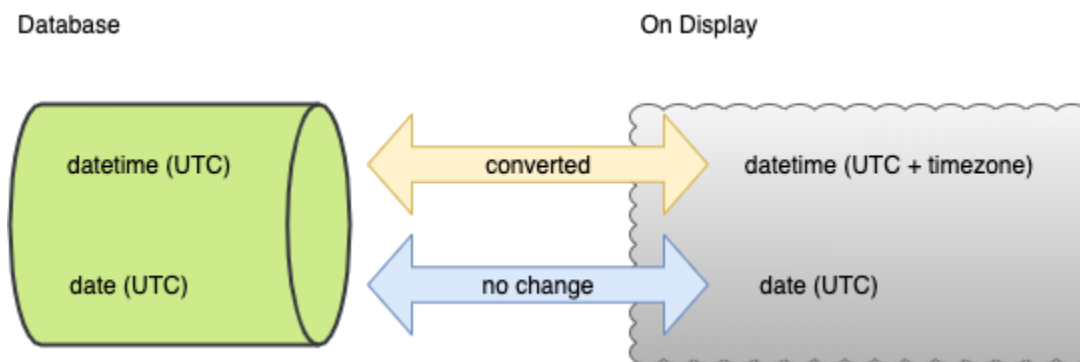
Figure 3: Datetime type is converted while date type remains the same without conversion

3 Data Processes (Common Data)

Common data structures, data conversion and resampling are described in this section while regional differences of data structure and process are mentioned in each main document.

3.1 Data structure

There are two types of database table: (1) spatial tables, which contain geographical location and can only be manipulated by spatial extension tools such as PostGIS, and (2) non-spatial tables, which can be manipulated by common database management system (DBMS) such as Postgres and MySQL without spatial extensions. Further, there are two sub-types of spatial data. One is (1-a) vector data, which comprises of geographical location with either points, lines or polygons in addition to general features, such as datetime (Burrough *et al.*, 2015). Another is (1-b) raster data, which contains non-human readable binary and geolocational data. In this study, raster data are wrapped in a column of database table. Common abstract classes and database table are introduced in the rest of this section. Note that classes and database tables are strongly coupled by ORM as mentioned above in this study. These are, therefore, considered to be synonym unless there is explicit illustration.

3.1.1 Vector class

Vector class represents entities in the real world using discrete elements such as points, lines and polygons with coordinates (Heywood, Cornelius and Carver, 2011; Boldstad, 2012). There are some common vector classes, such as fire history, ignition and vegetation in this prototype. Fire history class contains historical fires with corresponding attributes such as burnt area and name; Ignition class has datetime and location of an ignition and vegetation class contains an identifier for vegetation.

3.1.1.1 *Fire History*

Fire history table contains information about record fires with ignition datetime at least as below. Other contents can be varied among study areas and are mentioned in main document.

Table 5: Fire history table contains ignition datetime at least.

Field Name	Field Type	Description
Ignition_datetime	yyyy-MM-dd HH:mm:ss	(UTC)

Fire history class can not only contain historical fires but also be intelligently interrogated through the methods, which is the inner functions of the class. Some of them have already been implemented in previous prototype (Ozaki, Aryal and Fox-Hughes, 2019). These methods are overridden by child classes so that the historical fires can be adapted in various time-zones and map coordinate systems in this prototype (See below).

Table 6: Methods of fire history class

Method	Description
Radius(fire_name)	Radius of the circle whose area is equal to fire area whose name is fire_name. The radius can be used to measure the maximum range of firebrands to project. The equation is $radius = \sqrt{\left(\frac{area}{\pi}\right)}$. See section 4.2.3.
yearsSinceLast (point, burningAt)	This method is designed to measure how old a fuel is and helpful to measure the fuel load for some fire models such as buttongrass moorland fire model. There are two parameters: point indicates a location to examine and burningAt does a simulated time of study case fire, which should coincide with the counterpart in climate data such as temperature, cloud coverage and curing.
wasBurnt (point, fire_name)	This method is designed to indicate whether or not a cursor point has been burnt in the provided name, fire_name, yet. If the point location has already been burnt in the provided fire_name, the method returns true, otherwise false.

3.1.1.2   *Ignition table*

Ignition table is designed to contain simulation data by copying from original ignition tables such as ignition incident and lightning strikes. For instance, this table records a result of simulated lightning strikes with timestamps by referring to lightning table (see section 3.1.1.3) if the ignition is caused by a lightning strike. In addition, this table can contain multiple types of ignitions (see Table 7).

Table 7: Ignition record table is an output table to keep track of fire simulation.

Field Name	Field Type	Description
id	Integer	System unique id
version	Nullable Integer	Simulation version
incident_id	Nullable integer	See section 3.1.1.3
lightning_id	Nullable integer	See section 3.1.1.3
examined	Boolean	0: not examined yet (NY), 1: examined. See section 7.
Ignition_datetime	DATETIME WITHOUT TIME_ZONE	Ignition datetime as UTC. This field may be copied from lightning hit if the reason is a lightning strike.

3.1.1.3   *Ignition incident and Lightning hits*

Ignition incident table and lightning lit table contains original information of ignitions. Both resemble each other, and these contain locations and datetime of an ignition incident or a lightning hit. A study area can have multiple locations in different times.

Table 8: Ignition table contains ignition datetime

Field Name	Field Type	Description
hit_datetime	DATETIME WITHOUT TIME_ZONE	yyyy-MM-dd HH:mm:ss (UTC, naïve)

This class is referred by ignition hit class, which records simulated ignition (see 3.1.1.2).

3.1.1.4   *Thermal hotspots*

Thermal hotspot data are useful to verify or support fire history or ignition data. These spots are monitored with the infrared channels from two satellites: Suomi National Polar-orbiting Partnership Program (S-NPP) satellite and Himawari-8, which is a high temporal resolution geostationary satellite (Lee, 2014; Schroeder, 2017; Listi *et al.*, 2018, 2018; ORNL DAAC, 2018; JAXA, 2022). SNPP and Himawari-8 were launched in 2011 and 2016 respectively. Resolution varies between hotspot images. The temporal resolution in S-NPP data is poor with observations only six times a day at most (Lee, 2014; Schroeder, 2017; Wang, 2021), while spatial resolution is high, having 375 m pixels. On the other hand, spatial resolution in the Himawari-8 hotspot detections is low, with one km pixels, but temporal resolution is extremely good, every 10 minutes, due to the geostationary nature of the satellite, with multiple detections per hour (Yumimoto *et al.*, 2016; Listi *et al.*, 2018). Record structures exhibit in Table 9 and Table 10.

Table 9: Thermal hotspots from S-NPP

Field Name	Field Type	Description
latitude	Real number	This coordinate is recorded as WGS84
longitude	Real number	This coordinate is recorded as WGS84
bright_ti4	Real number	
scan	Real number	
track	Real number	
acq_date	String	yyyy-MM-dd format
acq_time	Integer	
satellite	String	
instrument	String	
confidence	String	
version	Integer	
bright_ti5	Real number	
frp	Real number	
daynight	String	D or N
type	Integer	

Table 10: Thermal hotspots from Himawari

Field Name	Field Type	Description
fid	Real number	This coordinate is recorded as WGS84
#obstime	QString	yyyy-MM-dd hh:mm:ss format

dettime	QString	yyyy-MM-dd hh:mm:ss format
sat	QString	
algo	QString	
okm	QString	
sampl	qlonglong	
line	qlonglong	
lon	double	This coordinate is recorded as WGS84
lat	double	This coordinate is recorded as WGS84
pixwid	double	
pixlen	double	
meant07	double	
meant14	double	
meantdt	double	
fire_idx	double	
fire	qlonglong	
test1_6	QString	
sunglint	double	
firepower	double	
freq	double	Fire intensity
fQC	qlonglong	
pixel	QString	

3.1.1.5   *Vegetation*

Structure of vegetation can vary throughout jurisdictions. The common field, vegetation group, is described below.

Table 11: General vegetation table

Field Name	Field Type	Description
veg_group	Varchar	Key for matching the fire model in the configuration file

3.1.1.6   *Geology*

Geology table is employed to identify a site productivity in buttongrass fire model and was acquired from GeoScience Australia with the scale, 1: 1 million (Geoscience Australia, 2020). The site productivity is low if a location contains quartzite. Otherwise, the productivity is medium (5.4). Main features of this table are described below.
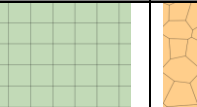
Table 12: General geology table

Field Name	Field Type	Description
stratno	Integer	Stratification number
name	Varchar	Name of stratification
description	Varchar	description

3.1.1.7 Prediction geometries

Prediction is a table for containing simulation results. Class and table for prediction are conceptual and therefore implemented by its child classes by following OOP (Figure 2). There are two types of geometry in Prototype 2: regular and irregular. Further, there are Delaunay and Voronoi in irregular shape while Diamond, Hexagon and Square in regular geometry as below.

Table 13: Geometries with average number of adjacent grids

Geometry	Delaunay	Diamond	Hexagon	Square	Voronoi
Image					
Type	Irregular	Regular	Regular	Regular	Irregular
ID	1	2	3	4	5
Average number of adjacent grids	12.51	7.96	5.84	7.93	5.96

The number of adjacent grids vary among these geometries. For instance, Delaunay has the most, approximately 12.5; Diamond and Hexagon follow it with approximately eight; Square and Voronoi have the least, approximately six. The average number of adjacent grids in fire geometries is approximately 8.04 and its angle is approximately $44.78° \approx 360°/8.04$. The number of adjacent grids is correlated with elapse. For example, Delaunay shows the shortest because Delaunay has more neighbour grids, approximately 12.5, than other geometries (Ozaki, Aryal and Fox-Hughes, 2019). That is, Delaunay has the most chances to search the shortest path of fire propagation. The attributes of all geometries are as addressed below.

Table 14: Prediction table

Field Name	Field Type	Description
assess	BYTE	0: Not accessed yet (NY), 1: Working in progress (WIP), 2: Done (DONE)
centroid_id	Integer	Foreign key
elapse	Nullable Big Integer	Shortest elapsed time since the initial ignition
elapse_max	Nullable Big Integer	Longest elapsed time
fire_channel	Integer	0: no lateral fire , 1: with lateral fire
fire_duration	Nullable Big Integer	This indicates how long fire stayed by subtracting elapse_max by elapse field
fire_intensity_max	Float	Maximum fire intensity computed by fire model
size	Integer	Side length of square grid which is used to generate polygon
spotting_distance	Float	Spotting distance
vorticity	Integer	similarly to fire_channel, 0: no lateral fire with vorticity, 1: with lateral fire with vorticity

Similar to the previous prototype, an elapse field represents elapsed time since the first ignition and an access field indicates either status 0 as not assessed yet (NY), 1 as working in progress (WIP), or 2 as done (DONE) (Ozaki, Aryal and Fox-Hughes, 2019). The elapsed time is the earliest time to reach the corresponding cell while elapse_max is the latest in order for computing the duration of fire staying in the cell into other column, fire_duration. An intensity of fire is contained into fire_intensity_max column and updated when the larger intensity is identified. Size column in Prototype 2 is a counterpart of zoom column in Prototype 1. It represents the length of a square side, which is used as a measurement to generate prediction polygons, and a scale category of prediction. In previous prototype, the zoom column in prediction indicates the scale such as small, medium and large. On the other hand, the size column in Prototype 2 contains the digit as a size of grid to represent a scale. Distance to the spotting fire is contained in the column, spotting_distance after calculated by fire models. The spotting fire is addressed further in 4.2.3. Both fire_channel and vorticity columns contain 1 if the lateral fire spread is identified otherwise 0. The lateral fire spread is further addressed in **Error! Reference source not f ound.**.

In the following section, process of prediction polygon is introduced.

3.1.1.8 *Process of prediction polygon*

Process of prediction polygon differs between regular and irregular geometries in QGIS (Ozaki, Aryal and Fox-Hughes, 2019). Steps of regular geometry, such as Diamond, Hexagon and Square, are simple as described below.

Table 15: Process of prediction polygon (regular geometry)

Step	Description
1	Extent of the study area is measured.
2	Height and width of the rectangle, which estimates each geometry, are measured.
3	Either Diamond, Hexagon or Square, is selected among regular geometries.
4	The polygons in previous step are generated.
5	Centroids for the above are generated.

Firstly, extent of study area is manually measured by overlapping other geospatial data such as fire history, vegetation and climate data on QGIS. Secondly, height and width of each rectangular grid, which is to estimate each geometry, are computed. For example, if x minimum is 430,000, x maximum is 530,000, y minimum is 5,190,000 and y maximum is 5,270,000 in the extent, then width and height of extent are as following.

$$width = x.max - x.min = 530,000 - 430,000 = 100,000$$

$$height = y.max - y.min = 5,270,000 - 5,190,000 = 80,000$$

Thirdly, a required geometry is generated by QGIS function. Lastly, centroids, which will be used to measure a distance from other grids, are created. The number of required centroids is calculated by dividing total extent by area of conceptual polygon size, such as $500m^2$.

$$\#centroid = \frac{extent}{polygonArea} = \frac{width \cdot height}{500^2} = \frac{100,000 \cdot 80,000}{500^2} = 32,000$$

Process for irregular geometry is addressed as below.

Table 16: Process of prediction polygon (irregular geometry)

Step	Description
1	Extent of study area is measured.
2	The number of random points is computed as seeds for irregular polygon.
3	Random points are generated with 80 metres as the minimum distance.
4	Irregular polygons are generated.
5	Centroids for prediction polygons are generated.

Similar to regular geometry, extent is measured at first. Then the number of random points, which will become seeds for generating irregular geometry such as Delaunay or Voronoi, is calculated. These points are generated with the minimum distance from other random points as 300 metres if conceptual square size is $500m^2$. This figure is necessary to empirically estimate by maximising the minimum distance so that each grid is evenly distributed by QGIS. The larger the distance is, the more chance to fail to generate. Then, prediction polygons are generated. Centroids of prediction are generated in the last. These centroids are employed to measure the distance from other grids in the fire prediction. The below figure shows an example of Delaunay and its centroid.
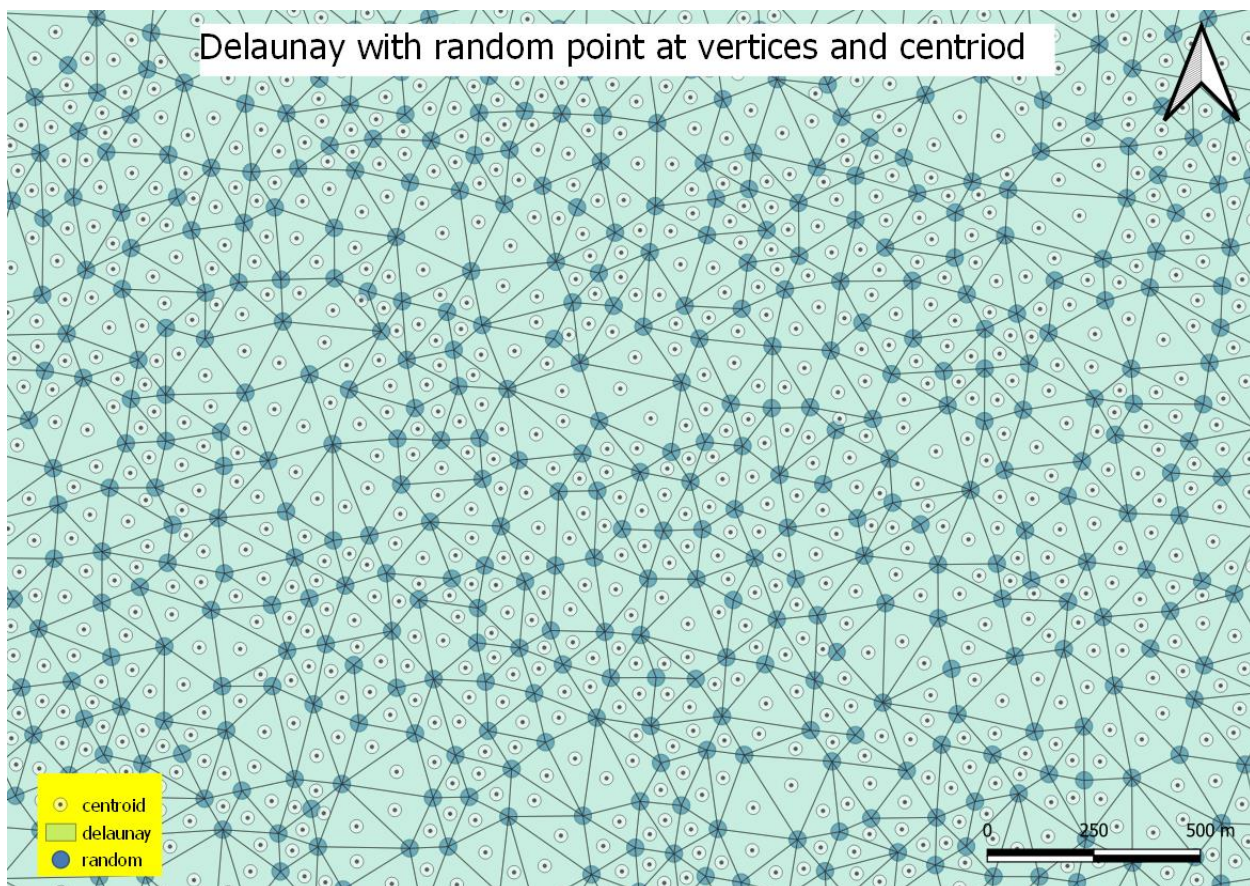

Figure 4: Delaunay polygons are generated based on random points as their vertices then a centroid is computed on each Delaunay.

3.1.2   Raster data

Raster class represents entities in the world by distributing in regular grids (Boldstad, 2012). There is a raster table and a band table in this prototype and are various records such as DEM; Relative Soil Moisture (AWAP), which is employed to estimate fuel moisture content in desert spinifex fire model; BARRA climate data such as temperature, curing, wind, in the raster table. The raster table contains study_area_id, raster as a rast column, metadata which is extra information from an original file, and type_id, which indicates a type of raster (see below).

Table 17: Raster table with study_area_id, type_id, rast, and metadata

Field Name	Field Type	Description
Id	Integer	System unique id
study_area_id	Integer	See section 7
type_id	Integer	See section 7
rast	Raster	NOT NULL
metadata	Text	Additional information from original file

Each raster record can relate to one or more bands, whose tables are designed to contain band information such as raster id, timestamp and metadata, as below.

Table 18: Band table with timestamp, metadata and raster id

Field Name	Field Type	Description
id	Integer	
dim_time	DATETIME WITHOUT TIME_ZONE	Timestamp as UTC
metadata	Text	Additional information from original file
raster_id	Integer	Foreign key

3.1.2.1   Resolution of raster data

Resolution of raster varies depending on original raster files. For instance, Relative Soil Moisture (AWAP) are the coarsest, $5\ km$; the climate data are the second coarsest, approximately $1.5\ km$; curing data directly retrieved from BoM is lightly finer, $453.78\ m$, than other climate data. Similarly, the wind data resampled by WindNinja is finer than original climate data. Note that size represents side length of each pixel. See below.

Table 19: Resolution of raster data

Raster type	Pixel size (metres)
DEM	27.05
AWAP	5,000
Wind generated by WindNinja	495.21
Curing from BoM	453.78
Other climate data	1,500

3.1.2.2   Digital Elevation Model (DEM)

Digital Elevation Models (DEMs) are one of common raster data and signify elevation (Boldstad, 2012). DEM can be retrieved from United States Geological Survey (USGS) through Earth Explorer, which is a guidance tool to obtain geospatial data (United State Geological Survey (USGS), 2020). Its data provider

is "SRTM 1 Arc-Second Global" and original resolution was approximately $27\ m$. Coordinate system of the original files is WGS 84 / UTM zone 55s (*USGS EROS Archive - Digital Elevation - Shuttle Radar Topography Mission (SRTM) 1 Arc-Second Global*, 2020). DEM is served as tiles and these tiles are merged at first if study area is covered by multiple tiles. Secondly, it is reprojected to local coordinate system such as GDA94 zone 55 (SRID: 28355) for consistency with other geo data in each study area. Thirdly, coverage area of the DEM is clipped. The Clipped DEM is lastly imported in the database. Note that resolution of the last prototype was $25\ m$ while it is about $27\ m$ in new prototype. This discrepancy is acceptable because resolution of other raster data, such as curing, wind data resampled by WindNinja, and other climate reanalysis data are still greater than that of DEM. See below.

Table 20: Process of DEM: merge, reprojection, clip and import to DB

#	Step name	Description
1	Merge	Four datasets were merged.
2	Reprojection	Reproject to local coordinate system
3	Clip	The data covering around the study area was clipped to save the space
4	Import to database	The data was imported into the database.

The table structure follows a raster structure (see Table 17 and Table 18).

3.1.2.3   Reanalysis Climate Data

BARRA is an abbreviation of "The Bureau of Meteorology Atmospheric high-resolution Regional Reanalysis for Australia" and reanalysis data for regional atmosphere. Its coverage areas are Australia, New Zealand and South Asia and resolution is approximately 12 km (Su *et al.*, 2019). Table structure follows a raster structure (see Table 17 and Table 18). Each climate raster record can relate to multiple band tables with different timestamps.

3.1.2.4   Curing Data

Curing signify percentage of cured or dead materials over total fuel complex including dead and alive in grassland (Andrews, Anderson and Anderson, 2006). The data are obtained from THREDDS while other climate data are from BARRA (*Centre for Australian Weather and Climate Research - List of THREDDS catalogs*, 2017). Resolution is approximately $500\ m$, which is finer than other climate data on BARRA-T, $1.5\ km$. There are some processes. Firstly, data quality is visually examined because curing is observed from satellite and coverage is often insufficient. Secondly, they are chronologically sorted and merged because these are separately distributed. Each original dataset is allocated into each band chronologically. In other words, curing data column shall relate to multiple band tables with different timestamps. Thirdly, map coordinate is reprojected for consistency with other geo data in each study area. Fourthly, the data covering the study area are clipped to save the space. After importing raster data, it is necessary to create band records with datetime column. See below.

Table 21: Process of curing data

#	Step name	Description
1	Qualification of coverage	Datasets are visually confirmed the quality of coverage of study area by inspecting its quality.
2	Sort and Merge	The datasets are chronologically sorted and allocated in each band in new dataset.

3	Reprojection	The datasets are reprojected to local coordinate system such as GDA94 zone 55 (SRID: 28355) for Tasmania, depending on study area.
4	Clip	The data covering around study area is clipped to save space.
5	Import to database	The raster data is imported into database.
6	Insert datetime	Band records with datetime column is inserted.

Its table structure follows a raster structure (see Table 17 and Table 18).

3.1.2.5   *Relative Soil Moisture (Upper Layer)*

Relative soil moisture illustrates the water fluxes regarding to the soil moisture modelled by Australian Water Availability Project (AWAP), which is a collaborated project among CSIRO Marine and Atmospheric Research (CMAR), the Bureau of Metrology (BoM), the Bureau of Rural Sciences (BRS). There are two layers for soil properties, upper (depth from 0 to 0.2 m) and lower (depth between 0.2 and 1.5 m). Desert Spinifex Model ingests an upper layer of relative soil moisture for calculation of the fuel moisture content (5.3.4). Relative soil moisture content is rasterised into fraction as seen in Figure 5 (Raupach *et al.*, 2009, 2012; CSIRO AWAP Team, 2014).
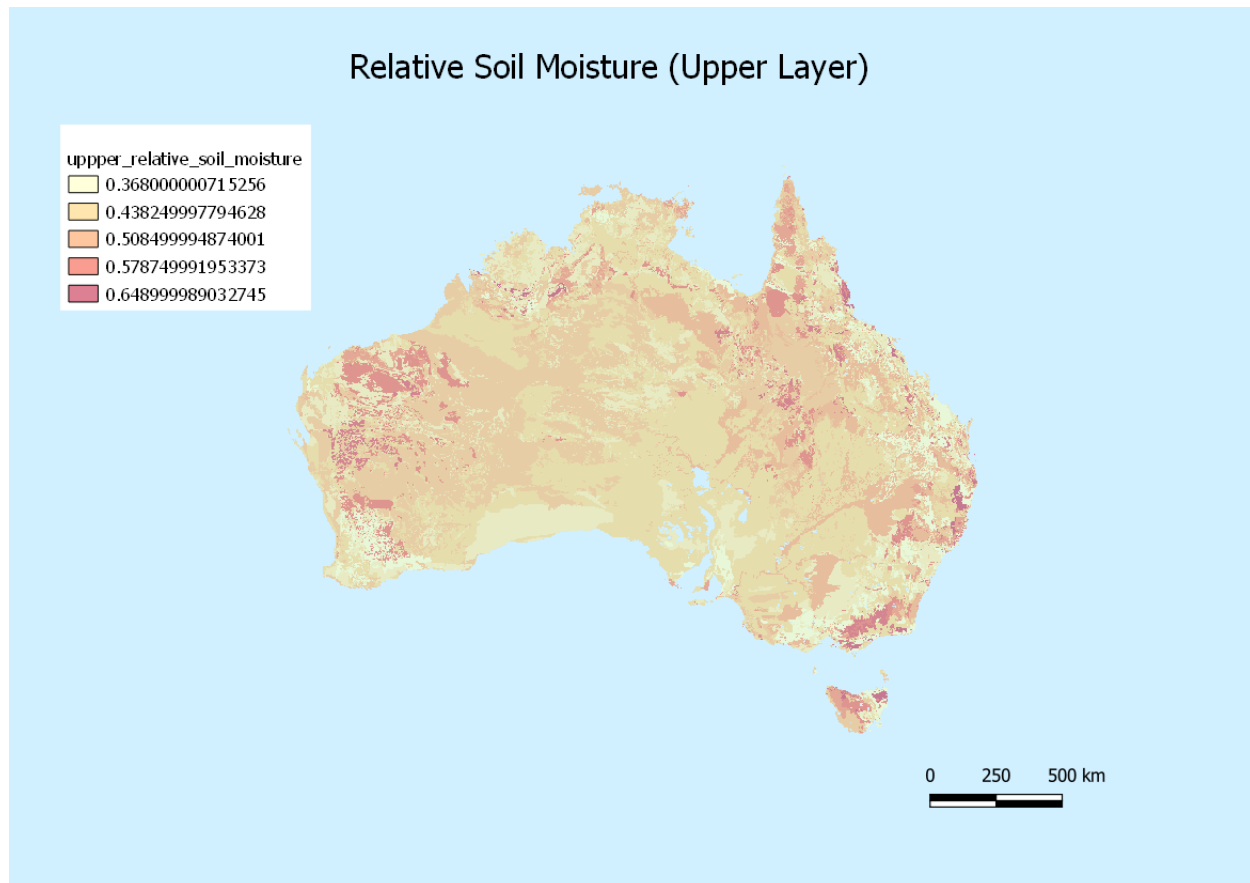

Figure 5: Upper relative soil moisture rasterised in fraction

Although map coordinate is originally GDA 94, which is equivalent to WGS84 for general purpose, it is not explicitly assigned any projection. It is, therefore, necessary to imprint WGS84 into the data in

advance. Then it is re-projected to appropriate coordinate system. Following process is the same as general steps. Details are described in 3.2.

3.1.3   Non-spatial data

Non-spatial data are described in this section.

3.1.3.1   *Version*

Version table is designed to manage simulation version and contains various information, such as id, geometry, timestamps as below. Its versioning flow is addressed in the section 4.1.

Table 22: Version table contains timestamps for simulation with geometry of prediction.

Field Name	Field Type	Description
id	Integer	Simulation version
geometry	Integer	Geometry id. See section 3.1.1.7.
started_at	DATETIME WITHOUT TIME_ZONE	Timestamp for simulation starting
updated_at	DATETIME WITHOUT TIME_ZONE	Timestamp for simulation updating
finished_at	Nullable DATETIME WITHOUT TIME_ZONE	Timestamp for simulation finishing

3.2   Data conversion

In general, geospatial data files are processed in several steps; quality is inspected by removing anomaly band; rest of bands are sorted by chronological order; reordered data are merged into a file; the coverage is clipped (Figure 6). After that, the data are imported into database. Note that some steps can be omitted dependant on nature of data. For instance, it is not necessary to sort bands chronologically in DEM because there is only a band.
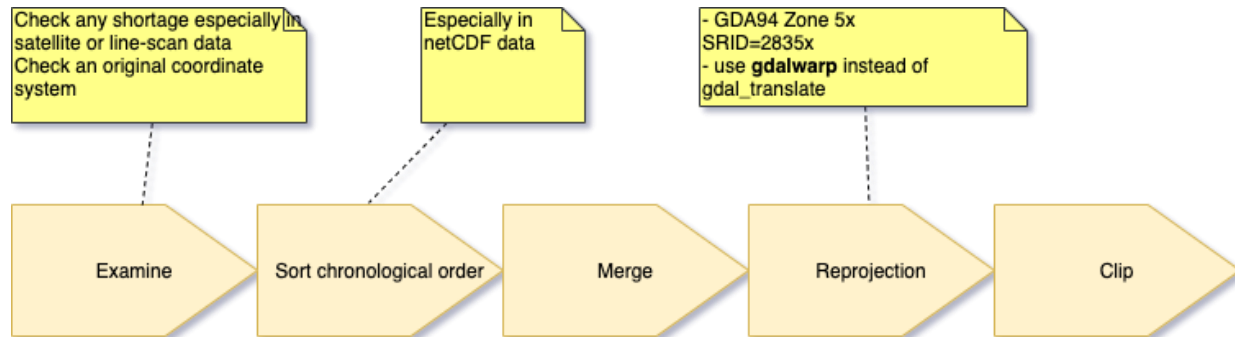
Figure 6: Common data process: Examining anomaly data, chronological sort, merging, reprojection and clipping

3.3   Resampling by WindNinja

Wind is one of significant factors of fire behaviour. It is necessary to use WindNinja to make wind data in BARRA more topographically sensitive because crude wind is not very topologically sensitive. WindNinja is a diagnostic tool and ingests various parameters such as DEM, direction and magnitude of wind, temperature, cloud cover, and refines wind speed and direction. There are some terrain specific parameters. For instance, diurnal wind option is capable of depicting diurnal airflow and is useful for diagnose valleys. Conservation of mass and momentum (CoMM) of wind is beneficial for analysis of lee side wind. However it spends from one to three hours per time episode to resample because it internally

calls OpenFoam which calculates Computer Fluid Dynamics (CFD) while it takes a several seconds at most without this option (Liu and Fang, 2019; Wagenbrenner *et al.*, 2019; Firelab, 2020).

There are two interfaces, Graphical User Interface (GUI) and Command Line Interface (CLI) as below.
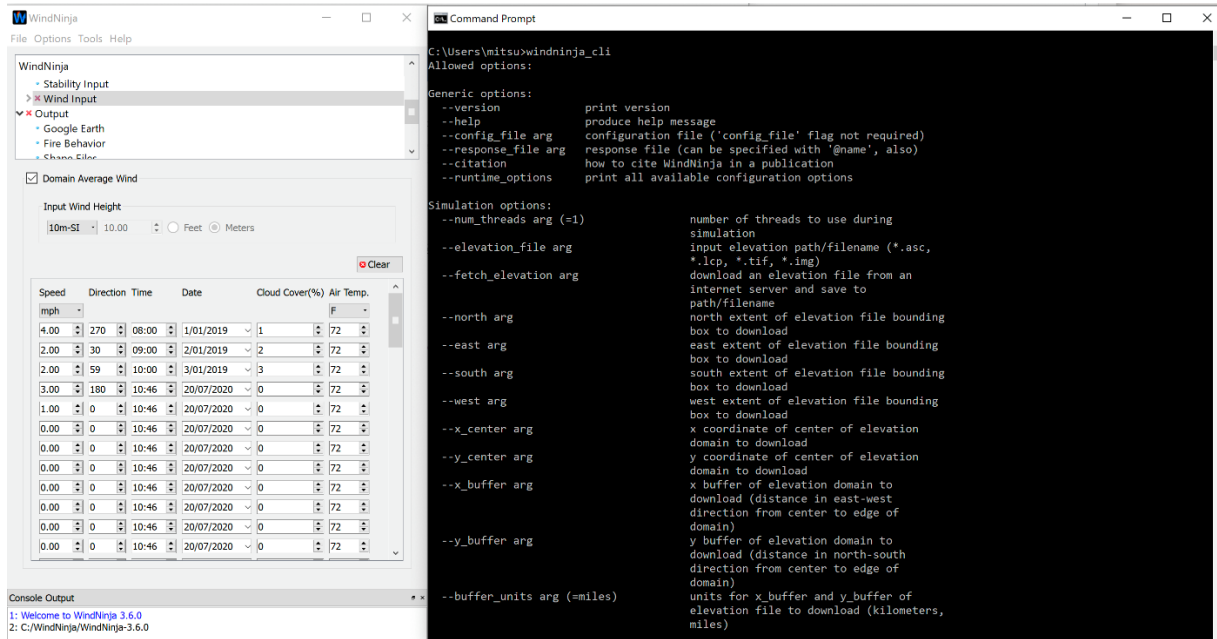
Figure 7: Two interfaces in WindNinja: (1) GUI on the left and (2) CLI on the right

CLI is employed because of a few reasons. The first is execution time. it may be necessary to execute WindNinja for a number of temporal bands. For example, if a fire is observed for two months and climate data are recorded hourly, approximately 24 hours × 30 days = 1,440 executions are necessary. The second is tolerance for human error. Although GUI is user-friendly and intuitive, manual input is human error prone while the CLI is suitable to be embedded in a system for automation. The third reason is that there are many more options in the CLI than the GUI. For instance, there are only two units for temperature, Fahrenheit (F) and Celsius (C) in the GUI. On the other hand, Kelvin (K) and Reaumur (R) in addition to F and C, are available in the CLI. Workflow for refinement of wind data by WindNinja is as below.
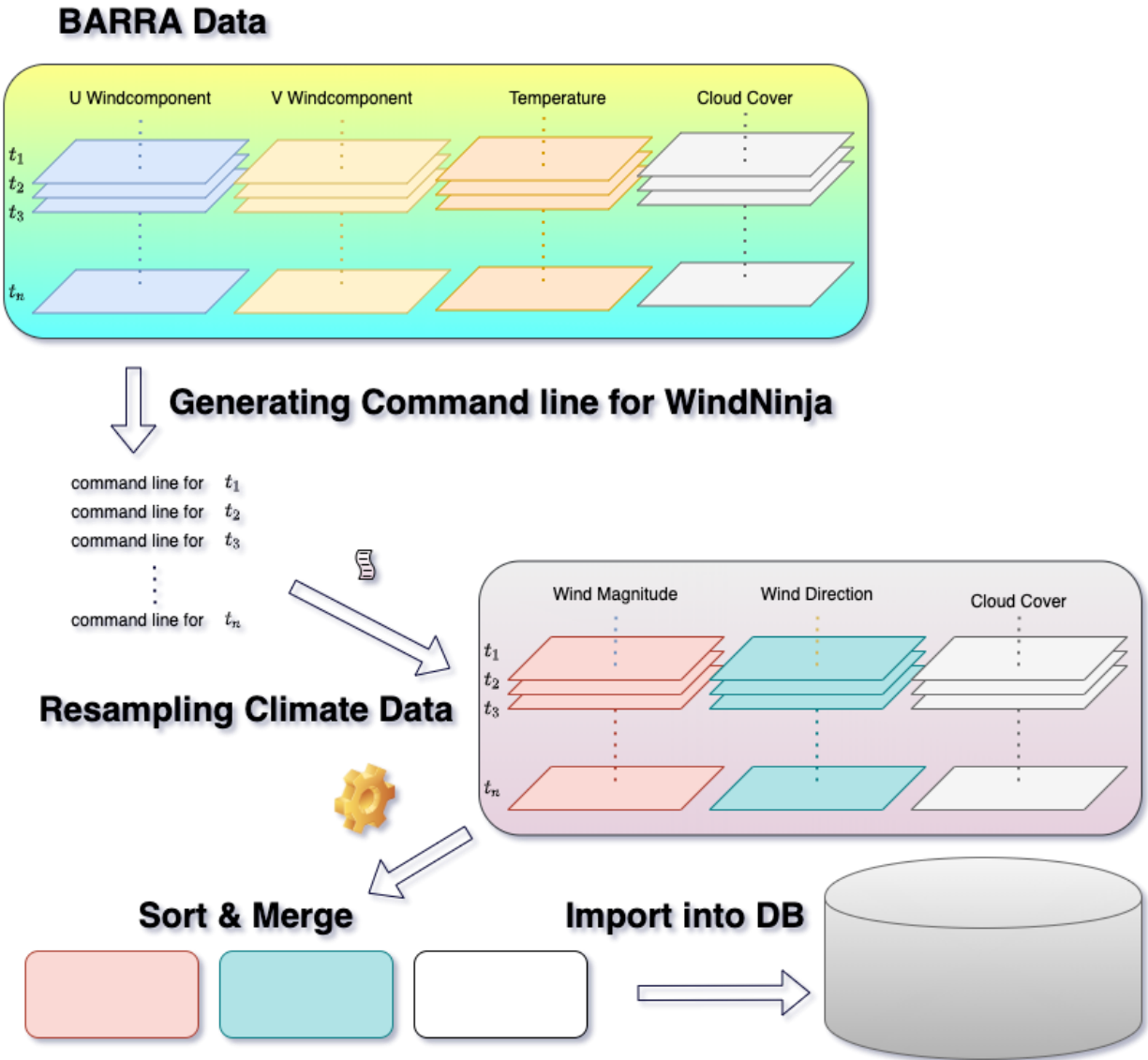
Figure 8: Process of resampling climate data: (1) climate data in each band and type are retrieved, (2) These parameters are written in a script for WindNinja command line interface, (3) The script is executed, (4) Output climate data are sorted order by time and (5) mered into each type of climate data and (6) These mashed up data are then imported into database

Firstly, BARRA climate data are retrieved at certain locational point as seeds to regenerate wind data. These data are temperature, cloud coverage, and wind component. Wind components are converted into speed and direction as mentioned in 4.4. Secondly, these climate data become parameters for CLI and written into a batch script. Thirdly, the script is executed and resampled wind speed and angle of toward wind. Fourthly, these resampled files are renamed so that they are chronologically sorted using UNIX script because the resampled files are named by WindNina and not sorted chronologically. Fifthly, these data are merged into each type of climate data with temporally separate bands. Lastly, these mashed up data are imported into database. Although cloud coverage data are also regenerated, the data stay unchanged from the original in the database. Therefore, the newly generated cloud coverage is not imported into the database.

4 Flow charts and diagrams

In this section, flow and process of various functions such as version control, class diagram for fire models, ignition, conversion of wind components, calculation of precipitation and conversion of measurement units, are described.

4.1 Version control

Version control allows the prototype to contain various combination of simulations. This function is beneficial when different configured values are ingested or when random selection is used, such as ignitions by lightning strikes. The version information is managed by version class as illustrated in 3.1.3.1. There are some entities are recorded by associating with version. For example, new record is created with version in ignition table when ignition point is unknown. In terms of prediction tables, they are cloned by appending version id to their table name. For instance, Delaunay table, riveaux_delaunay is cloned as riveaux_delaunay_0001 where 0001 indicates a backup version. In the same manner, centroids of prediction tables such as riveaux_centroiddelaunay, are also cloned with version id. All in all, new record is added in the ignition table while whole tables are cloned with regard to the predictions when version is incremented. See below.

Versioning

When version is created anew, new record is added in ignition table

while new table is created as backup for predictions.
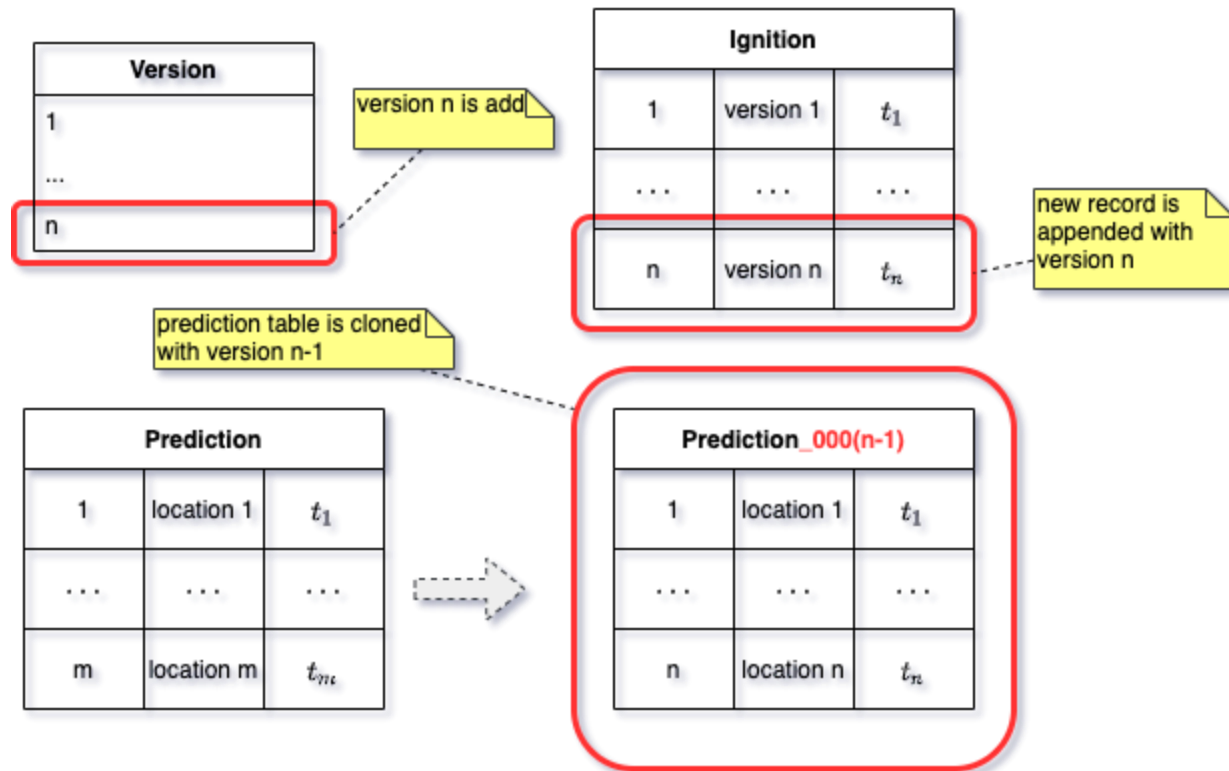
Figure 9: In version control, new record is added in the ignition while new clone is generated with current version number for prediction tables.

4.2   Prediction of fire propagation

Some functions are inherited from the previous prototype and others are revised regarding to simulation of fire propagation. Firstly, status of prediction (assess) is renewed. Then an extended overall flow of prediction is illustrated. Thirdly, spotting fire, which was one of promised functions from the previous study is described.

4.2.1   Assess status on prediction grids

A prediction grid is implemented in prediction polygons such as Delaunay, Diamond, Hexagon, Square and Voronoi, and contains various properties, such as ID, assess status and elapse. Assess is a status, which can be either, **Not Yet (NY)**, **Work In Progress (WIP)** or **Done (DN)**. With WIP assess, the elapse can be updated to smaller number while DN assess is not updated anymore unless this cell is reported as re-ignition point addressed in the section 4.3.3. The elapse property indicates either time since ignition as seconds when a cell is burnable or minus one when the cell is not burnable. The elapse can be computed until the grid status becomes DN to seek the shortest time from neighbours as seen below.
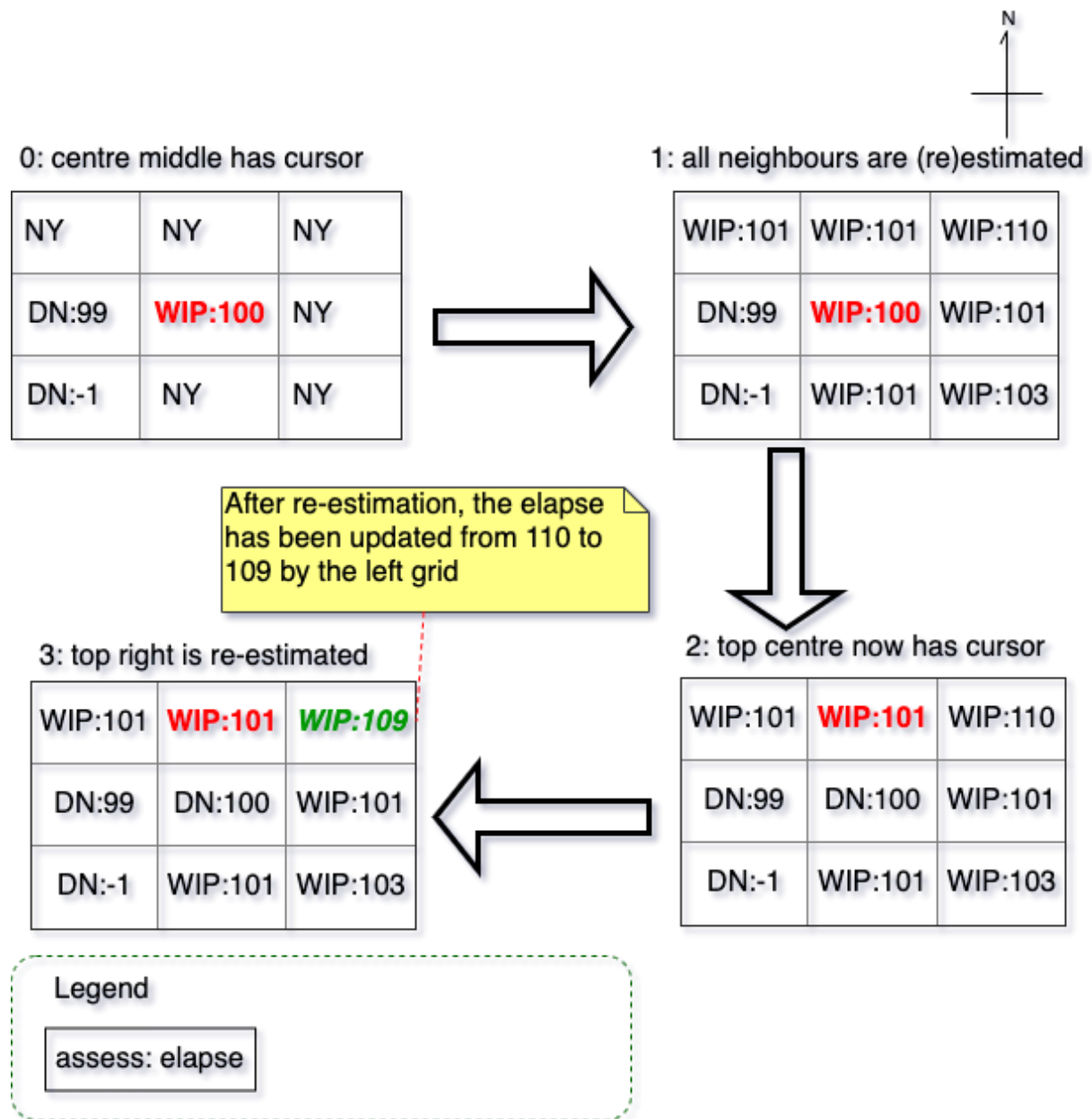
Figure 10: Assess status flow to find the shortest path. Each grid has an assess status in either Not Yet (NY), Work In Progress (WIP) and Done (DN). For instance, (0) a central grid has a cursor; its neighbour in the west has completed assessed with an elapse 99; the one in the southwest has also completed by negative one indicating not burnable; other adjacent neighbours have never been assessed and therefore their assesses are still NY. (1) The shortest path is determined as 100 from all neighbours. (2) Hence the central status becomes DN and cursor moves up to the north, which has one of the next shortest elapses with WIP. (3) From the point of a prediction in the northeast, now the shortest elapse decreases to 109, cited from (Ozaki, Aryal and Fox-Hughes, 2019).

This elapse is measured from not only adjacent polygons but also a spotting fire, which is new function in this prototype mentioned in 4.2.3. In terms of realisation of fire propagation, a cursor moves to the grid which contains the next youngest elapse and the status, WIP as below.
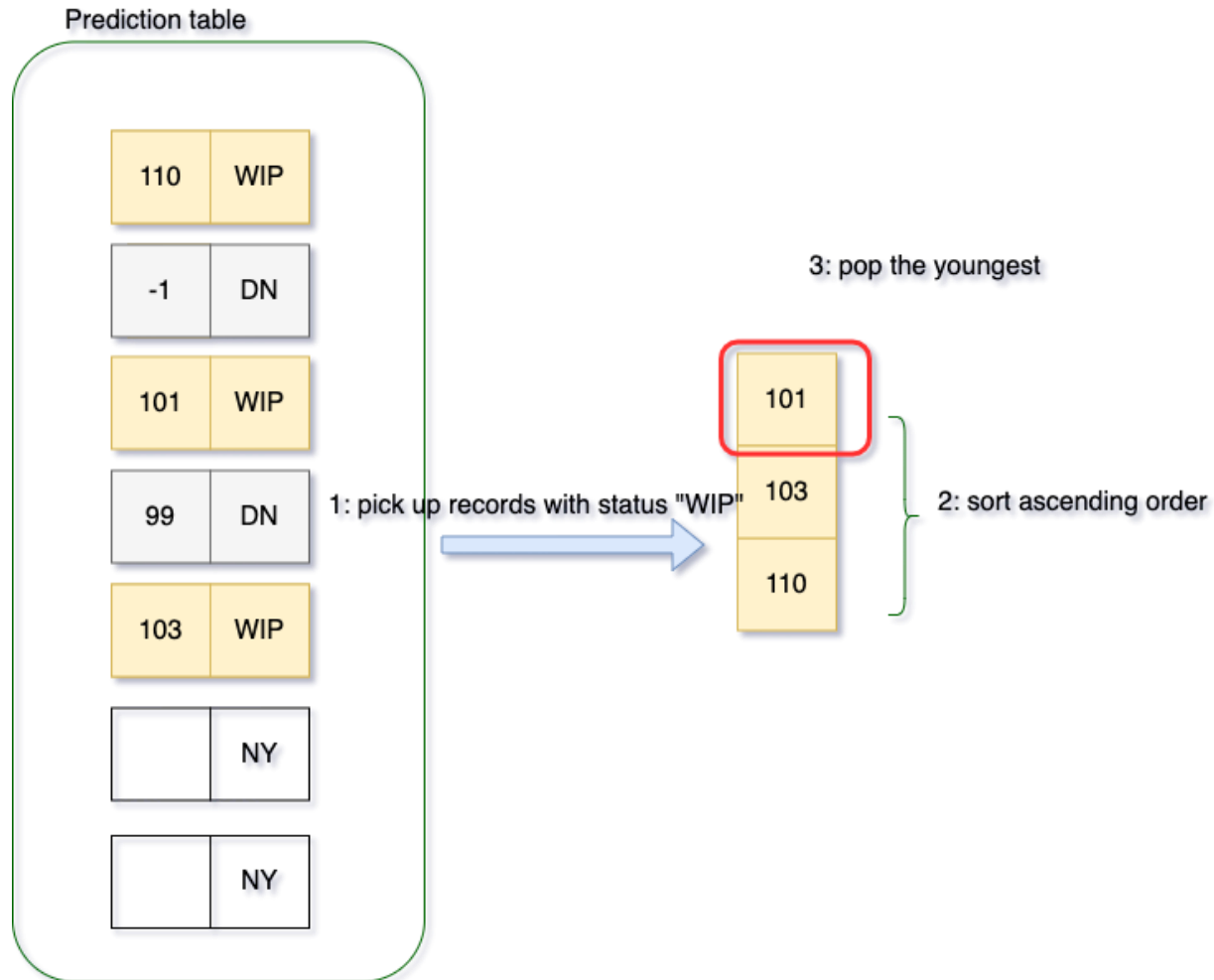
Figure 11: Storage of elapse and assess status. Database table contains these properties. System selects the youngest elapse from the table. Cited from (Ozaki, Aryal and Fox-Hughes, 2019)

With regard to an unburnt grid with minus one elapse, its assess status is different from the previous prototype, Prototype 1. Minus one is attributed to an unburnt grid and became assess DN immediately in Prototype 1. These unburnt cells were not assessed again because these were considered to be confirmed in the previous prototype. In contrast, the grids with minus one elapse are ascribed to Work In Progress (WIP) in this prototype so that they can be assessed again from other neighbours or spotting fires as seen below.
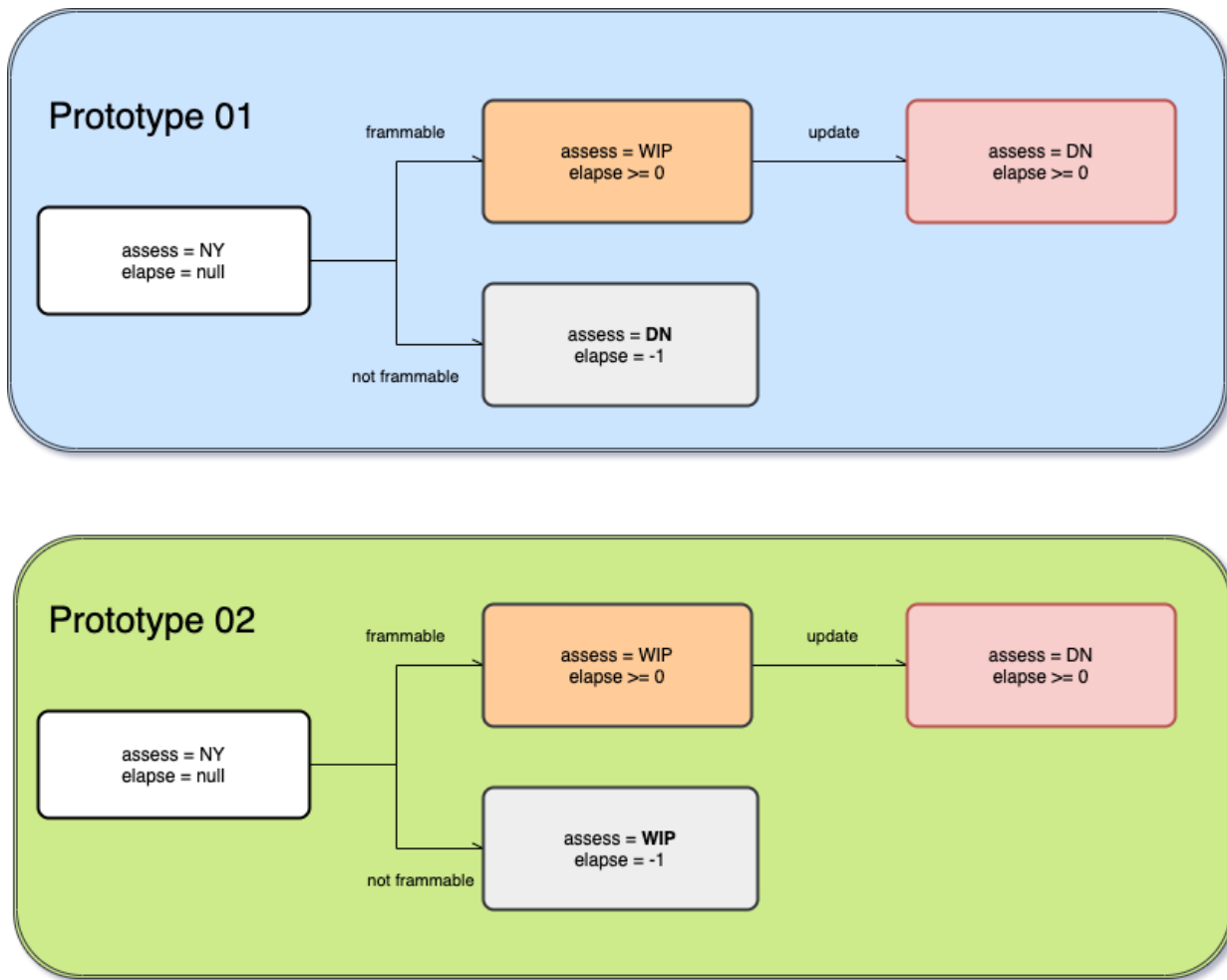
Figure 12: An unburnt status has been changed. In previous version, assess has been assigned as Done (DN) with elapse -1 once the cell was found not to be burnable. On the other hand, the unburnt cell stays Work In Progress (WIP) in Prototype 2 so that this cell can be examined from adjacent or spotting fire again.

It was possible to confirm that a location did not catch fire from another cell by any reasons such as lack of parameters because fire models in Prototype 1 did not equip with probability to make decision, i.e., "go" or "not-go" as described in section 5.4.1. In other words, cells could have had any positive elapse or zero if they were found to be burnable by calculation of rate of spread of fire in the previous prototype. However, it is necessary to re-evaluate un-burnable areas in this prototype because the same location can be evaluated as burnable or un-burnable by probability of catching fire with different time. For instance, a cell can be high-potentially burnt in day-time due to high temperature while it can be low probability with low temperature at night. In addition, a fire can intrude from not only adjacent grids by multiple ignitions function as mentioned in section 4.3, but also by spotting fire addressed in the section 4.2.3. Note that this change has an impact on verification. That is, unburnt areas are not counted in as fire area in this prototype because unburnt grids stay WIP (Table 23).

Table 23: Different unburnt assessment (elapse=-1) between Prototype 1 and 2

Prototype	Assess	Description
1	DN	Once the cursor location was assessed as DN, it could not be assessed again.

| 2 | WIP | Because assess status is WIP, it can be re-evaluated. This is beneficial for multiple ignitions, firebrands, as well as fire models which equip probability for fire spread. |

4.2.2   Flow chart of fire prediction

Overall flow of fire simulation is illustrated in this section. Prediction flow of fire propagation has been extended in this study from the previous study. This system is capable of multiple ignitions and introduces new fire models (see below).
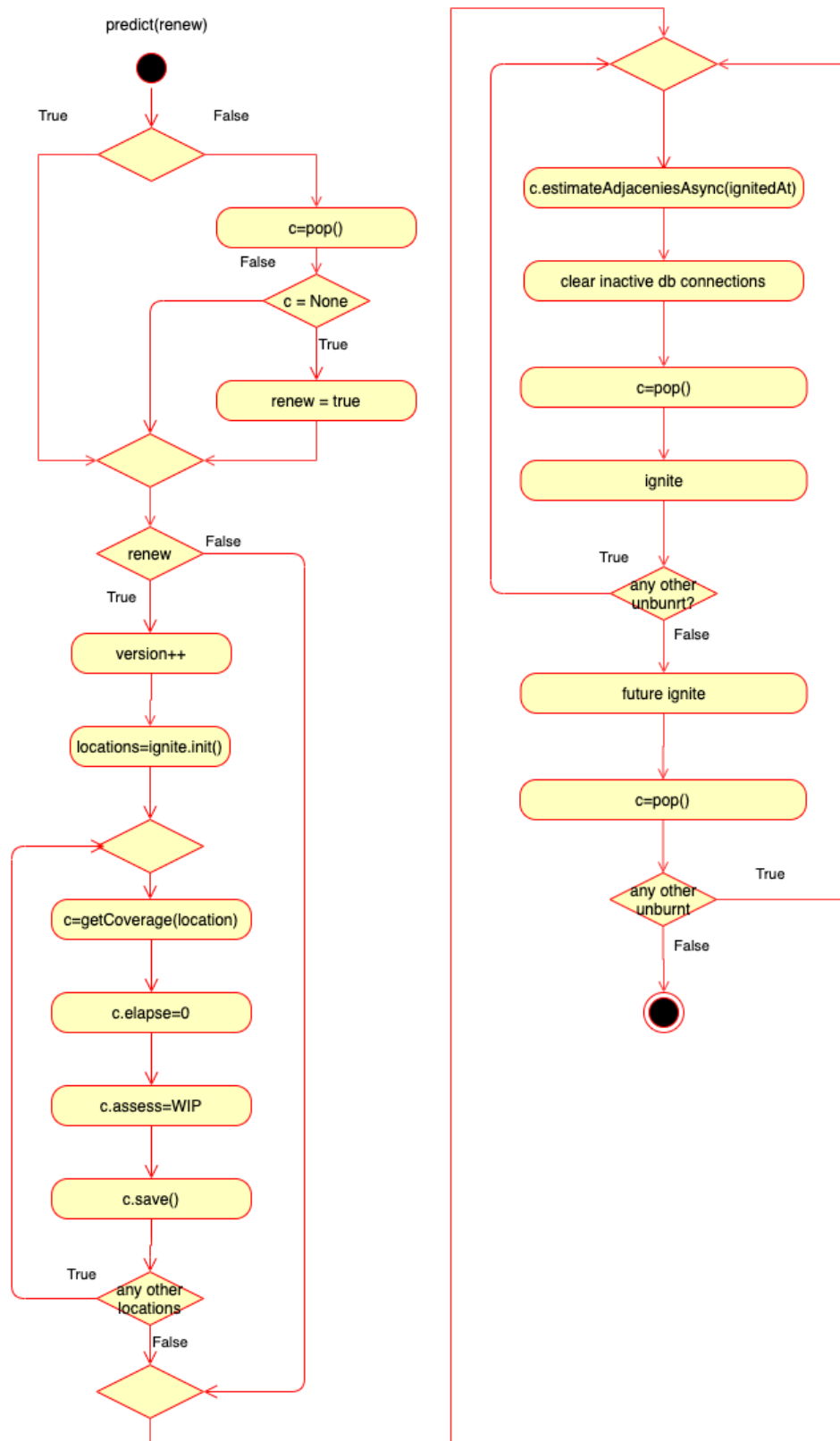
Figure 13: Flow of fire prediction with multiple ignition points

Prototype 2 can either start simulation from the scratch or take up where it left last time. If new start is selected by user, previous prediction table are cloned with on-going version; current prediction tables are formatted with elapse=None and assess=NY; version is incremented; prediction at the youngest ignition point is retrieved; its neighbours are schedule to predict in a queue; and assess status of the current prediction becomes DN with the shortest elapse from its neighbours. If a continue mode is selected, the prediction record, whose elapse is the youngest with assess status, WIP, is retrieved; its neighbours are scheduled; and the assess status of the current prediction becomes DN with the shortest elapse from neighbours. In either case, recent ignitions, which have not been triggered yet, are searched after a cursor moves from one to another. New prediction record is scheduled if there is any ignition. In addition, a future ignition is searched if all predictions caused by past ignitions are depleted.

4.2.3   Adjacent cells and cells within spotting distances

There are two ways for fire to transfer to a grid. One is that a fire moves onto adjacent grids, and another is a spotting fire.

Firstly, adjacent cells are re-defined in this prototype. The adjacent cells were defined as the grids which share boarder with others in previous prototype. However, they often overlap each other in the process of generating grids in QGIS. Therefore, the neighbour grid is re-defined as the grid which touches other grids or overlaps with others as below.
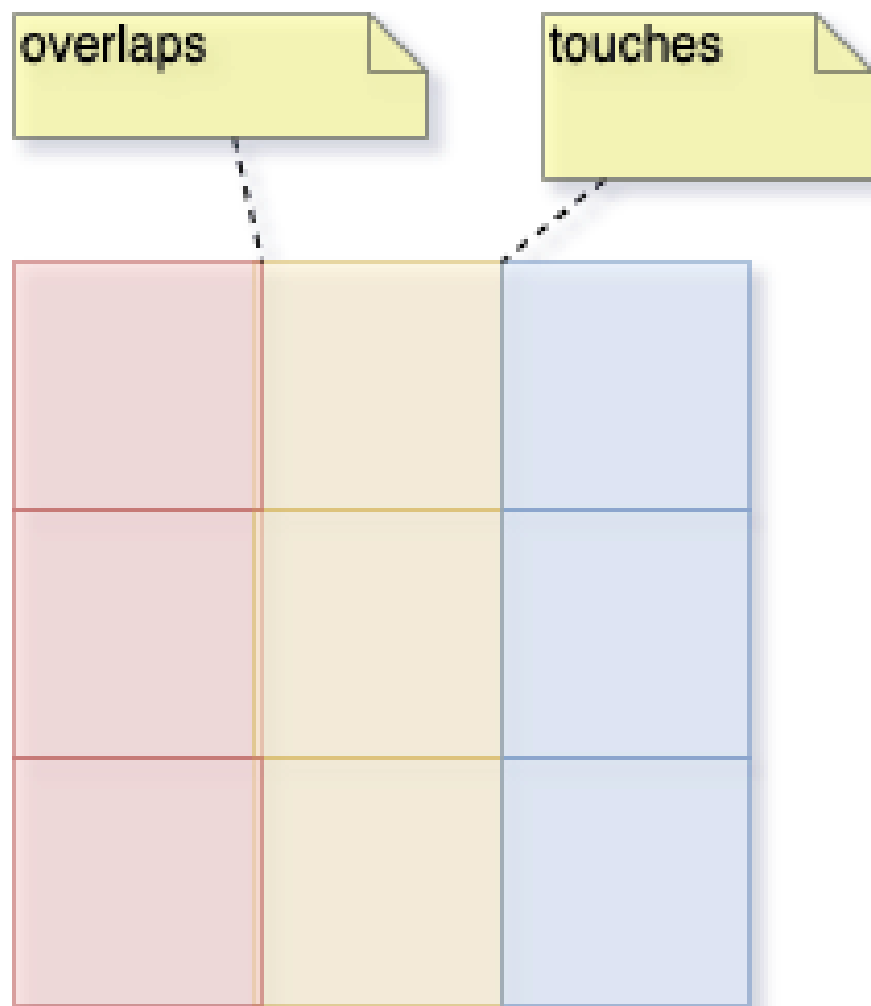
Figure 14: Adjacent grids either share border or overlap with other grids.

Secondly, spotting fire range is defined. Firebrands can ignite not only immediate adjacent cells but also remote fuels. That is, burnt area only affects imminent adjacent cells if there is no spotting fire as seen on the left (Figure 15). On the other hand, if there is a spotting fire in Forest fire model, cells within a spotting distance are examined. The spotting distance is 300 metres in an example on the right (Figure 15).
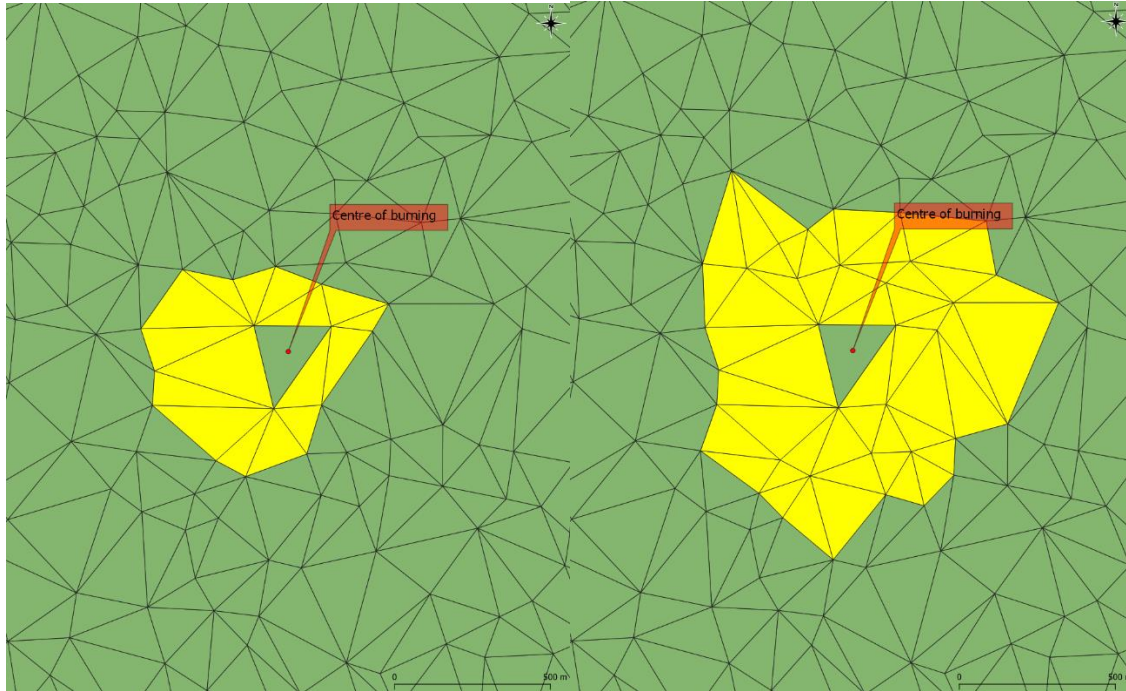
Figure 15: Influence of on-going fire. Left figure indicates that only adjacent cells are imminently affected if a spotting distance is zero. Right figure shows that all area within a spotting range is examined if a spotting occurs.

There are two contrivances in implementation of the spotting fire.

The first is spotting distance. According to the experiment conducted by Hall et al., a transported distance of firebrand of *Eucalyptus viminalis* can be more than 20 km (Hall *et al.*, 2015). Cruz et al. state that distance can excess 30 km in eucalyptus forests (Cruz *et al.*, 2012). However, it is necessary to limit the distance in the prototype because of an extent of geospatial data. The maximum radius is calculated form a fire isochrone in this prototype.

$$r = \sqrt{\frac{Area}{\pi}}$$

Where Area and r indicates burnt area in each study and a radius of the circle whose area is equivalent of the burnt area respectively (Figure 16).
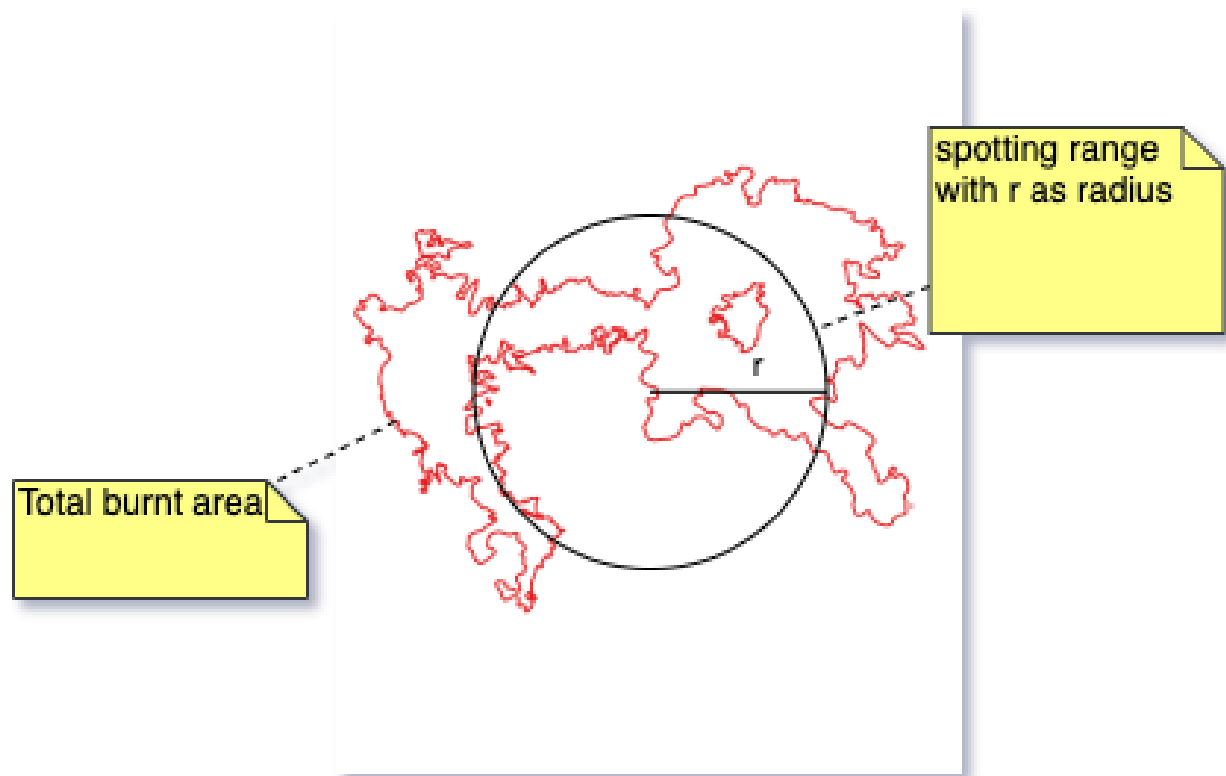
Figure 16: Maximum range of spotting fire is the radius of the circle which area is commensurate with the total burnt area

Another contrivance is probability of spotting fire and branched fire spread. It is necessary to select spotting points in a range because fire indeed spreads from each anew spotted area instead of burning whole area at once. In this prototype, therefore, spotting areas are randomly selected with configured probability. In this way, whole area in spotting range will be affected from new spotting locations (Figure 17).
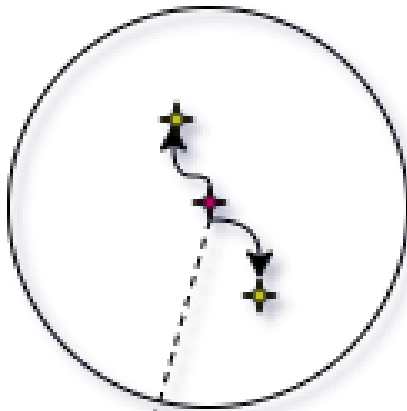
Figure 17: Firebrands are transported within a spotting distance. Then fires spread from each spotting point.
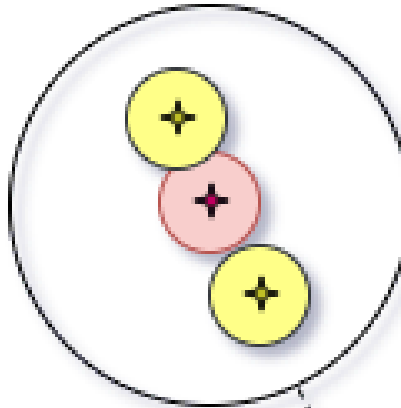
4.2.4   Mask of fire isochrone

Mask of fire isochrone allows the simulation to start near the predecessor fire isochrone. Fire isochrones are observed data and often contain end time of the fire in the isochrone. This temporal information can be used to start the fire simulation in the descendent isochrone. Assume there are the fire isochrones: A and B (Figure 18).
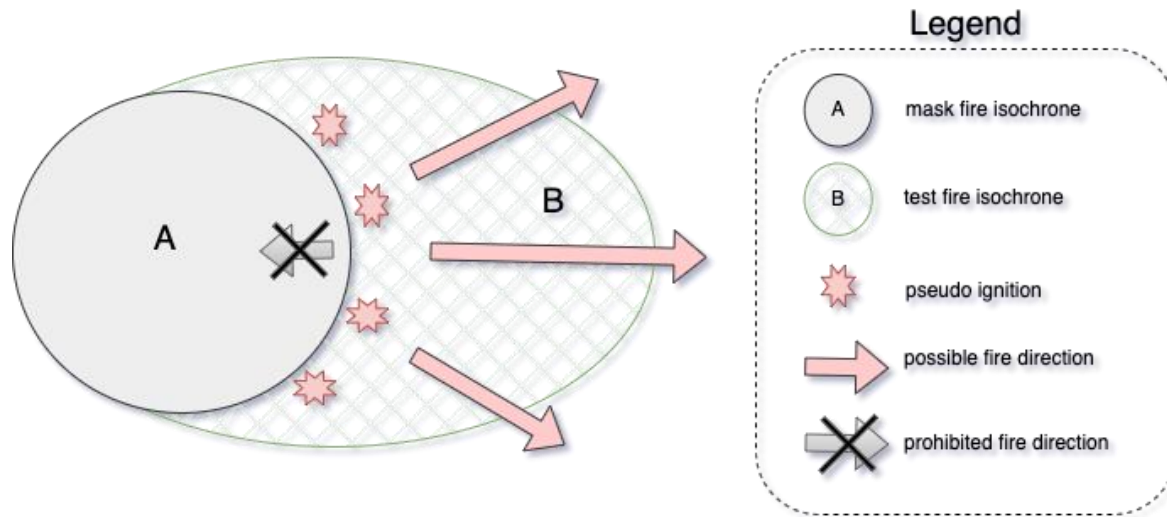
Figure 18: Mask of fire isochrone allows fire simulation to resume fire at the end of predecessor isochrone.

A is an ancestor of B and ended at t_A. Then t_A becomes the ignition points near the border between A and B. In addition, A can be configured as mask isochrone so that the fire cannot propagate back into isochrone A.

4.2.5   Terrain filter

Terran filter allows detection of lateral fire channelling which is a highly atypical fire channel caused by an interaction of horizontal vortex and a lee-slope fire (Figure 19). This type of fire channel is a rapid fire spread transverse to both synoptic wind and downslope wind (Sharples *et al.*, 2011, 2017; Sharples, McRae and Wilkes, 2012).
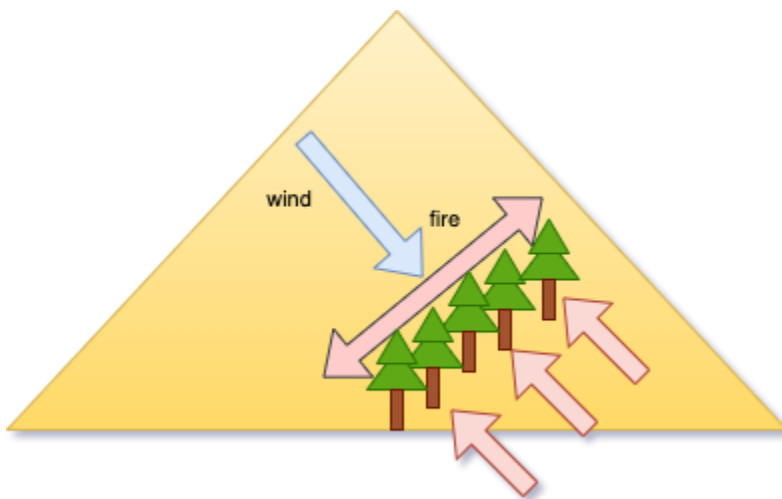
Figure 19: Fire spreads perpendicular to the wind coming in due to the disturbance of the forest.

There are several conditions for the fire channel to take place such as (1) slope angle is larger than a threshold; (2) the gap of terrain aspect and coming wind direction must be smaller than a threshold; (3) wind magnitude is greater than a threshold, (4) fuel type is forest and (5) fuel load is greater than a threshold (Table 24 and Figure 20).

Table 24: Conditions of lateral fire spread. It is necessary for the lateral fire spread to meet all the condition.

#	Condition	Note
1	$\gamma_s \geq \sigma$	γ_s is topographic slope and σ is a configured threshold whose default value is 10.5^o .
2	$\theta \leq \delta$	$\theta = \|\theta_w - \gamma_a\|$ where θ is the gap between the direction of coming wind and aspect of the slope. δ is a configured threshold whose default value is 40°
3	$V_w \geq \nu$	V_w is wind speed ($km \cdot h^{-1}$) and ν is a configured threshold whose default value is $20\ km \cdot h^{-1}$.
4	$veg \in forest$	Vegetation type is a member of forest.
5	$L_f \geq \lambda$	L_f is fuel load (tonne) and λ is a configured threshold whose default value is $15\ tonnes$.
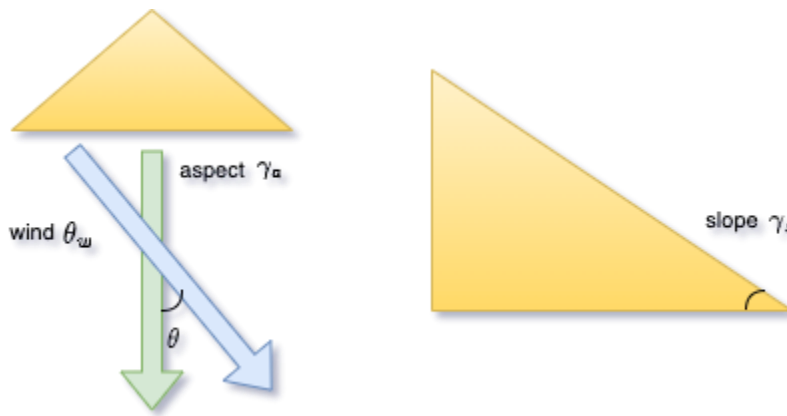
Figure 20: The gap between wind direction coming in and slope aspect exhibits on the left while right shows slope angle

These thresholds are configured. In addition, this type of the spread often produces spotting fire because a required fuel type is forest (Sharples, McRae and Wilkes, 2012; Sharples *et al.*, 2017). The spotting fire can be used by configuration (4.2.3).

4.2.6   Fire severity

Fire severity indicates cumulative damage on vegetation and is represented by normalised burnt ratio (dNBR) (Ndalila, Williamson and Bowman, 2018; Wentao and Yu, 2020). The average and type of dNBR are determined from fire severity data within a prediction grid (Figure 21).

Figure 21: Fire severity is calculated within a prediction grid.
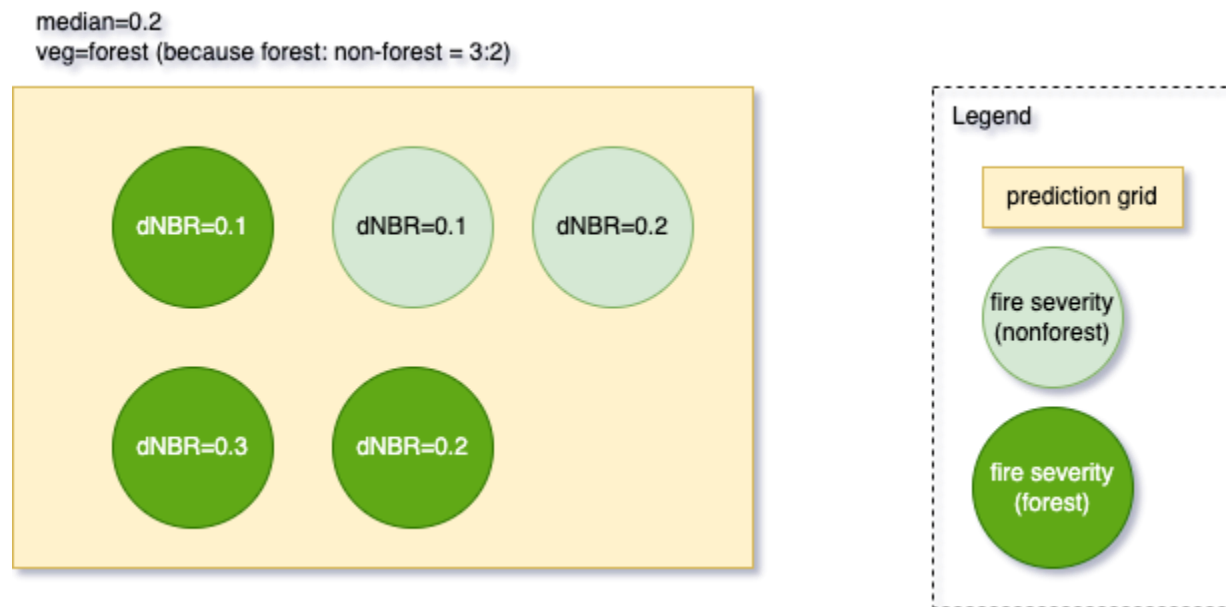
Vegetation type is also determined because severity class varies between forest and non-forest.

4.3   Ignition

An ignition point of bushfire is a centre of fire spreading and can be triggered by anthropogenic activities or natural phenomenon. There was only one ignition in previous system while Prototype 2 allows configuring multiple locations and times for ignitions. Ignition class manages ignitions by connecting not only ignition table but also lighting and ignition incident table in database (Figure 22)

Figure 22: Ignition class has various properties: ignited datetime, examined status, incident id, lightning id and version id as well as methods to generate ignition points both randomly and statically, the first ignition point, recent non-examined ignition points and future ignition points.

In depth, there are some attributes such as timestamp and several methods to retrieve and to register ignitions from either database tables or configuration files with such as all incidents in the observed area of fire (batchGenelateIgnitionByAllIncidens); all lightning hits in a fire isochrone from lightning table (batchGenerateIgnitionByAllLightnings); individual lighting hits from configuration file (batchGenerateIgnitionByLightningIDs); individual location and time from configuration file (batchGenerateIgnitionByLocationsAndTimes) and randomly selected lightning hits (generateIgnitionsAtRandomLightning).

In the following sections, random selection is described further in 4.3.1; mechanism of how to retrieve an ignition is addressed in 4.3.2; and multi-ignitions and propagation to surroundings are illustrated in 4.3.3.

4.3.1   Selection of random lighting hits

Randomly selection of lighting hits (generateIgnitionsAtRandomLightning) is described in this section. In general, an average of probability of fire ignition from a lightning hit is approximately, 0.006 at most (Dowdy and Mills, 2009; Bushfire CRC, 2011).

$$P = 0.006$$

Now the number of ignitions is calculated by multiplying the number of lightning hits with probability (P) as followings:

$$n_{ignition} = count(hit_{lightning}) \cdot P$$

where $n_{ignition}$ states the number of ignitions and $count(hit_{lightning})$ signifies the number of lightning hits. For example, in case that 100 lightning hits were recorded within a burnt area, then there are 0.6 ignitions by the general probability. However, studied fires have been confirmed that there was at least one ignition. Therefore, the number of ignitions is calculated in the prototype as following,

$$n_{ignition} = max(count(hit_{lightning}) \cdot P, 1)$$

Where the max function chooses the greatest value among the given values, which means at least one ignition is guaranteed. Note that this probability (P) is configurable in this prototype.

Now ignition points are selected using mathematical combination. The number of combinations ($n_{combination}$) is calculated as following:

$$n_{combination} = \binom{hit_{lightning}}{n_{ignition}}$$

All combinations, which are non-order-sensitive sets, can be retrieved by Python function, <u>combinations</u> (Python Software Foundation, 2020a). For example, if there are 500 hits and 3 ignitions are expected, then the number of combinations ($n_{combination}$) falls on 20,708,500, which can be calculated by $\binom{500}{3}$ as below.
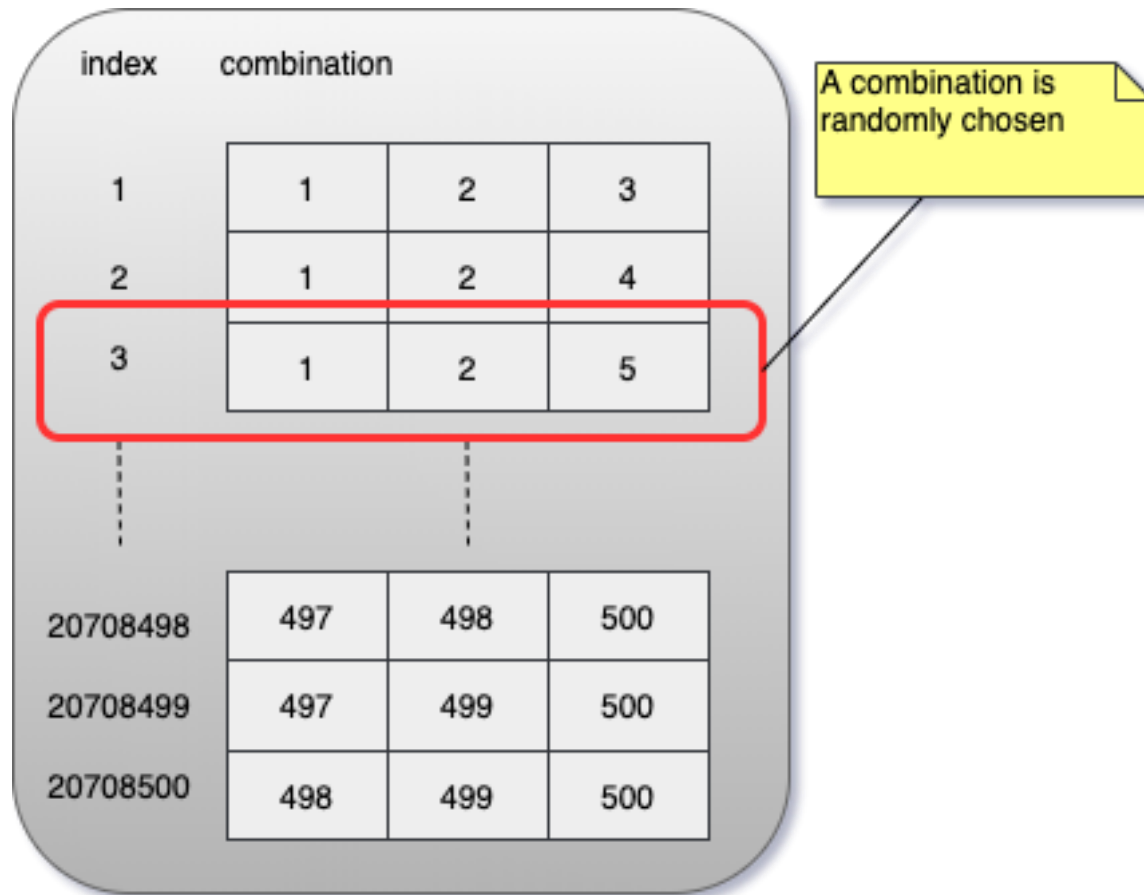
Figure 23: Among the generated combinations, a pattern is randomly chosen.

Then a combination is randomly chosen by a random function in Python (Python Software Foundation, 2020b). In the example above, the row with the index 3 is chosen, which contains lightning 1, 2, and 5 as ignition points.

4.3.2   Retrieval of ignitions

There are three methods to retrieve ignition points by Ignition class. Once ignition points are generated either randomly or statically, the earliest ignition is retrieved as a starting point of prediction regardless of examined status using the method, *getFirstIgnition* in Figure 24 (1). While a fire propagation is being executed, a cursor seeks recent ignitions which have not been examined yet through the method, *getRecentIgnitions* in Figure 24 (2). If there are any unexamined ignitions, these are considered as new ignitions if the area **has not been burnt** yet. When the fire propagation has already been predicted with past ignitions, the system tries to find any future ignitions by the method, *getFutureIgnitions* in Figure 24 (3). If there are any future ignitions, then prediction resumes from these ignition points. In either case, the ignition status needs to be changed to examined=True, if it is examined in fire propagation.

(1) Ignitio.getFirstIgnition(t)

Ignition table		
version	**datetime**	**examined**
1	t_1	True/False
1	t_2	False
1	t_3	False
1	t_4	False
1	t_5	False

(2) Ignitio.getRecentIgnitions(t, version_id)

Ignition table		
version	**datetime**	**examined**
1	t_1	True
1	t_2	False
1	t_3	False
1	t_4	False
1	t_5	False

(3) Ignitio.getFutureIgnitions(t, version_id)

Ignition table		
version	**datetime**	**examined**
1	t_1	True
1	t_2	True
1	t_3	True
1	t_4	False
1	t_5	False

Figure 24: How Ignition class methods, such as (1) the first ignition point, (2) recent non-examined ignition points and (3) ignition points in the future, retrieve ignition points.

4.3.3   Parallel fire propagation and re-ignition

Multiple ignitions allow to fire propagate simultaneously. For instance, there are some ignition points which ignite in different time. Each ignition keeps its own elapse for fire spreading. Although these ignition points simulate igniting as registered, the elapse can vary because the elapse is a calculation result of rate of fire spread on each fire model (Figure 25).
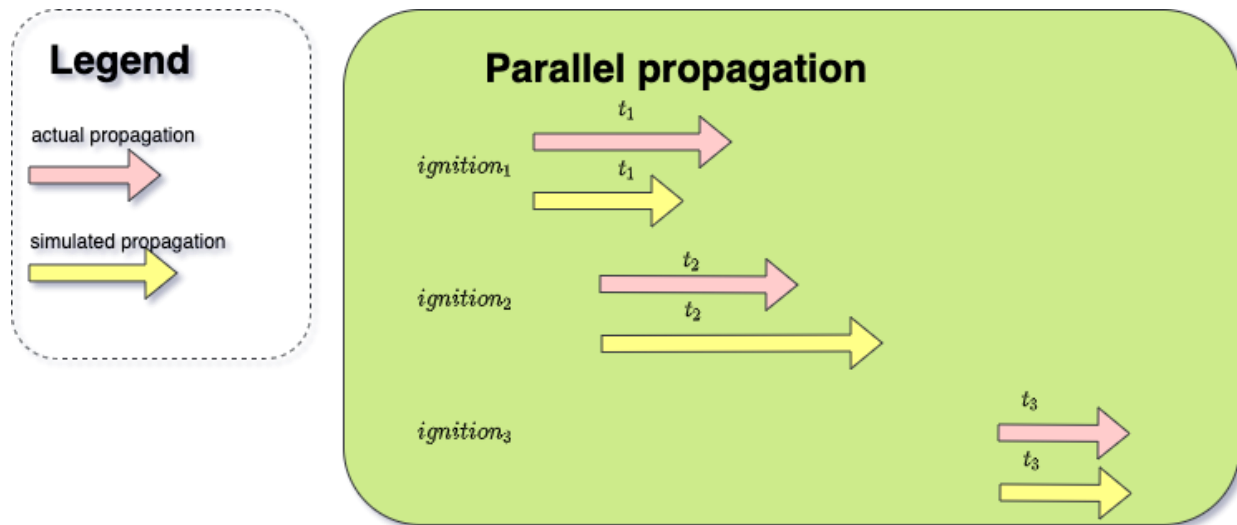
Figure 25: Parallel fire propagation allows fires spreading by their own paces simultaneously.

In addition, the location which failed to propagate, can be reignited if the location is registered with another incident (Figure 26). For instance, there are two incidents registered, t_1 and t_5 in ignition point 1. Firstly, t_1 failed to propagate fire at ignition point 1. After for a while, the scheduled t_5 is triggered. Because t_5 is under favourable condition to propagate the fire, the fire keeps propagating at the same location this time. On the other hand, t_6 cannot propagate fire at ignition point 2 because t_2 has already burnt surrounding areas entirely.
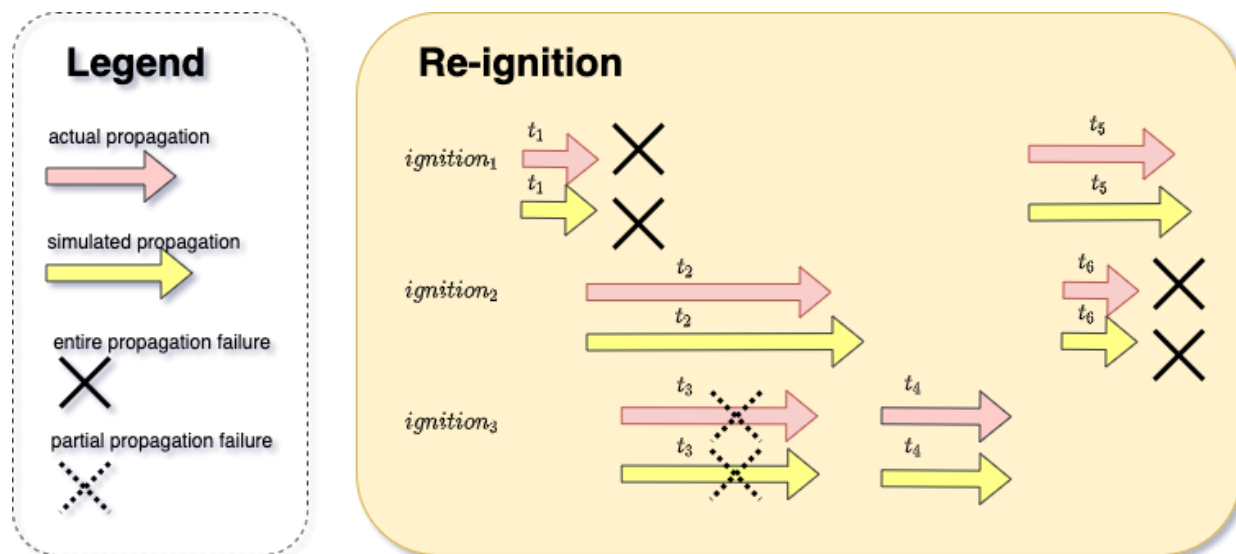
Figure 26: A fire can ignite again in the same location when it failed to propagate previously if another fire incident is registered.

If there were some unburnt areas around ignition point 3 and condition was favourable to catch a fire for t_4, t_4 could have caught the fire on rests of neighbours in turn.
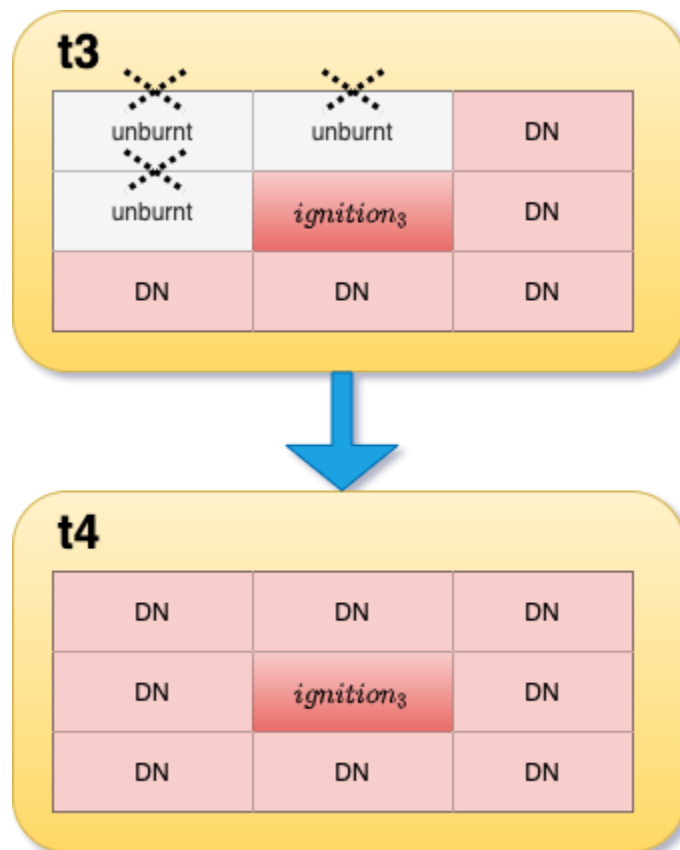
Figure 27: Mechanism of re-ignition on partial unburnt neighbours

4.4   Wind Component

Wind magnitude is one of variables to calculate a rate of spreading fire (ROS) in fire models (See section 5). There are some processes to ingest wind magnitude and these steps are illustrated in this section.

4.4.1   Zonal and meridian wind

U-V component is a format of crude wind in BARRA. It is necessary to compute this magnitude before the crude data are resampled to be topographically sensitive by Windninja (3.3). U components indicate zonal or latitudinal, i.e., easterly or westerly, while v components show meridional or longitudinal, i.e., northerly or southerly as seen below (Holloway, 1967; American Meteorological Society, 2020).
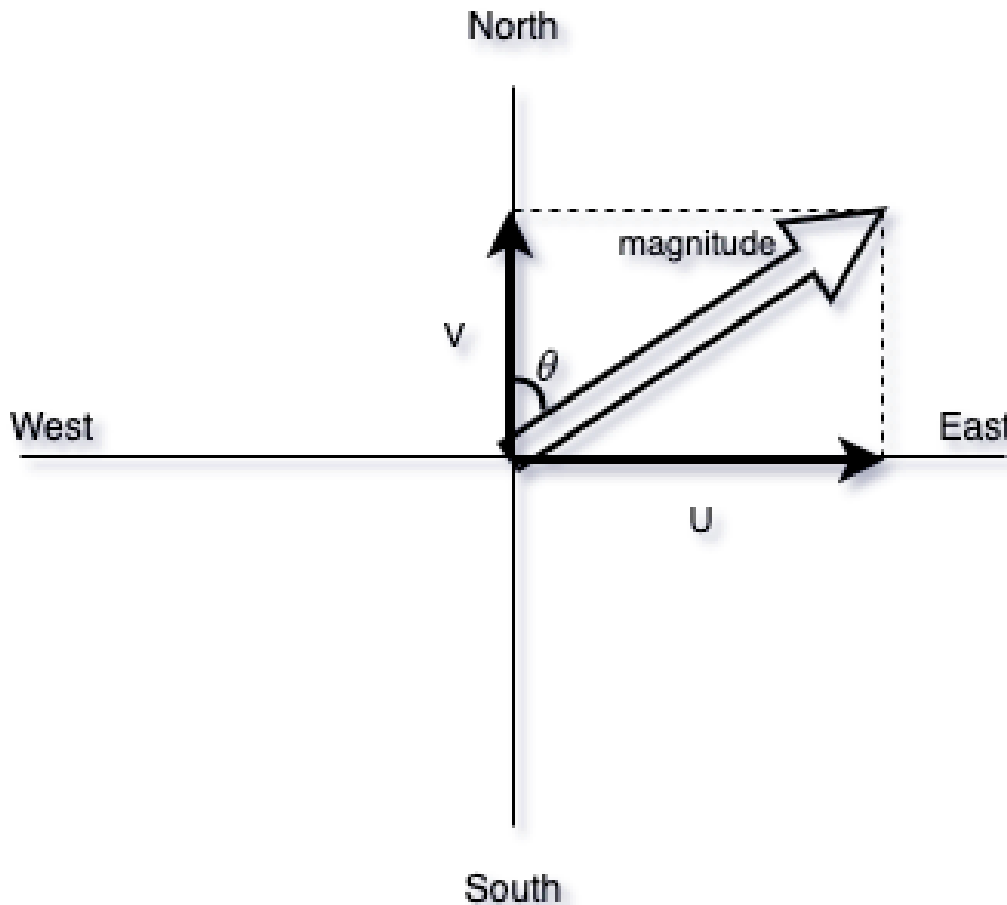
Figure 28: U-V wind components: a hypotenuse shows wind magnitude and θ does a toward direction of the wind adapted from (Holloway, 1967)

Wind magnitude is calculated as hypotenuse with Pythagorean theory as following,

$$hypotenuse =| \sqrt{(opposite^2 + adjacent^2)} \ |$$

Hence, the wind magnitude is as following:

$$windmagnitude =| \sqrt{(u^2 + v^2)} \ |$$

With regard to the angle of wind direction (θ), it is possible to obtain it using arc tangent.

$$\theta = arctan\left(\frac{opposite}{adjacent}\right)$$

However, it is necessary to be cautious about the baseline because the angle is against not horizontal but vertical axis. Therefore, the equation is as following:

$$\theta = arctan\left(\frac{u}{v}\right)$$

Note that the wind direction indicates **outflow** and measurement unit for the produced wind magnitude is ms^{-1} in BARRA data (The Australasian Fire and Emergency Service Authorities Council (AFAC), 2020).

4.4.2   Inversion of wind

There are a couple opportunities to invert wind direction. Namely, inversion of wind direction is required for WindNinja when input data are outflow because this tool ingests inflow (Firelab, 2020). In addition, this inflow needs to invert to outflow again to estimate alignment of fire as mentioned in section 5.12.

The wind direction is basically converted by adding 180 °. However, it is also necessary to subtract 360 ° if the total angle surpasses 360 ° as below (Ozaki, Aryal and Fox-Hughes, 2019).

Inversion of direction of Wind to outward
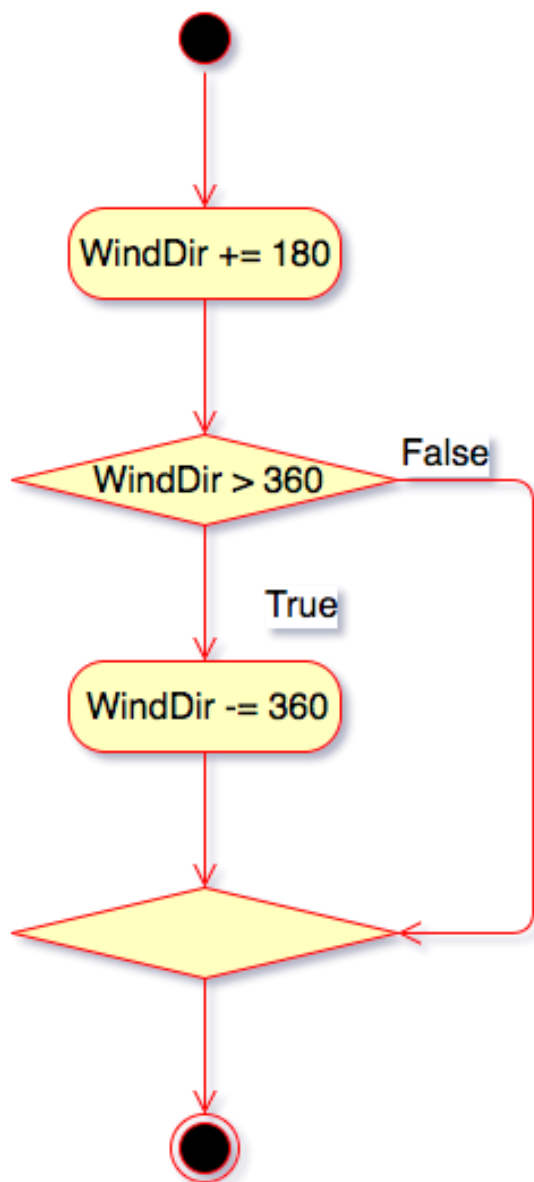
Figure 29: Inversion of wind direction cited from (Ozaki, Aryal and Fox-Hughes, 2019)

4.5　Precipitation for the last 48 hours

Precipitation is ingested in Buttongralss moorland fire model (5.4). The total precipitation can be calculated from precipitation record in raster table as below.
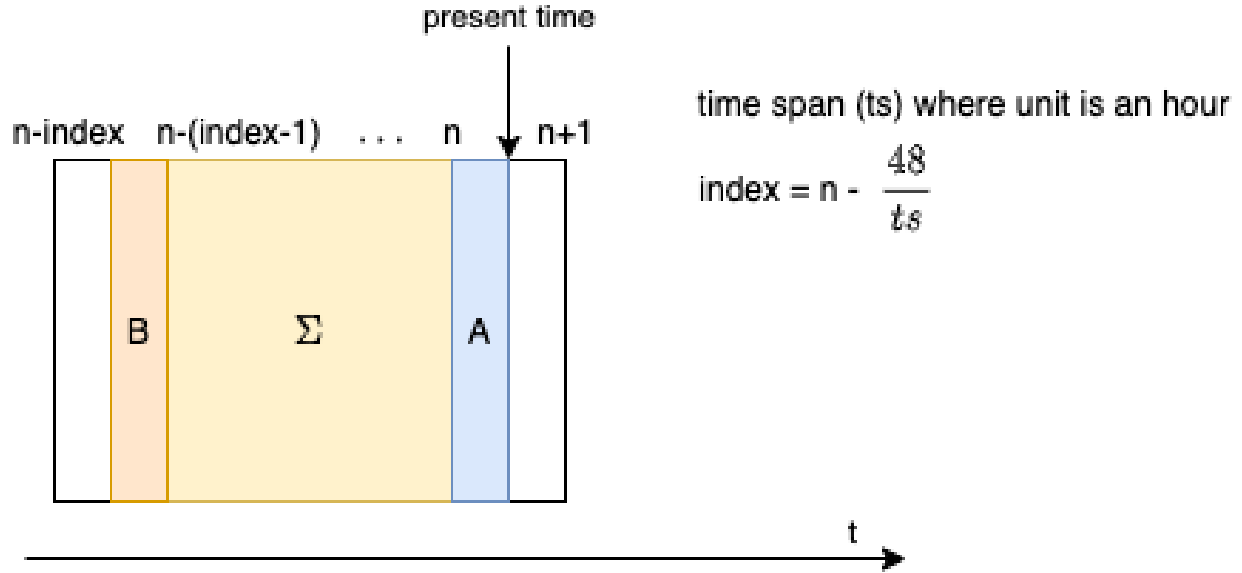
Figure 30: Total precipitation in the last 48 hours

Firstly, time interval (dim_time) between bands are calculated from present time. Unit of timespan (ts) is hour. For instance, if a cursor is between band n and band n+1, ts is as following.

$$ts = band[n+1].dim\_time - band[n].dim\_time.$$

Then the remnant from the closest time band is calculated. For example, if current time band n is 12:00:00, time span is 1 hour and the present time is 12:12:00, the remnant is 12 minutes, that is 0.2 hours. Thirdly, the remnant value, i,e, precipitation, is computed by multiplying with the average of two bands.

$$Value\ A = \frac{(band[n].value + band[n+1].value)}{2} \cdot \frac{Remnant}{timespan}$$

The remnant for the youngest time band, which indicates 48 hours, is calculated.

$$head = n - \frac{48}{ts}$$

$$valueB = \frac{(band[head].value + band[head+1].value)}{2} \cdot (1 - Remannt)$$

Then, total is calculated by adding the middle summation of values and remnants.

$$total = valueA + \sum_{i=head+1}^{n} (band[i].value) + valueB$$

if temporal data are depleted, i.e. head-min<0, the youngest bands are repeatedly used.

$$total = valueA + \sum_{i=min+1}^{n} (band[i].value) + (\Delta) \cdot min.value$$

Where $\Delta = (min - head + (1 - Remnant))$

4.6   Time since last precipitation

Last precipitation is one of variables in Buttongrass moorland fire model (5.4). It can be obtained by descending precipitation bands and finding non-zero value in the bands until a cursor moves from present time to the youngest among bands as seen below.
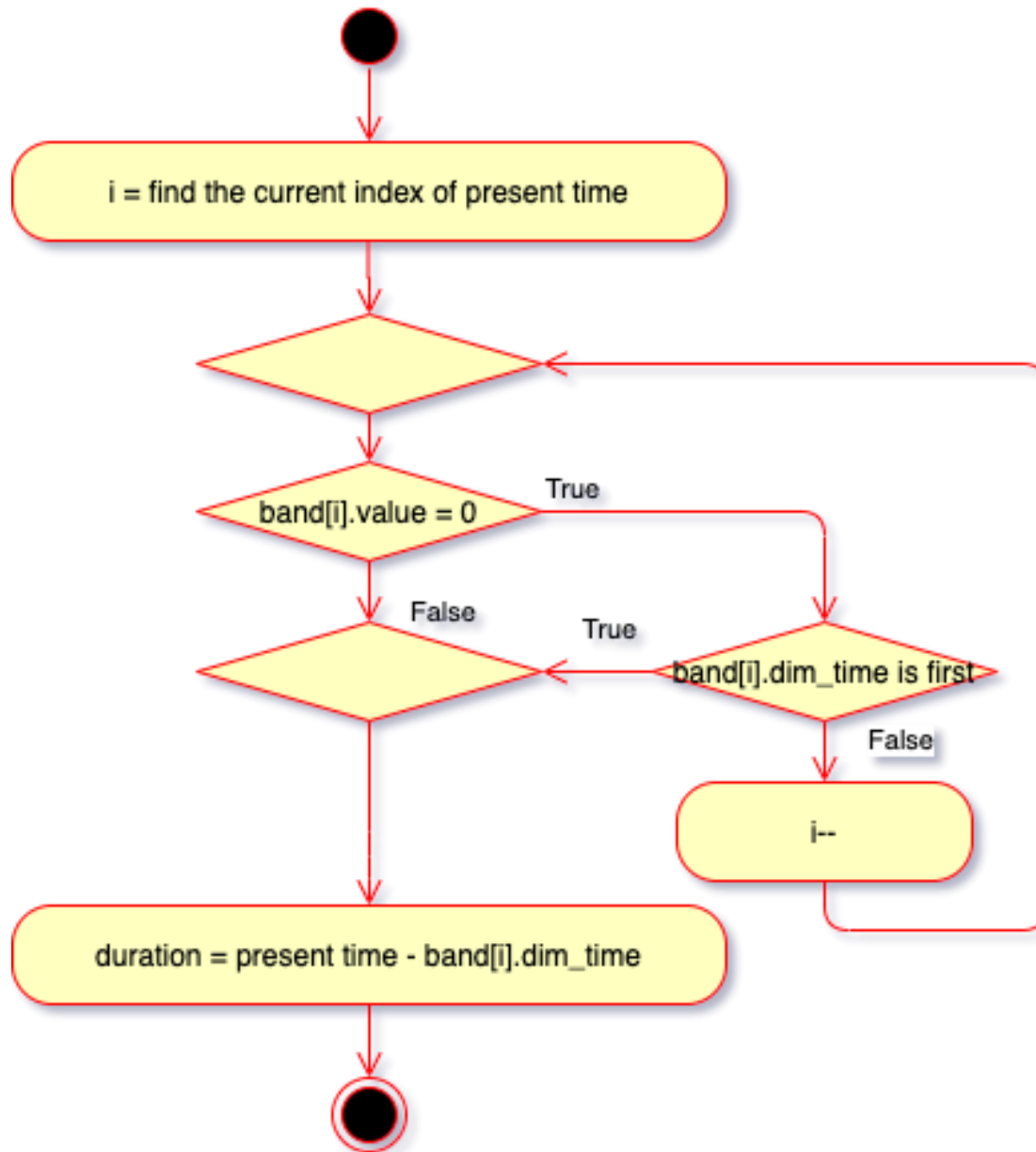
Figure 31: Last precipitation = present time – non-zero band's time

4.7   Unit conversion

There are some functions to convert unit in Prototype 2.

4.7.1 Conversion of Kelvin and Celsius

Kelvin can be converted to Celsius by subtracting 273.15. That is, Celsius = Kelvin − 273.15.

4.7.2 Conversion of kilograms per square metres for millimetres.

Since 1 kilogram of water is approximately a litre, 0.001 m^3, the height of the precipitation per m^2 is equivalent to 1 millimetre.

$$\frac{1kg}{m^2} = \frac{0.001m^3}{m^2} = 0.001\, m = 1\, mm$$

4.8 Class diagram of fire models

There are eight fire models in this prototype as meticulously explained in section 5. Overall diagram is illustrated in this section in advance.

There are some common features shared by multiple fire models. The below figure shows conceptual hierarchy of fire model classes.
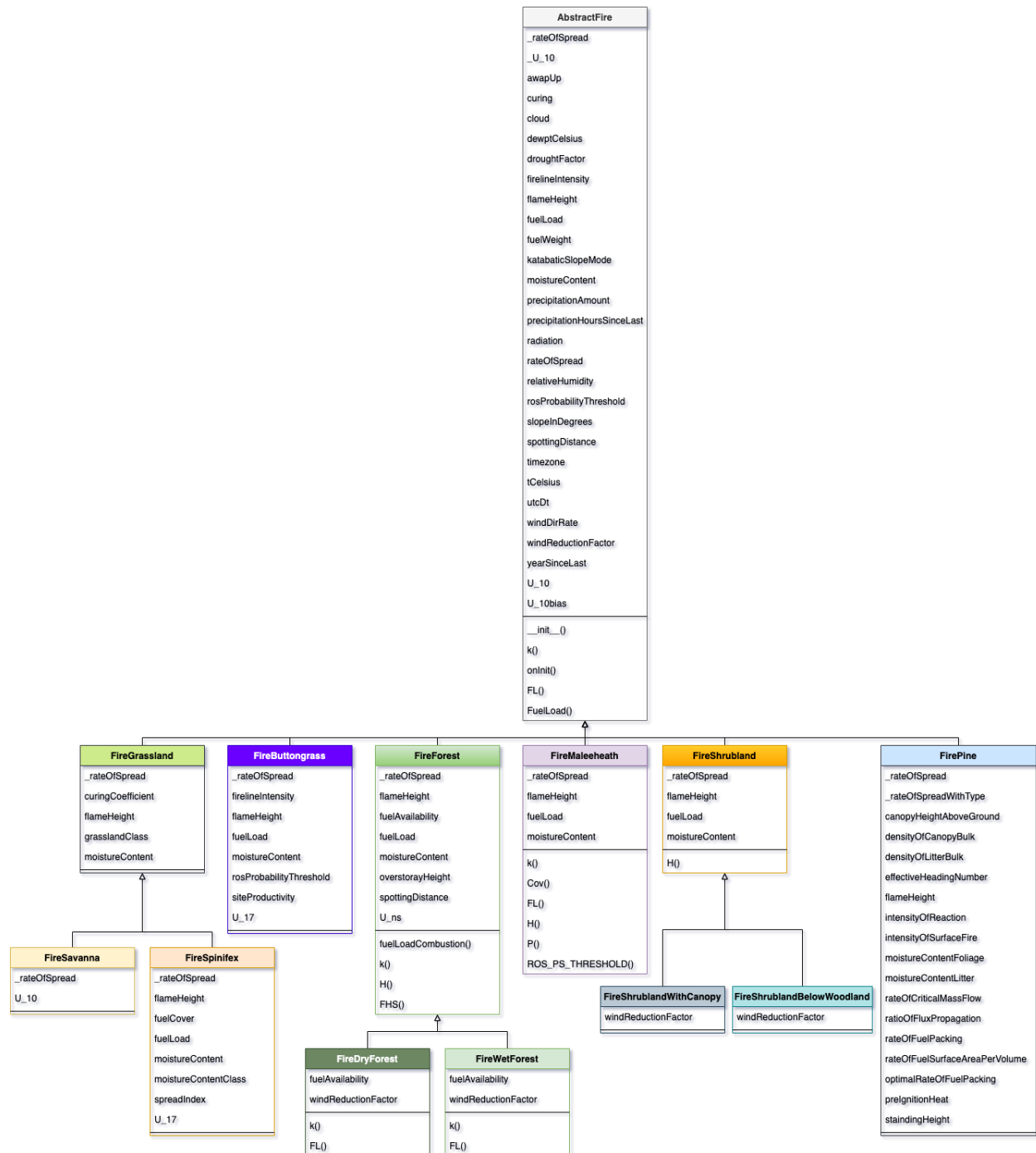
Figure 32: UML class diagrams for fire models

For instance, U_10 indicates wind magnitude at 10 metres height and ingested by all concrete models. Therefore, U_10 belongs to *AbstractFire* class so that inherited classes can share it according to Object-Oriented Programming (OOP). Because child classes either inherit or override behaviours from their parent class, this concept is useful to economise and maintain programming codes.

5 Fire models

Fire models and their corresponding functions such as slope, measurement of distance, adjustment of wind magnitude for its direction, sigmoid function, as well as difference from previous prototype, are addressed in this section. Prototype 2 comprises of eight existing fire models which will be integrated in Research Prototype (Table 25 and Figure 33).

Table 25: Fire Danger Rating Models proposed by Research Prototype project cited from (The Australasian Fire and Emergency Service Authorities Council (AFAC), 2020)

#	Fire Behaviour Model	Short Name	Reference	Fuel Type
1	CSIRO Grassland fire spread model	Grassland	(Cheney, Gould and Catchpole, 1998; Miguel G Cruz *et al.*, 2015)	Continuous grasslands
2	CSIRO Grassland for northern Australia model	Savanna	(Cheney, Gould and Catchpole, 1998; Miguel G Cruz *et al.*, 2015)	Grassy woodlands and open forests
3	Desert spinifex model	Spinifex	(Burrows, Gill and Sharples, 2018)	Hummock grasslands
4	Buttongrass moorlands model	Buttongrass	(Marsden-Smedley and Catchpole, 1995b)	Buttongrass moorlands
5	Dry Eucalypt Forest Fire Model (DEFFM or "Vesta")	Forest	(Cheney *et al.*, 2012)	Shrubby dry eucalypt forests
6	Mallee heath model	Mallee heath	(Cruz *et al.*, 2013)	Semi-arid mallee heath
7	Heathland model	Shrubland	(Anderson *et al.*, 2015)	Temperate shrublands
8	Adjusted Pine model	Pine	Cruz (pers. Comm.)	Pine plantations
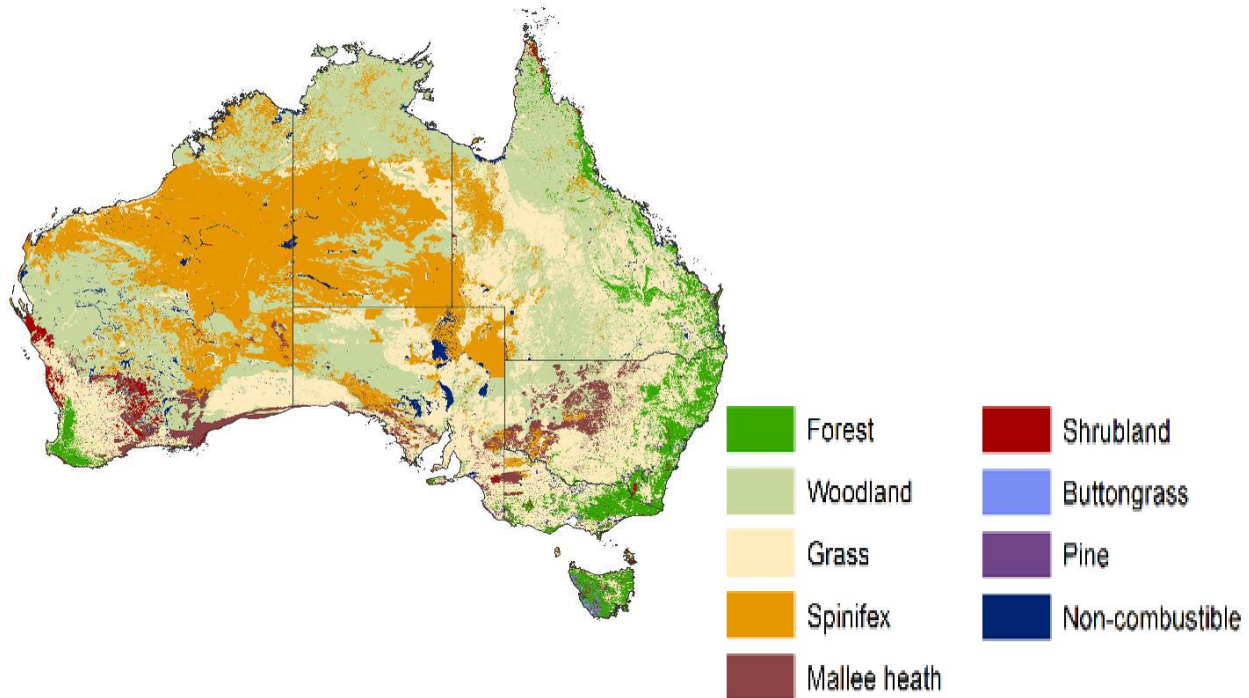
Figure 33: Distribution of major fuel types in Australia adapted from (The Australasian Fire and Emergency Service Authorities Council (AFAC), 2020)

A fire model is selected in accordance with vegetation type, which can be retrieved from various datasets depending on a jurisdiction. Therefore, it is necessary to match fuel model with local vegetation data. Selection of fire models and local vegetation is described in each study area. In this section, each fire model with general fuel type is described.

5.1 CSIRO grassland fire spread model (Grassland) (Anderson *et al.*, 2015)

CSIRO grassland fire spread model is called grassland model and designed to predict a fire spread in homogeneous grassland with measurement of wind speed at 10 metres high above the ground, dead fuel moisture content, which is defined when fuel moisture content is below 30 % (Aguado *et al.*, 2007), and curing or greenness of vegetation (Cheney, Gould and Catchpole, 1998; Allan *et al.*, 2003; The Australasian Fire and Emergency Service Authorities Council (AFAC), 2020). In this section, components of this fire model, such as type, fuel load, the fire rate of spread (ROS), fire moisture content (θMC), curing coefficient ($\Theta curing$), fuel intensity and fuel height are addressed.

5.1.1 Three types of grassland model

There are three sub-models in this grassland fire model: natural, grazed and eaten out grassland models depending on the fuel loads (Table 26).

Table 26: Classes of grassland by fuel loads (5.1.2) as a threshold: natural, grazed and eaten out

#	Grassland classes	Fuel load (tonnes per hectares)	Description
1	Natural grassland	≥ 6	Undistributed or un-grazed
2	Grazed grassland	> 3 and < 6	cut

3	Eaten out grassland	≤ 3	e.g. low wetland (The Australasian Fire and Emergency Service Authorities Council (AFAC), 2020) p119

Note that default values of fuel load are illustrated in the below section.

5.1.2 Fuel Load

This prototype employs default values of fuel loads for this fire model depending on regions by following that the Research Prototype utilises these values (The Australasian Fire and Emergency Service Authorities Council (AFAC), 2020). The default fuel loads in tonnes per hectare are clustered in either 1.5, 3.0, 4.5 and 6.0 depending on climate zones such as the desert, grassland, subtropical & temperate, and equatorial & tropical zone respectively as below. For example, East coastal areas have default fuel loads as 4.5 tonnes per hectare.

Figure 34: Guideline for fuel load (tonnes per hectare): desert (1.5), grassland (3.0), subtropical & temperate (4.5), and equatorial & tropical (6.0) cited from (The Australasian Fire and Emergency Service Authorities Council (AFAC), 2020)

5.1.3 Fire rate of spread (ROS)

There are separate equations of fire rate of spread (ROS) in three different classes of grassland models. Wind speed is one of important variables in ROS to establish a condition of equation and this speed is considered at the height of 10 meters above the ground.

In each grassland class, there are two equations for ROS. The first equation is for when wind speed is less than 5 km per hour while another is with an exponential function when the wind speed at 10 m above 5 km per hour. Three classes and their equations are as following.

Natural grassland model (Class 1):

When a 10 m wind speed < 5 kmh^{-1},

$$\text{ROS}_{\text{natural}} = (0.054 + 0.269 \cdot \text{U}_{10}) \cdot \Phi_{\text{MC}} \cdot \Phi_{\text{curing}} \times 1000$$

When a 10 m wind speed ≥ 5mh^{-1},

$$\text{ROS}_{\text{natural}} = (1.4 + 0.838 \cdot (\text{U}_{10} - 5)^{0.844}) \cdot \Phi_{\text{MC}} \cdot \Phi_{\text{curing}} \times 1000$$

Notations are in Table 27:

Table 27: Notation of grassland class 1

Notation	Description
ROS	Rate of spread in m h^{-1}. Note that it therefore is necessary to divided by 1000 if km h^{-1} is required as a unit.
U_{10}	10 m wind speed (km h^{-1})
Φ_{MC}	Fuel moisture coefficient (See 5.1.4)
Φ_{curing}	Curing coefficient (See 5.1.5)

Grazed or cut grassland model (Class 2):

When a 10 m wind speed < 5 kmh^{-1},

$$\text{ROS}_{\text{grazed}} = (0.054 + 0.209 \cdot \text{U}_{10}) \cdot \Phi_{\text{MC}} \cdot \Phi_{\text{curing}} \times 1000$$

When a 10 m wind speed ≥ 5mh^{-1},

$$\text{ROS}_{\text{grazed}} = (1.1 + 0.715 \cdot (\text{U}_{10} - 5)^{0.844}) \cdot \Phi_{\text{MC}} \cdot \Phi_{\text{curing}} \times 1000$$

Notation is described above.

Eaten out grassland model (Class 3):

When a 10 m wind speed < 5 kmh^{-1},

$$\text{ROS}_{\text{eatenout}} = \frac{1}{2} \cdot (0.054 + 0.209 \cdot \text{U}_{10}) \cdot \Phi_{\text{MC}} \cdot \Phi_{\text{curing}} \times 1000$$

When a 10 m wind speed ≥ 5mh^{-1},

$$\text{ROS}_{\text{eatenout}} = (0.55 + 0.357 \cdot (\text{U}_{10} - 5)^{0.844}) \cdot \Phi_{\text{MC}} \cdot \Phi_{\text{curing}} \times 1000$$

Although the case in which the eaten out ROS at wind speed 10 m is less than 5 km h^{-1}, has not been examined yet, spread speed is attributed as **half** of that in $\text{ROS}_{\text{natural}}$ or $\text{ROS}_{\text{grazed}}$ (Cheney, Gould and Catchpole, 1998). Notation is described above.

5.1.4   Fuel moisture content (Φ_{MC})

Fuel Moisture Content (Φ_{MC}) is part of variables for ROS and ingests dead fuel moisture content (MC). Equation of MC between 2 and 24 % is as following (The Australasian Fire and Emergency Service Authorities Council (AFAC), 2022):

$$MC = 9.58 - 0.205 \cdot T + 0.138 \cdot RH$$

Now MC is conditionally substituted in Φ_{MC} (Table 28).

When MC < 12 %,

$$\Phi_{MC} = exp(-0.108 \cdot MC)$$

When MC > 12 % and $U_{10} < 10 \ km \ h^{-1}$,

$$\Phi_{MC} = 0.684 - 0.0342 \cdot MC$$

When MC > 12 % and $U_{10} > 10 \ km \ h^{-1}$,

$$\Phi_{MC} = 0.547 - 0.0228 \cdot MC$$

Table 28: Summary of Equations and conditions of MC

MC	U_{10}	Equation of Φ_{MC}
< 12	-	$\Phi_{MC} = exp(-0.108 \cdot MC)$
> 12	$< 10 \ km \ h^{-1}$	$\Phi_{MC} = 0.684 - 0.0342 \cdot MC$
> 12	$> 10 \ km \ h^{-1}$	$\Phi_{MC} = 0.547 - 0.0228 \cdot MC$

Notations are described below.

Table 29: Notation of variables for MC

Notation	Description
MC	Moisture content of dead grass
T	Temperature ($C \ °$)
RH	Relative humidity (%)
U_{10}	10 m wind speed (km h^{-1})

5.1.5   Curing coefficient (Φ_{curing})

Curing coefficient (Φ_{curing}) signifies percentage (%) of grass curing and is one of variables for rate for fire spread (ROS). The minimum Φ_{curing} is 21 % to have an impact on ROS (Miguel G Cruz *et al.*, 2015). That is, when the curing ≥ 21,

$$\Phi_{curing} = \frac{1.036}{1+103.989 \cdot exp(-0.0996 \cdot (curing-20))}$$

Otherwise,

$$\Phi_{curing} = 0$$

5.1.6 Fireline intensity

Fireline Intensity is calculated as following (The Australasian Fire and Emergency Service Authorities Council (AFAC), 2020):

$$I_B = h \cdot w \cdot ROS$$

Table 30: Notation of variables for fire intensity

Notation	Description
I_B	Fireline intensity (kWm^{-1})
h	Heat yield constant as 18,600 $kJkg^{-1}$
w	Fuel load in kg m^{-2} Note that it is necessary to multiply 0.1 to convert $FuelLoad_{combustion}$ from $\frac{tonnes}{ha}$ to $\frac{kg}{m^2}$
ROS	Rate of spread in ms^{-1} ($1ms^{-1} = 3600\ mh^{-1}$)

5.1.7 Flame height

There are two equations for flame height depending on grassland class. The first equation is for natural (class 1) grasslands.

$$F_{height} = 2.66 \cdot \left(\frac{ROS}{3600}\right)^{0.295}$$

The second is for grazed (class 2) and eaten out (class 3) grasslands.

$$F_{height} = 1.12 \cdot \left(\frac{ROS}{3600}\right)^{0.295}$$

(The Australasian Fire and Emergency Service Authorities Council (AFAC), 2020)

5.2 CSIRO for northern Australia model (Savanna)

CSRIO grassland fire spread model (Grassland) addressed in section (5.1) is adapted to model fire behaviour in woodland-like vegetation by multiplying a coefficient with its rate of spread of fire (ROS). This adapted model is called CSIRO for northern Australia model and is also as known as Savanna. The condition for the ROS coefficient is wind speed. The rate of spread of fire can also be reduced by vegetation type since the wind speed can be mitigated by the structure of the heterogeneous vegetation mixed with grasses and trees. The wind speed at the height between 2 and 10 meters above the ground and a rate of spread of fire after reduction are below (The Australasian Fire and Emergency Service Authorities Council (AFAC), 2020).

Table 31: Ratio of wind speed and spread of fire in open grassland, short tree forest and tall forest adapted from (The Australasian Fire and Emergency Service Authorities Council (AFAC), 2020)

Type of vegetation	ratio of wind speed above the ground between 2 and 10 m	ratio of ROS
Open grasslands	.8	1.0
Woodlands (5-7 m height)	.6	.5
Open forest (10-15 m height)	.42	.3

5.3 Desert spinifex model (Spinifex)

Spinifex model names after Spinifex, the perennial grass, which is mainly pervasive in remote and arid landscapes. It often incurs severe bushfires (Burrows, Gill and Sharples, 2018).

5.3.1 Fire rate of spread (ROS)

There are a few steps in a desert spinifex model to calculate a fire rate of spread (ROS). Firstly, a spread index (SI) is calculated. Then the probability of spread (P), which signifies continuity of fuels, is determined by ingesting SI as an independent variable of logistic sigmoid function. Finally, the ROS is computed using SI (Burrows, Gill and Sharples, 2018).

Spread Index (SI) is computed as following:

$$SI = 0.412 \cdot U_{1.7} + 0.311 \cdot c - 0.676 \cdot m - 4.073$$

Note that the above equation is newer version than that in the Research Prototype as advised in the notation of the prototype.

Now probability (P) is calculated using sigmoid function (see section 5.13) to normalise the probability between 0 and 1.

$$P = \frac{1}{(1 + exp(-SI))}$$

If P is greater than 0.5 then the fire rate of spread (ROS) is calculated,

$$ROS = 40.982 \cdot \frac{U_{1.7}^{1.399} \cdot C^{1.201}}{m^{1.699}}$$

Where

$$U_{1.7} = 0.305 \cdot U_{10}$$

If P is equal to or less than 0.5, zero is assigned to ROS.

(Burrows, Gill and Sharples, 2018)

Table 32: Notation of desert spinifex ROS

Notation	Description
SI	Spread index indicates likelihood of fire spread. Likely to spread when SI is greater than 0
P	Likelihood of fire spread and ranges between 0 and 1. Likely to spread when SI is greater than 0.5.
ROS	Rate of fire spread in (m h^{-1}).
U_{10}	Wind speed at the height of 10 m above the ground in (km h^{-1}).
$U_{1.7}$	Wind speed at the height of 1.7 m above the ground in (km h^{-1}).
c	Fuel coverage in %. Spinifex regardless of dead or alive, and any other vegetation which height is $\leq$ 1.5 m. See 5.3.3.
m	Mean fuel moisture content in clump profile of spinifex (%). See 5.3.4.

5.3.2 Fuel load (FL_{ns})

Fuel load (FL_{ns}) is a variable to calculate flame height and its equation follows the AFAC Technical Guide as below (The Australasian Fire and Emergency Service Authorities Council (AFAC), 2022):

If productivity =1

$$FL_{ns} = 2.046 \cdot TSF^{0.42}$$

else if productivity>1

$$FL_{ns} =$$

Table 33: Constant for fuel load

TSF (years)	Productivity=2		Productivity=3	
	Spinifex=Open	Spinifex=Woodland	Spinifex=Open	Spinifex=Woodland
<1	1.28	2.01	3.58	3.78
1–2	2.39	3.4	5.25	5.11
2–3	3.36	4.38	6.73	5.95
3–4	4.21	5.06	8.05	6.49
4–5	4.96	5.53	9.21	6.84
>5	5.6	5.86	13.34	7.38

Table 34: Notation of fuel load

Notation	Description
FL_{ns}	Fuel load in (tonnes ha^{-1})
TSF	Time since fire in years
Productivity	In configuration for now $\in$ [1: low, 2: medium, 3: high]
Spinifex type	In configuration for now $\in$ [0: Open, 1: Woodland]

5.3.3   Fuel cover (c)

Fuel cover (c) is a variable to calculate ROS and its equation follows the AFAC Technical Guide as below (The Australasian Fire and Emergency Service Authorities Council (AFAC), 2022):

If productivity=1

$$c = 26.20 \cdot TSF^{0.227}$$

If productivity>1

$$c = 39.3 \cdot TSF^{0.227}$$

Table 35: Notation of fuel cover

Notation	Description
c	Fuel cover in (%)
TSF	Time since fire in years
Productivity	In configuration for now $\in$ [1: low, 2: medium, 3: high]

5.3.4 Fuel moisture content (m)

Fuel moisture content (m) is a variable to calculate ROS. There are five classes in fuel moisture content dependent on the age of spinifex fuels as below.

Table 36: Moisture class with the age of spinifex fuels adapted from (Burrows, Liddlelow and Ward, 2014; The Australasian Fire and Emergency Service Authorities Council (AFAC), 2022)

Class	Age (time since fire in years)	Cover spinifex live (%)	Cover spinifex dead (%)
1	$TSF < 3$	15-30	0
2	$3 \leq TSF < 11$	30-40	<5
3	$11 \leq TSF < 16$	35-45	5-10
4	$16 \leq TSF < 21$	40-50	10-15
5	$21 \leq TSF$	30-40	30-40

The details of each class are addressed in the following sections.

5.3.4.1 Class 1 moisture content

Moisture content for class 1 is the same as the one for grassland fire spread model. See section 5.1.4.

5.3.4.2 Class 2 moisture content

There are two different equations for class 2 in original papers: Research Prototype and Burrows et al (2014). This document follows the Research Prototype, which includes the equation conceived by the Burrows (Burrows, Liddlelow and Ward, 2014; The Australasian Fire and Emergency Service Authorities Council (AFAC), 2020).

$$MC_{class2} = 40 \cdot AWAP_{uf} + 13$$

Table 37: Notation of moisture content

Notation	Description
MC_{classx}	Moisture content for class X
$AWAP_{uf}$	Relative monthly soil moisture [upper layer] (%) obtained from http://www.csiro.au/awap/ (Raupach *et al.*, 2009, 2012; CSIRO AWAP Team, 2014). Detail of the data is described in 3.1.2.5.

5.3.4.3 Class 3 moisture content

Class 3 moisture content is as following.

$$\text{threshold} = MC_{class2} - \left(\frac{1}{0.03 \cdot RH}\right) \cdot 1.5$$

$$MC_{class3} = 0.14, if\ threshold \leq 0.14$$

$$MC_{class3} = \text{threshold, otherwise}$$

Table 38: Notation of moisture content

Notation	Description
MC_{classx}	Moisture content for class X where x indicates the number of classes

RH	Relative humidity (%)

5.3.4.4 Class 4 moisture content

Class 4 moisture content is as following.

$$\text{threshold} = MC_{class2} - \left(\frac{1}{0.03 \cdot RH}\right) \cdot 2.5$$

$$MC_{class4} = 0.13, if\ threshold\ \leq 0.13$$

$$MC_{class4} = \text{threshold, otherwise}$$

Table 39: Notation of moisture content

Notation	Description
MC_{classx}	Moisture content for class X where x indicates the number of classes
RH	Relative humidity (%)

5.3.4.5 Class 5 moisture content

Class 5 moisture content is as following.

$$\text{threshold} = MC_{class2} - \left(\frac{1}{0.03 \cdot RH}\right) \cdot 3.5$$

$$MC_{class5} = 0.12, if\ threshold\ \leq 0.12$$

$$MC_{class5} = \text{threshold, otherwise}$$

Table 40: Notation of moisture content

Notation	Description
MC_{classx}	Moisture content for class X where x indicates the number of classes
RH	Relative humidity (%)

5.3.4.6 Dead fuel moisture content

Dead fuel moisture content is calculated as followed (The Australasian Fire and Emergency Service Authorities Council (AFAC), 2022) :

$$FMC = 2.279 + 0.160107 \cdot RH - 0.14784 \cdot T + 7$$

Table 41: Notation of moisture content

Notation	Description
MC_{classx}	Moisture content for class X where x indicates the number of classes
RH	Relative humidity (%)
T	Temperature ($C\,°$)

5.3.5   Fireline intensity

Fire Intensity is calculated as following (The Australasian Fire and Emergency Service Authorities Council (AFAC), 2022):

$$I_B = h \cdot w \cdot ROS$$

Table 42: Notation of variables for fire intensity

Notation	Description
I_B	Fireline intensity (kWm^{-1})
h	Heat yield constant as 16,700 $kJkg^{-1}$
w	Fuel load in kg m^{-2} (1 kg m^{-2} = 10 $tonnes\ ha^{-2}$) (see 5.3.2) Note that it is necessary to multiply 0.1 to convert $FuelLoad_{combustion}$ from $\frac{tonnes}{ha}$ to $\frac{kg}{m^2}$
ROS	Rate of spread in ms^{-1} (1ms^{-1} = 3600 mh^{-1}) (see 5.3.1)

5.3.6   Flame height

Flame height is calculated as following (The Australasian Fire and Emergency Service Authorities Council (AFAC), 2020, p. 101):

$$F_{height} = 0.097 \cdot ROS^{0.424} + 0.102 \cdot FL_{ns}$$

Table 43: Notation of head-fire frame height of desert spinifex

Notation	Description
F_{height}	Flame height in (m)
ROS	Rate of spread in (m h^{-1})
FL_{ns}	Fuel load in (tonnes ha^{-1})

5.4   Buttongrass moorlands model (Buttongrass)

Buttongrass moorland is treeless vegetation community with buttongrass and moorland refers to heathland and morass (Marsden-Smedley and Catchpole, 1995a). Buttongrass is highly flammable and rampant more than 7,000 km^2 in south-west and west Tasmania (Marsden-Smedley, Catchpole and Pyrke, 2001). For instance, it is burnable up to 27 % fuel moisture and three years older and can keep burning even on natural fire breaks such as on water and minerals as well as manmade infrastructures such as roads (Marsden-Smedley, Catchpole and Pyrke, 2001; The Australasian Fire and Emergency Service Authorities Council (AFAC), 2020).

5.4.1   Fire rate of spread (ROS)

There are a few steps to calculate fire rate of spread (ROS). Firstly, the equation of the linear regression (z) for the probability is calculated as following:

$$z = -1.0 + 0.68 \cdot U_{1.7} - 0.07 \cdot MC - 0.0037 \cdot U_{1.7} \cdot MC + 2.1 \cdot D$$

Where

Fire Simulator – Prototype 2

$$U_{1.7} = \frac{U_{10}}{1.2}$$

Note that this equation is addressed in (Marsden-Smedley, 2009).

Table 44: Notation of variables for the logistic function

Notation	Description
$U_{1.7}$	Wind speed at 1.7 m above the ground as the surface wind speed in (km h^{-1})
U_{10}	Wind speed at 10 m above the ground in (km h^{-1})
MC	Dead fuel moisture content in (%)
D	Site productivity: low=0 and medium=1. The Research Prototype uses a default value as 1. In contrast, this productivity is dynamically selected by lithological components in Prototype 2.

Then the probability of the continuity of fire spread (P) is computed using linear regression (z) and sigmoid function (see section 5.13) to normalise the probability so that it can be between 0 and 1.

$$P = \frac{1}{(1+exp(-z))}$$

If P is greater than 0.5, rate of fire spread (ROS) is calculated in m h^{-1} by multiplying the original equation, ($\frac{m}{min}$) with $\frac{60\,min}{h}$ (Marsden-Smedley and Catchpole, 1995b; The Australasian Fire and Emergency Service Authorities Council (AFAC), 2020).

$$ROS = 0.678 \cdot U_{1.7}^{1.312} \cdot exp(-0.0243 \cdot MC) \cdot \left(1 - exp(-0.116 \cdot TSF)\right) \times 60$$

Otherwise, the ROS is assigned to 0 in the same manner as the one in Spinifex (see 5.3.1).

Note that the probability was not taken into account in Buttongrass model, in Prototype 1. This concept is anew introduced by following another Marsden's paper and Research Prototype. However, threshold 0.5 is on the discretion of Research Prototype only (Marsden-Smedley, Catchpole and Pyrke, 2001; The Australasian Fire and Emergency Service Authorities Council (AFAC), 2020). Therefore, the threshold is configurable with the default value, 0.5, for experimental purpose in Prototype 2.

Table 45: Notation of variables for ROS

Notation	Description
$U_{1.7}$	Wind speed at 1.7 m above the ground as the surface wind speed in (km h^{-1})
U_{10}	Wind speed at 10 m above the ground in (km h^{-1})
MC	Dead fuel moisture content in (%)
TSF	Time since fire in (years)
ROS	Rate of spread in (m h^{-1})

In addition, site productivity is dynamically selected in accordance with a geological component in Prototype 2 follows the constant number in Research Prototype. That is, it is low (=1) if quartzite is contained, otherwise it is medium (=2) in Prototype 2. Although the original literature of Research Prototype (Marsden-Smedley, Catchpole and Pyrke, 2001) states different numbers, these figures were integrated in the later paper (Marsden-Smedley, 2009). This comparison is summarised below.

Table 46: Comparison of definition in site productivity

Fire Simulator – Prototype 2

Reference of site productivity	Research Prototype		Marsden-Smedley, Catchpole and Pyrke		Prototype 2	
Equation	ROS probability	Fuel load	ROS probability	Fuel load	ROS probability	Fuel load
Low	1	1	0	1	1	1
Medium	2	2	1	2	2	2

The geological information is retrieved from geology table (3.1.1.6).

5.4.2 Moisture content (MC)

Moisture content (MC) is a variable for ROS. An equation for a moisture content of buttongrass moorland is expressed as below (The Australasian Fire and Emergency Service Authorities Council (AFAC), 2020):

$$MC = Rf + Hf$$

Where

$$Rf = 67.128 \cdot \left(1 - exp(-3.132 \cdot rain)\right) \cdot exp(-0.0858 \cdot t)$$

$$Hf = exp(1.660 + 0.0214 \cdot RH - 0.0292 \cdot T_{dew})$$

Table 47: Notation of variables for moisture content

Notation	Description
MC	Dead fuel moisture content in (%)
Rf	Rainfall factor
Hf	Humidity factor
Rain	The amount of precipitation in the past 48 hours in (mm). See 4.5.
t	Time after the last precipitation (h). See 4.6.
RH	Relative humidity in (%)
T_{dew}	Dew-point temperature in ($C°$)

5.4.3 Fuel load

Fuel load is a variable to calculate fire intensity. The fuel load of buttongrass moorlands can be calculated based on the average diameter of fuel, which is approximately 1.5 mm for both low and medium productivity as following (Marsden-Smedley and Catchpole, 1995b; The Australasian Fire and Emergency Service Authorities Council (AFAC), 2020):

$$Fuel_{low} = 11.73 \cdot \left(1 - exp(-0.106 \cdot TSF)\right)$$

$$Fuel_{med} = 44.61 \cdot \left(1 - exp(-0.041 \cdot TSF)\right)$$

$$Dead_{low} = (0.873 \cdot (1 - exp(-0.036 \cdot TSF))) \cdot Fuel_{low}$$

$$Dead_{med} = (0.950 \cdot (1 - exp(-0.054 \cdot TSF))) \cdot Fuel_{med}$$

Table 48: Notation of variables for fuel load

Notation	Description
$Fuel_{low}$	Fuel load in total for low productivity location in (tonnes ha^{-1})
$Fuel_{med}$	Fuel load in total for medium productivity location in (tonnes ha^{-1})
$Dead_{low}$	Dead-fuel load in total for low productivity location in (tonnes ha^{-1})
$Dead_{med}$	Dead-fuel load in total for medium productivity location in (tonnes ha^{-1})
TSF	Time since fire in years

5.4.4 Fireline intensity

Fire Intensity is calculated as following (The Australasian Fire and Emergency Service Authorities Council (AFAC), 2020, p. 101):

$$I_B = h \cdot w \cdot ROS$$

Table 49: Notation of variables for fire intensity

Notation	Description
I_B	Fireline intensity (kWm^{-1})
h	Heat yield constant as 19,900 $kJkg^{-1}$
w	Fuel load for both low and mid productivity site in kg m^{-2}. Note that it is necessary to multiply 0.1 to convert $FuelLoad_{combustion}$ from $\frac{tonnes}{ha}$ to $\frac{kg}{m^2}$. See 5.4.3.
ROS	Rate of fire spread in ms^{-1} (1ms^{-1} = 3600 mh^{-1})

5.4.5 Flame height

Flame height is calculated as following (Marsden-Smedley and Catchpole, 1995b; The Australasian Fire and Emergency Service Authorities Council (AFAC), 2020):

$$F_{height} = 0.148 \cdot I_B^{0.403}$$

Table 50: Notation of head-fire frame height of Tasmania grassland moorland

Notation	Description
F_{height}	Flame height in (m)
I_B	Fireline intensity (kWm^{-1})

5.5 Dry and wet eucalypt forest fire model (Forest)

Dry eucalypt forest fire model is as known as Vesta or DEFFM. This model is employed not only for dry eucalypt forest but also wet forest as well as other forests with variables to distinguish them in Prototype 2 until further forests models are ready to operate. The short name of this model is Forest.

5.5.1 Fire rate of spread (ROS)

Fire rate of spread (ROS) is calculated by multiplying several components: wind ($\Phi 1$), fuel attributes ($\Phi 2$), moisture content ($\Phi 3$) and slope ($\Phi 4$) as following (Cheney *et al.*, 2012; The Australasian Fire and Emergency Service Authorities Council (AFAC), 2020).

$$ROS = \Phi 1(wind) \cdot \Phi 2(fuel\ attributes) \cdot \Phi 3(moisture\ content) \cdot \Phi 4(slope)$$

$\Phi 1(wind)$ and $\Phi 2(fuel\ attributes)$ are described together below because these conditions are strongly connected. Then $\Phi 3(moisture\ content)$ is described in 5.5.3 and $\Phi 4(slope)$ is a common function throughout fire models and therefore addressed in 5.9.

5.5.2 $\Phi 1(wind)$ and $\Phi 2(fuel\ attributes)$

The $\Phi 1(wind) \cdot \Phi 2(fuel\ attributes)$ are variables for ROS. There are two equations for wind and fuel attributes, which are variables of the fire rate of spread (ROS) in dry eucalypt forest with shrubs underneath depending on the availability of fuel hazard scores (FHS) (Cheney *et al.*, 2012; The Australasian Fire and Emergency Service Authorities Council (AFAC), 2020).

The $\Phi 1(wind) \cdot \Phi 2(fuel\ attributes)$ for the ROS irregularly varies if the wind speed at 10 m is equal to or less than 5 km h^{-1}. Therefore, a constant value is employed as:

$$\Phi 1(wind) \cdot \Phi 2(fuel\ attributes) = 30\ \text{m}\ h^{-1}$$

If the wind speed is greater than 5 km h^{-1}, the equation for FHS version is as following (Cheney *et al.*, 2012):

$$\Phi 1(wind) \cdot \Phi 2(fuel\ attributes)$$
$$= 30 + 1.5308 \cdot (U_{10} - 5)^{0.8576} \cdot FHS_s^{0.9301} \cdot (FHS_{ns} \cdot H_{ns})^{0.6366} \cdot 1.03$$

Fuel hazard scores are visual estimation of potential fuel hazards between 0 and 4 in five fuel layers: (0) overstory tree canopy bark, (1) intermediate tree canopy bark, (2) elevated fuel layer, (3) near surface fuel layer and (4) surface fuel layer (Gould, McCaw and Cheney, 2011). Further, five Fuel Hazard Ratings (FHR) are categorised based on FHS (Cheney *et al.*, 2012). Since the equation for FHR version, which is non-available of FHS, is not intuitive, the Research Prototype does not use FHR but FHS version. Therefore, the FHR version is omitted in this document by following the Research Prototype.

To make wind ($\Phi 1$) and fuel attributes ($\Phi 1$) more realistic , the Research Prototype replaces the wind speed at 10 m (U_{10}) with the one near surface (U_{ns}) at wind speed > 5 km h^{-1} as below (The Australasian Fire and Emergency Service Authorities Council (AFAC), 2020). Note that comparison of wind speed also replaces U_{ns} with U_{10} for consistency.

$$\Phi 1(wind) \cdot \Phi 2(fuel\ attributes)$$
$$= 30 + 1.5308 \cdot (\boldsymbol{U_{ns}} - 5)^{0.8576} \cdot FHS_s^{0.9301} \cdot (FHS_{ns} \cdot H_{ns})^{0.6366} \cdot 1.03$$

Where

$$U_{ns} = \frac{3.0 \cdot U_{10}}{wind\ reduction\ factor}$$

Wind reduction factors vary depending on vegetation attributes (Cruz *et al.*, 2018). In the Research Prototype, **3** and **5** are substituted to the wind reduction factors of dry and wet forests respectively (The Australasian Fire and Emergency Service Authorities Council (AFAC), 2020).

Table 51: Notation of variables for wind and fuel attributes

Notation	Description
ROS	Rate of spread in (m h^{-1})
U_{10}	Wind speed at 10 m above the ground in (km h^{-1})
U_{ns}	Wind speed near surface
FHS_s	Surface fuel hazard score range from 0 and 4. Default value is 3.5 for both dry and wet forest.
FHS_{ns}	Near surface fuel hazard score range from 0 and 4. Default value is 3 for both dry and wet forest.
H_{ns}	Near surface fuel height (cm). Default value is 25.
Wind reduction factor	Fuel type specific (Cruz *et al.*, 2018). Default values are **3** and **5** for dry and wet forest respectively.

In terms of fuel hazard scores (FHS), Gould et al (2011) introduce a visual estimation method meticulously (Gould, McCaw and Cheney, 2011). This method is ideal if each entity such as bark, density, structure and litters, can be measured. However, it is not pragmatic to collect this information in large burnt areas. Therefore, the simple default values from the Research Prototype are employed in this study as below.

Table 52: Default Values applied from (The Australasian Fire and Emergency Service Authorities Council (AFAC), 2020)

Dry/Wet eucalypt forests	Dry eucalypt forest	Wet eucalypt forest
FHS_s	3.5	3.5
FHS_{ns}	3	3
H_{ns}	25	25
Wind reduction factor (cm)	**3**	**5**

5.5.3 $\Phi3(moisture\ content)$

Moisture content ($\Phi3$) is a variable for ROS depending on moisture contents (MC) If moisture content is equal to or less than 4, $\Phi3$ is 2.31. If MC is larger than 20, $\Phi3$ is 0.05. Otherwise, $\Phi3$ is multiplication of a constant value, 18.35, and MC powered by a constant value, -1.495 as following (The Australasian Fire and Emergency Service Authorities Council (AFAC), 2022).

If MC $\leq$ 4

$$\Phi3(moisture content) = 2.31$$

Else If 4 < MC $\leq$ 20

$$\Phi3(moisture content) = 18.35 \cdot MC^{-1.495}$$

else if MC > 20

Fire Simulator – Prototype 2

$$\Phi3(moisturecontent) = 0.05$$

Where

$$MC = a + b \cdot RH - c \cdot T$$

Where a, b and c are coefficients as following depending on the period.

Table 53: Coefficients in MC with three periods

Period	Period with condition	a	b	c
1	Clear skies, 12:00 – 17:00, October-March	2.76	0.124	0.0187
2	Cloudy, other daylight hours	3.60	0.169	0.0450
3	Night-time	3.08	0.198	0.0483

Note: Clear sky is equivalent to cloud coverage = 0 and other daylight hours is between 6:00 and 18:00 in Prototype 2.

Table 54: $\Phi3(moisturecontent)$ variables

Notation	Description
MC	Moisture condition for periods in (%)
RH	Relative humidity in (%)
T	Temperature in (C °)

5.5.4   Spotting distance

Spotting fire is an attribute of Vesta and can be applied optionally in this prototype. A range of spotting fire is estimated as following (The Australasian Fire and Emergency Service Authorities Council (AFAC), 2020).

When ROS < 150 mh^{-1}

Spotting distance = 50

Else

Spotting distance = $\left| 176.969 \cdot arctan(FHS_s) \cdot \left(\frac{ROS}{U_{10}^{0.25}}\right)^{0.5} + 1568800 \cdot FHS_s^{-1} \cdot \left(\frac{ROS}{U_{10}^{0.25}}\right)^{-1.5} - 3015.09 \right|$

Table 55: Notation of variables for spotting distance

Notation	Description
Spotting distance	Spotting distance in (m)
ROS	Rate of spread in (m h^{-1})
U_{10}	Wind speed at 10 m above the ground in (km h^{-1})
FHS_s	Surface fuel hazard score range from 0 and 4. Default value is 3.5 for both dry and wet forest.

5.5.5 Fuel load

Fuel load is a variable to calculate fire intensity and is the accumulation ($\text{FuelLoad}_{\text{acc}}$) of the fuel layers based on flame height (The Australasian Fire and Emergency Service Authorities Council (AFAC), 2020).

Whenever a flame occurs,

$$\text{FuelLoad}_{\text{acc}} = FuelLoad_s + FuelLoad_{ns}$$

In addition, if the flame height > 1 m, a bark and elevated layers are added as following.

$$\text{FuelLoad}_{\text{acc}} = \text{FuelLoad}_{\text{acc}} + FuelLoad_{el} + FuelLoad_b$$

Further, if the flame height > (the height of overstorey) $\cdot \frac{2}{3}$

$$\text{FuelLoad}_{\text{acc}} = \text{FuelLoad}_{\text{acc}} + FuelLoad_o$$

Where

$$FuelLoad_x = FL_x \cdot \left(1 - exp(-k_x \cdot TSF)\right)$$

Note that subscripts x for FuelLoad, FL and k can be either, s, ns, el, b or o, which indicates surface, near surface, elevated, bark or overstory respectively.

Table 56: Variables for flame heigths

Notation	Description
$FuelLoad_x$	Fuel Load in (tonnes ha^{-1}) where x indicates a layer in {s, ns, el, b, o}
FL_x	Constant state fuel in each fuel layer in (tonnes ha^{-1}) see Table 57 for dry and Table 58 for wet forests
k_x	Fuel accumulation rate in each fuel layer in (tonnes ha^{-1}). See Table 59 for dry and Table 60 for wet forests
TSF	Time since fire in (years)

*Table 57: Constant value of **dry** forests for FL_x adapted from (The Australasian Fire and Emergency Service Authorities Council (AFAC), 2020)*

FL_x	Constant
FL_s	14
FL_{ns}	3.5
FL_{el}	4
FL_b	5
FL_o	**6**

*Table 58: Constant value of **wet** forests for FL_x adapted from (The Australasian Fire and Emergency Service Authorities Council (AFAC), 2020)*

FL_x	Constant
FL_s	14
FL_{ns}	3.5
FL_{el}	4
FL_b	5
FL_o	**8**

*Table 59: Constant value of **dry** forests for k_x adapted from (The Australasian Fire and Emergency Service Authorities Council (AFAC), 2020)*

k_x	Constant
k_s	**0.3**
k_{ns}	0.2
k_{el}	**0.2**
k_b	0.1
k_o	**0.30**

*Table 60: Constant value of **wet** forests for k_x adapted from (The Australasian Fire and Emergency Service Authorities Council (AFAC), 2020)*

k_x	Constant
k_s	**0.35**
k_{ns}	0.2
k_{el}	**0.15**
k_b	0.1
k_o	**0.35**

5.5.6 Fuel availability

All the more, fuel load in forest for combustion can be expressed as following (The Australasian Fire and Emergency Service Authorities Council (AFAC), 2020).

$$FuelLoad_{combustion} = Fuel_{availability} \cdot FuelLoad_x$$

where if the forest is for **dry** eucalypts

$$Fuel_{availability} = DF \cdot 0.1$$

Else If the forest is for **wet** eucalypts

$$Fuel_{availability} = \left(\frac{1.008}{1 + 104.9 \cdot exp(-0.9306 \cdot DF \cdot C1)} \right)$$

where

$$C1 = 0.1 \cdot (KBDI \cdot (0.0046 \cdot W^2 - 0.0079 \cdot W - 0.0175) - 0.9167 \cdot W^2 + 1.5833 \cdot W + 13.5)$$

Table 61: Variables for fuel availability for combustion

Notation	Description
$FuelLoad_{combustion}$	Fuel load for combustion in (tonnes ha^{-1})
$Fuel_{availability}$	Fraction of fuel availability range between 0 and 1

DF	Drought factor
C1	The standard structure adjustment $\in [0, 1]$
KBDI	The ketch-Bryam drought index (mm)
W	Wind reduction factor $\in [3, 5]$

5.5.7 Fireline intensity

Fire Intensity is calculated as following (The Australasian Fire and Emergency Service Authorities Council (AFAC), 2020):

$$I_B = h \cdot w \cdot ROS$$

Table 62: Notation of variables for fire intensity

Notation	Description
I_B	Fireline intensity (kWm^{-1})
h	Heat yield constant as 18,600 $kJkg^{-1}$
w	$0.1 \cdot FuelLoad_{combustion}$ ($kg\ m^{-2}$)
ROS	Rate of spread in ms^{-1} ($1ms^{-1} = 3600\ mh^{-1}$)

5.5.8 Flame height

Flame height is calculated using rate of spreading (ROS) and the height of elevated fuel as following (The Australasian Fire and Emergency Service Authorities Council (AFAC), 2020):

$$F_{height} = 0.0193 \cdot ROS^{0.723} \cdot exp(0.64 \cdot H_{el}) \cdot 1.07$$

Table 63: Notation of frame height

Notation	Description
F_{height}	Flame height in (m)
ROS	Rate of spread in (ms^{-1})
H_{el}	Elevated fuel height in (m) = 1.5 m as default

5.6 Mallee heath model (Mallee heath)

There are two fire models for the shrublands. One is for semi-arid shrublands and another is other shrublands. The former is called **Mallee heath model** and described in this section while the latter is called **Heathland model** and illustrated in the section (5.7).

5.6.1 Moisture Content (MS)

Firstly, a moisture Content (MC) in % is defined prior to the definition of the fire rate of spread (ROS). MC is ingested by ROS in the rest of sections. MC comprises of MC_1 and MC_2.

$$MC = MC_1 + MC_2$$

Where MC_1 is conceived by (Miguel G. Cruz *et al.*, 2015).

$$MC_1 = 4.79 + 0.173 \cdot RH - 0.1 \cdot (T - 25) - \Delta \cdot 0.027 \cdot RH$$

In addition, the Research Prototype takes into account recent precipitation as below (The Australasian Fire and Emergency Service Authorities Council (AFAC), 2020).

$$MC_2 = 67.128 \cdot \left(1 - exp(-3.132 \cdot rain)\right) \cdot exp(-0.0858 \cdot TSR)$$

Table 64: Notation of variables for MC

Notation	Description
MC	Moisture content in (%).
RH	Relative humidity in (%)
T	Temperature in (C °)
Δ	1: high solar radiation, that is, during from 12:00 to 17:00 in daylight saving (October to March) and sunny, 0: else
rain	Amount of precipitation in the last 48 hours in (mm)
TSR	Time since cessation of last precipitation including drizzle in (hours)

5.6.2 Fire rate of spread (ROS)

There are a few steps to predict fire propagation: (1) probability for binary decision-making, that is, "go" or "no-go", (2) identification of fire types, surface or crown fire, and (3) rate of spread (ROS).

Firstly, probability (P_{spread}) is computed by employing sigmoid function (see section 5.13) for logistic regression (Cruz *et al.*, 2013; The Australasian Fire and Emergency Service Authorities Council (AFAC), 2020).

$$P_{spread} = \frac{1}{1 + exp(-z)}$$

Where

$$z = 14.624 + 0.2066 \cdot U_{10} - 1.8719 \cdot MC - 0.30442 \cdot Cov_o$$

When $P_{spread} < 0.5$, the fire is not enough strong to keep propagating and the status is therefore "no-go", otherwise the process goes to the next step.

Table 65: Notation of variables for probability

Notation	Description
P_{spread}	Probability of spread between 0 and 1
U_{10}	Wind speed at 10 m above the ground in (km h^{-1})
MC	Moisture content in (%) described in 5.6.1.
Cov_o	Coverage of overstorey in (%). Here Research Prototype uses the default value **18**.

Secondly, type of fire (P_{crown}) is identified by sigmoid function as following.

$$P_{crown} = \frac{1}{1 + exp(-z)}$$

Where

$$z = -11.138 + 1.4054 \cdot U_{10} - 3.4217 \cdot MC$$

Table 66: Notation of variables for probability

Notation	Description
P_{crown}	Normalized probability of crown between 0 and 1
U_{10}	Wind speed at 10 m above the ground in (km h^{-1})
MC	Moisture content in (%) described in 5.6.1.

Thirdly, two ROS models, surface ROS (ROS_s) and crown ROS (ROS_c), are defined to calculate the total ROS later depending on the P_{crown}. Note that the unit of original equations for both ROSs (Miguel G. Cruz *et al.*, 2015) are ($\frac{m}{min}$), while the Research Prototype converts to ($\frac{m}{h}$) by multiplying it by ($\frac{60\,min}{1\,h}$) to be consistent.

$$ROS_s = 3.337 \cdot U_{10} \cdot exp(-0.1284 \cdot MC) \cdot H_o^{-0.7073} \times 60$$

$$ROS_c = 9.5751 \cdot U_{10} \cdot exp(-0.1795 \cdot MC) \cdot \left(\frac{Cov_o}{100}\right)^{0.3589} \times 60$$

P_{crown} is rounded before ROS is conditionally calculated based on P_{crown}. That is, $P_{crown}\ is\ attributed\ as$ 0 when $P_{crown} \le 0.01$ and When P_{crown} is ascribed as 1 when $P_{crown} > 0.99$ (Miguel G. Cruz *et al.*, 2015).

$$P_{crown} = 0, P_{crown} \le 0.01$$

$$P_{crown} = 1, P_{crown} > 0.99$$

Finally, total ROS is computed by adding up both possibilities for the crown fire as below (Miguel G. Cruz *et al.*, 2015).

$$ROS = (1 - P_{crown}) \cdot ROS_s + P_{crown} \cdot ROS_c$$

Table 67: Notation of variables for ROS

Notation	Description
ROS_s	Surface fire rate of spread in (mh^{-1})
ROS_c	Crown fire rate of spread in (mh^{-1})
U_{10}	Wind speed at 10 m above the ground in (km h^{-1})
H_o	Height of the Mallee storey (m). Default value is **4.5**.
MC	Moisture content in (%) described in 5.6.1.
P_{crown}	Normalized probability of crown between 0 and 1
Cov_o	Coverage of overstorey in (%). Here Research Prototype uses the default value, **18**.

5.6.3   Fuel load

Fuel load is a variable to calculate fire intensity. There are three fuel load equations for each fuel layers: surface ($FuelLoad_s$), overstorey ($FuelLoad_o$) and crown ($FuelLoad_c$) respectively. Definition of each fuel load is as following:

$$FuelLoad_s = FL_s \cdot \left(1 - exp(-k_s \cdot TSF)\right)$$

$$FuelLoad_o = FL_o \cdot \left(1 - exp(-k_o \cdot TSF)\right)$$

$$FuelLoad_c = FuelLoad_s + FuelLoad_o$$

Table 68: *Variables for fuel load*

Notation	Description
$FuelLoad_s$	Fuel Load for surface fires in (tonnes ha^{-1})
$FuelLoad_o$	Fuel Load for overstorey in (tonnes ha^{-1})
$FuelLoad_c$	Fuel Load for crown fires in (tonnes ha^{-1})
FL_s	Constant state fuel for surface in each fuel layer in (tonnes ha^{-1}). See Table 69.
FL_o	Constant state fuel for overstorey in each fuel layer in (tonnes ha^{-1}). See Table 69.
k_s	Fuel accumulation rate for surface fuel in each fuel layer in (tonnes ha^{-1}). See Table 69.
k_o	Fuel accumulation rate for overstorey fuel in each fuel layer in (tonnes ha^{-1}). See Table 69.
TSF	Time since fire in (years)

Table 69: *Constant value of* **Mallee heath** *adapted from (The Australasian Fire and Emergency Service Authorities Council (AFAC), 2020)*

FL_x	Constant
FL_s	3
FL_o	1
k_s	0.2
k_o	0.2

P_{crown} is rounded for consistency of ROS before accumulation of fuel load ($FuelLoad$) is conditionally calculated based on P_{crown} in this study. That is, P_{crown} *is attributed as* 0 when $P_{crown} \leq 0.01$ and When P_{crown} is ascribed as 1 when $P_{crown} > 0.99$. That is,

$$P_{crown} = 0, P_{crown} \leq 0.01$$

$$P_{crown} = 1, P_{crown} > 0.99$$

Finally, cumulative fuel load is computed by adding up the both possibilities for the crown fire as below.

$$FuelLoad = FuelLoad_s + P_{crown} \cdot FuelLoad_c$$

5.6.4   Fireline intensity

Fire Intensity is calculated as following (The Australasian Fire and Emergency Service Authorities Council (AFAC), 2020):

$$I_B = h \cdot w \cdot ROS$$

Table 70: *Notation of variables for fire intensity*

Notation	Description
I_B	Fireline intensity (kWm^{-1})
h	Heat yield constant as 18,600 $kJkg^{-1}$
w	Fuel load ($FuelLoad$) converted to kg m^{-2} *by multiplying* $1000kg/10000m^2$ *i.e.* 0.1
ROS	Rate of spread in ms^{-1} ($1ms^{-1} = 3600\ mh^{-1}$)

5.6.5 Flame height

Flame height has strong correlation with Fireline intensity (I_B) and the height can be empirically inducted as following (Cruz *et al.*, 2013):

$$F_{height} = exp(-4.142) \cdot I_B^{0.633}$$

Table 71: Notation of frame height

Notation	Description
F_{height}	Flame height in (m)
I_B	Fireline intensity (kWm^{-1}) as mentioned above.

5.7 Heathland model (Shrubland)

Heathland model is a fire model for shrublands excluding semi-amid shrublands and its short name is Shrubland.

5.7.1 Moisture Content (MS)

Firstly, moisture content (MC) in % is defined because MC is ingested in fire rate of spread (ROS) in the rest of sections. MC consists of MC_1 and MC_2.

$$MC = MC_1 + MC_2$$

Where MC_1 is conceived by (Miguel G. Cruz *et al.*, 2015).

$$MC_1 = 4.37 + 0.161 \cdot RH \cdot -0.1 \cdot (T - 25) - \Delta \cdot 0.027 \cdot RH$$

In addition, the Research Prototype takes into account recent precipitation as below (The Australasian Fire and Emergency Service Authorities Council (AFAC), 2020).

$$MC_2 = 67.128 \cdot \left(1 - exp(-3.132 \cdot rain)\right) \cdot exp(-0.0858 \cdot TSR)$$

Table 72: Notation of variables the probability

Notation	Description
MC	Moisture content in (%).
RH	Relative humidity in (%)
T	Temperature in (C °)
Δ	1: during high solar radiation (sunny and from 12:00 to 17:00 in October to March), 0: else
rain	Amount of precipitation in the last 48 hours in (mm)
TSR	Time since cessation of the last precipitation including drizzle in (hours)

5.7.2 Fire rate of spread (ROS)

Now, a fire rate of spread (ROS) is estimated as following.

When $U_{10} < 5km \; h^{-1}$ (Anderson *et al.*, 2015),

$$ROS = [ROS_0 + 0.2 \cdot (5.6715 \cdot (5 \cdot WRF)^{0.9102} - ROS_0) \cdot U_{10}] \cdot H_{el}^{0.2227} \cdot exp\,(-0.0762 \cdot MC) \times 60$$

else

$$ROS = 5.6715 \cdot (WRF \cdot U_{10})^{0.9102} \cdot H_{el}^{0.2227} \cdot exp(-0.0762 \cdot MC) \times 60$$

ROS is further adjusted by sigmoid function because the ROS was found to be unrealistically high in the result (The Australasian Fire and Emergency Service Authorities Council (AFAC), 2022).

$$ROS_{adj} = \frac{ROS}{1 + \exp\big(-(16.57 + 1.188 \cdot U_{10} - 2.705 \cdot MC)\big)}$$

Table 73: Notation of variables for ROS

Notation	Description
ROS	Rate of spread in (m h^{-1})
ROS_0	*Rate of spread (ROS) in 0 wind at 0 MC at 1.0 m height.* R_0= 5 m min^{-1} (This converts into **300** m h^{-1} in ROS calculation)
ROS_{adj}	ROS adjusted by AFDRS
WRF	Wind reduction factor: **0.667** is for shrublands without canopy and **0.35** is for ones below woodland.
U_{10}	Wind speed at 10 m above the ground in (km h^{-1})
H_{el}	Elevated height in (m) = **1.3** m as a default value in the Research Prototype
MC	Moisture content in (%)

5.7.3 Fuel load

Fuel load is a variable to calculate fire intensity and estimated as following:

$$FuelLoad = FL \cdot \big(1 - exp(-k \cdot TSF)\big)$$

Table 74: Variables for fuel load

Notation	Description
$FuelLoad$	Fuel Load in (tonnes ha^{-1})
FL	Constant state fuel in (tonnes ha^{-1}). Default value is **20**.
k	Fuel accumulation rate for fuel in (tonnes ha^{-1}). Default value is **0.2**.
TSF	Time since fire in (years)

5.7.4 Fireline intensity

Fire Intensity is calculated as following (The Australasian Fire and Emergency Service Authorities Council (AFAC), 2020):

$$I_B = h \cdot w \cdot ROS$$

Table 75: Notation of variables for fire intensity

Notation	Description
I_B	Fireline intensity (kWm^{-1})
h	Heat yield constant as 18,600 $kJkg^{-1}$

w	Fuel load ($FuelLoad$) converted to kg m^{-2} by multiplying $1000kg/10000m^2$ i.e. 0.1
ROS	Rate of spread in ms^{-1} ($1ms^{-1} = 3600\ mh^{-1}$)

5.7.5 Flame height

Flame height has strong correlation with Fireline intensity (I_B) and the height can be empirically computed as following (Cruz *et al.*, 2013):

$$F_{height} = exp(-4.142) \cdot I_B^{0.633}$$

Table 76: Notation of frame height

Notation	Description
F_{height}	Flame height in (m)
I_B	Fireline intensity (kWm^{-1}) as mentioned above.

5.8 Adjusted pine model (Pine)

The Research Prototype employs CSRIO SPARK for the pine plantation models (Miller *et al.*, 2015; The Australasian Fire and Emergency Service Authorities Council (AFAC), 2020). SPARK is a fire prediction tool using the level set method, which is capable of plugging in user define fire propagation models. Fire perimeter is measured instead of physical models in this model because calculation of perimeter is faster than the physical computational fluid dynamics (CFD) (Miller *et al.*, 2015). Although the Research Prototype postulates that it refers the framework from Spark, details of equations have not been stated in the original paper or operational level yet in Research Prototype. Therefore, this study only defines these equations by following the Research Prototype (Miller *et al.*, 2015; The Australasian Fire and Emergency Service Authorities Council (AFAC), 2020). This model will be implemented once further details are announced.

5.8.1 Fuel moisture content ($M_{foliar}\ and\ M_{litter}$)

Two moisture contents for foliar and litter has been released (The Australasian Fire and Emergency Service Authorities Council (AFAC), 2022).

Foliar moisture content is calculated as below

$$m_{foliar} = 150 - 5 \cdot DF$$

Litter fuel moisture is calculated in the simple way.

$$m_{litter} = 4.3426 + 0.1188 \cdot RH - 0.0211T$$

Table 77: M_{litter} variables

Notation	Description
m_{foliar}	Foliar moisture content
DF	Drought factor
m_{litter}	Moisture condition for periods in (%)

| RH | Relative humidity in (%) |
| T | Temperature in (C °) |

5.8.2   Fire rate of spread (ROS)

Fire rate of spread (ROS) in pine plantation model is conditionally predicted by selecting either surface ROS ($ROS_{surface}$), active crown fire ROS (ROS_{active}) or passive crown fire ROS ($ROS_{passive}$)(Cruz, Alexander and Fernandes, 2008). In prior to this condition, some parameters are defined.

Firstly, wind speed at stand height ($U_{StandHeight}$) and at flame height ($U_{FlameHeight}$) are defined.

$$U_{StandHeight} = U_{10} \cdot \frac{ln(\frac{0.36 \cdot h}{0.13 \cdot h})}{ln(\frac{10 + 0.36 \cdot h}{0.13 \cdot h})}$$

$$U_{FlameHeight} = U_{StandHeight} \cdot exp(-0.48)$$

Table 78: Notation of variables of wind speed at various heights

Notation	Description
$U_{StandHeight}$	Wind speed at stand height in (kmh^{-1})
$U_{FlameHeight}$	Wind speed at flame height in (kmh^{-1})
U_{10}	Wind speed at 10 m height in (kmh^{-1})
h	Stand height in (m) [TBA]

Secondly, a wind coefficient (C_{wind}) is estimated.

$$C_{wind} = C \cdot \left(54.68 \cdot U_{FlameHeight}\right)^B \cdot \left(\frac{P}{P_o}\right)^E$$

Where

$$B = 0.02562 \cdot \sigma^{0.54}$$

$$C = 7.47 \cdot exp(-0.133 \cdot \sigma^{0.55})$$

$$E = 0.715 \cdot exp(-0.000359 \cdot \sigma)$$

Table 79: Notation of variables of wind coefficient (C_{wind})

Notation	Description
P	Rate of fuel packing [TBA]
P_o	Optimal P [TBA]
σ	Rate of fuel surface area per volume (m^{-1}) [TBA]

Thirdly, surface ROS ($ROS_{surface}$) is defined.

$$ROS_{surface} = 18.288 \cdot \frac{R \cdot X \cdot (1 + C_{wind})}{\rho \cdot N_h \cdot h_p}$$

Table 80: Notation of variables of surface ROS ($ROS_{surface}$)

Notation	Description
$ROS_{surface}$	Surface ROS in (m h^{-1})
ρ	Density of a litter bulk [TBA]
N_h	The effective heating number [TBA]
h_p	Pre-ignition heat [TBA]
R	Intensity of reaction [TBA]
X	Ratio of flux propagation [TBA]

Fourthly, active crown fire ROS (ROS_{active}) is defined.

$$ROS_{active} = 661.26 \cdot U_{StandHeight}^{0.8966} \cdot \rho_{canopy}^{0.1901} \cdot exp(-0.1714) \cdot m_{litter}$$

Table 81: Notation of variables of active crown fire ROS (ROS_{active})

Notation	Description
ROS_{active}	Active crown fire ROS in (m h^{-1})
ρ_{canopy}	Density of the canopy bulk (kg m^{-3}) (Cruz, Alexander and Fernandes, 2008) [TBA]
$U_{StandHeight}$	Wind speed at stand height in (kmh^{-1}) as mentioned above
m_{litter}	Moisture content of the litter in (%) see 5.8.1

Fifthly, passive crown fire ROS ($ROS_{passive}$) is defined (Cruz, Alexander and Wakimoto, 2005).

$$ROS_{passive} = ROS_{active} \cdot exp(-CAC)$$

Where CAC indicates the criteria for active crowning defined below (Cruz, Alexander and Fernandes, 2008):

$$CAC = \frac{ROS_{active} \cdot \rho_{canopy}}{60 \cdot f}$$

Table 82: Notation of variables of passive crown fire ROS ($ROS_{passive}$)

Notation	Description
$ROS_{passive}$	Passive crown fire ROS in (m h^{-1})
ROS_{active}	Active crown fire ROS in (m h^{-1})
CAC	Criterion for active crowning
ρ_{canopy}	Density of the canopy bulk (kg m^{-3}) (Cruz, Alexander and Fernandes, 2008)
f	Rate of the critical mass flow for solid crown flame. Default value is **3.0** (Cruz, Alexander and Fernandes, 2008).

Before integrating three rates of spread, the last condition, crowing ratio (r_c) is articulated (The Australasian Fire and Emergency Service Authorities Council (AFAC), 2020).

$$r_c = \frac{I}{I_{critical}}$$

Where I indicates intensity of surface fire and $I_{critical}$ is the threshold of the intensity of surface fire for the ignition, which is calculated as below.

$$I_{critical} = \left(0.01 \cdot H_{CanopyBase} \cdot h_i\right)^{1.5}$$

Where $H_{CanopyBase}$ is the canopy height above the ground in (m) and h_i indicates the heat of ignition as below.

$$h_i = 460 + 25 \cdot m_{foliar}$$

Table 83: Notation of variables for conditions of ROS

Notation	Description
r_c	Crowing ratio
I	Intensity of surface fire [TBA]
$I_{critical}$	Minimum intensity of surface fire to ignite crown
$H_{CanopyBase}$	Canopy height above the ground in (m) [TBA]
h_i	Heat of ignition
m_{foliar}	Moisture content of foliage in (%) see 5.8.2

Finally, the rate of spread is selected. If the crowning ration (r_c) is equal to or greater than 1 and the criterion of active crowning (CAC) is greater than 1, an active crowning fire ROS (ROS_{active}) is chosen. If r_c is equal to or greater than 1, the CAC is equal to or less than 1 and the passive crowning fire ROS ($ROS_{passive}$) is greater than the surface ($ROS_{surface}$), the $ROS_{passive}$ is chosen, otherwise the $ROS_{surface}$ is selected (See below).
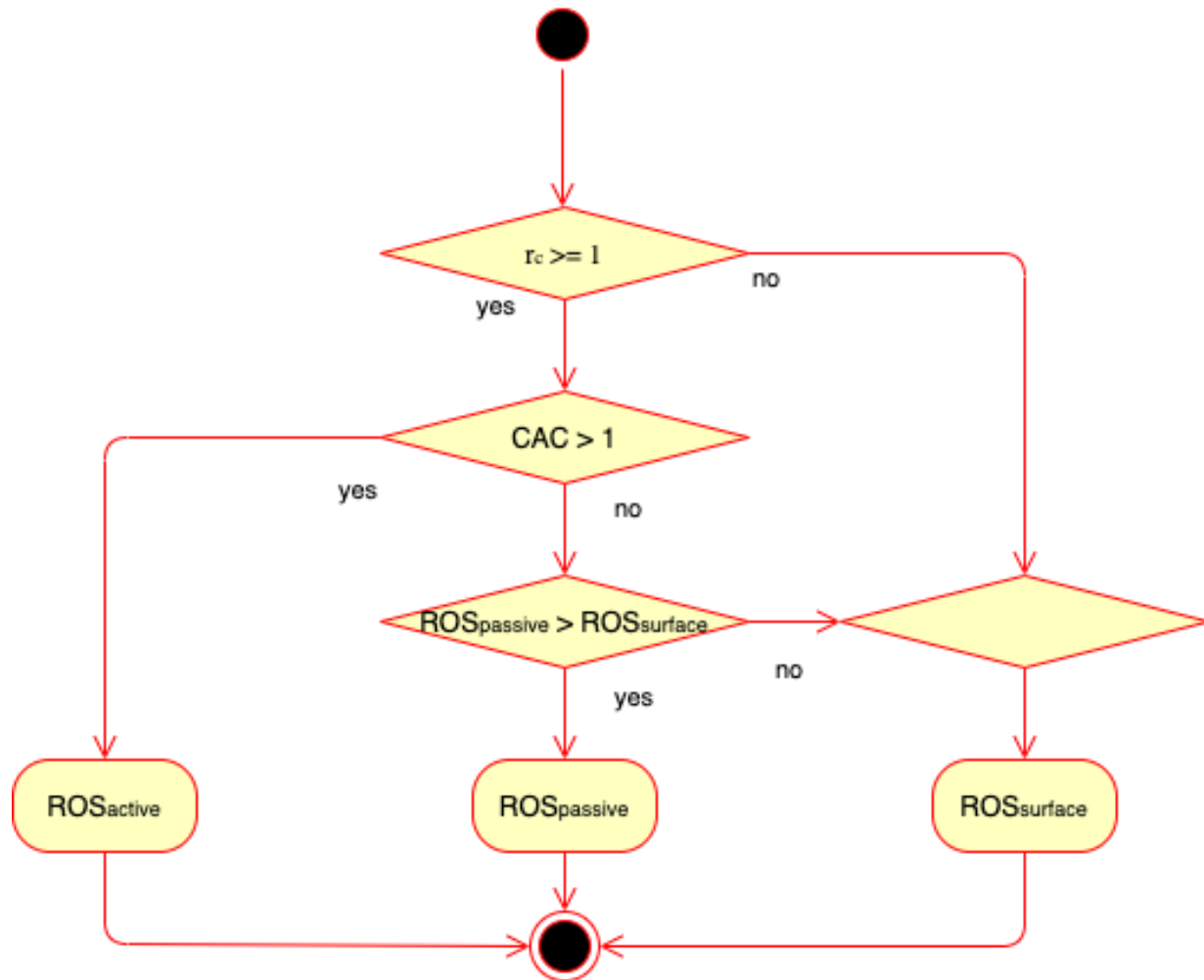
Figure 35: Selection of ROS: ($ROS_{surface}$, ROS_{active} or $ROS_{passive}$) adapted from (Cruz, Alexander and Fernandes, 2008)

5.8.3   Fireline intensity

Fire Intensity is calculated from the equation of ratio of crowning (r_c):

$$I = r_c \cdot I_{critical}$$

Table 84: Notation of fire intensity

Notation	Description
I	Intensity of surface fire
r_c	Crowing ratio
$I_{critical}$	Minimum intensity of surface fire to ignite crown

5.8.4   Flame height

Flame height is calculated from intensity and stand height (The Australasian Fire and Emergency Service Authorities Council (AFAC), 2020):

$$F_{height} = 0.07755 \cdot I^{0.46} + \Delta \cdot h$$

Table 85: Notation of frame height

Notation	Description
F_{height}	Flame height in (m)
I	Fireline intensity (kWm^{-1}) as mentioned above. [TBA]
Δ	1: if the ROS is ROS_{active}, 0: $else$
h	Stand height in (m) [TBA]

5.9 Slope influence on ROS

Slope has an impact on fire rate of spread (ROS) throughout the fire models mentioned above. Although the slope effects has not been implemented in Research Prototype yet, they are addressed as topographical effects for ROS by McArthur and Sullivan et al (Noble, Gill and Bary, 1980; Sullivan *et al.*, 2014; The Australasian Fire and Emergency Service Authorities Council (AFAC), 2020). Both anabatic (uphill) slope and katabatic (downhill) slope equations are addressed in this section.

5.9.1 Anabatic ROS

Anabatic ROS ($ROS_{anabatic}$) is defined as following (Noble, Gill and Bary, 1980):

$$ROS_{anabatic} = ROS \cdot exp(0.0687 \cdot \theta)$$

Table 86: Notation of variables of uphill ROS ($ROS_{anabatic}$)

Notation	Description
$ROS_{anabatic}$	Anabatic fire rate of spread in (m h^{-1})
ROS	Fire rate of spread in the plane in (m h^{-1})
θ	Slope of ground surface in (°)

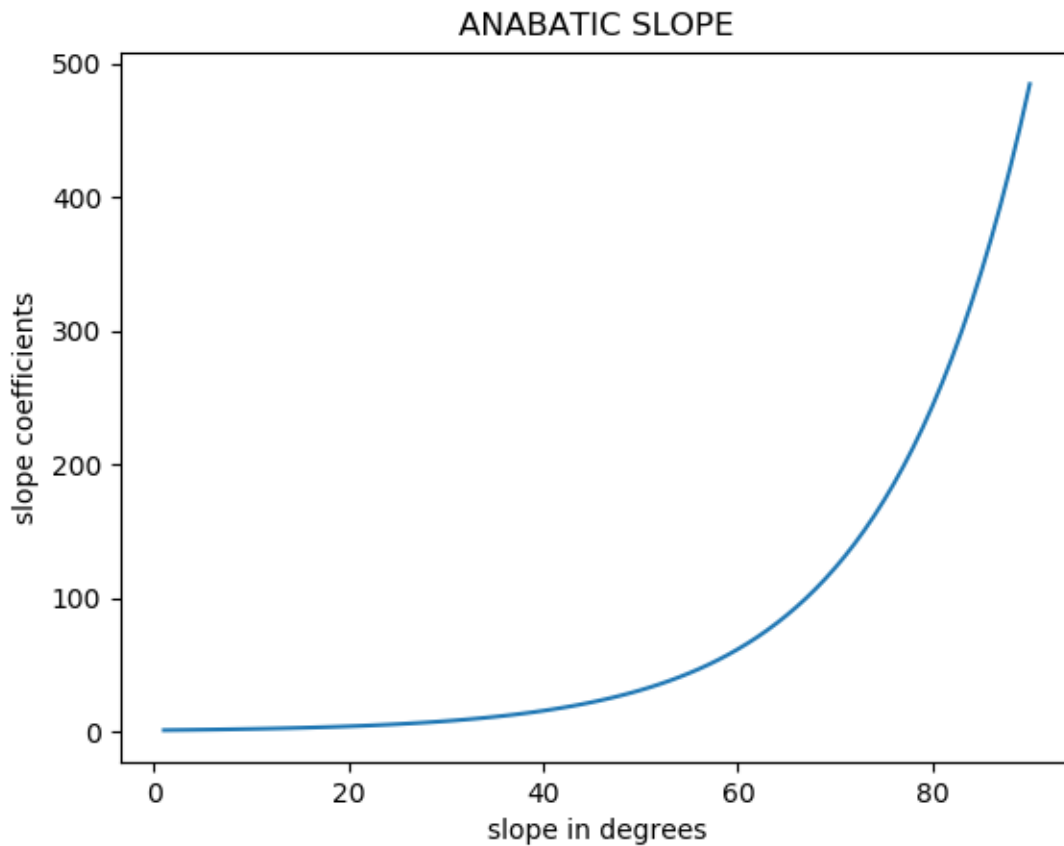The more angular slope is, the more coefficient increases as below.

Figure 36: ROS coefficient trend for anabatic slope

Slope angle in degrees is illustrated in the section 5.9.2.

5.9.2   Katabatic ROS

Sullivan (2014) proposes two equations for katabatic slope as seen below . (1) One takes the projected or plan distance, which is equivalent to base distance of trigonometry and (2) another does the ground or linear, which falls on hypotenuse. In terms of landscape scale, the former is suitable for large size and the latter is for smaller size (Sullivan *et al.*, 2014; The Australasian Fire and Emergency Service Authorities Council (AFAC), 2020).
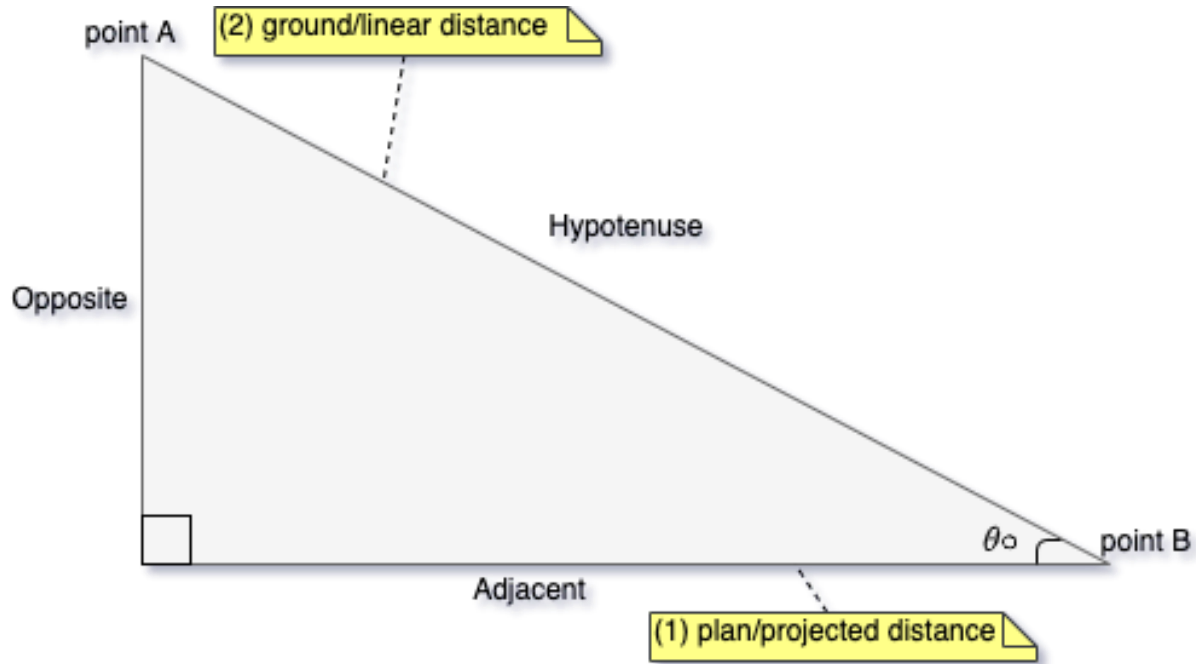
Figure 37: Katabatic slope distances :(1) plan/projected (2) ground/linear distance

Slope angle in degrees (θ) can be calculated as following:

$$\theta = tan\left(\frac{opposite}{adjacent}\right)$$

Where the opposite length is the subtraction of point B from point A vertically using DEM by assuming that fire proceeds from point A to B (Figure 37). Either coefficient is ingested into fire rate of spreading (ROS).

$$ROS_{katabatic} = ROS \cdot slope_{katabatic}$$

(1) Equation of $slope_{katabatic}$ along plan/projected distance is following.

$$slope_{katabatic} = \frac{2^{-\frac{\theta}{10}}}{2^{\left(1-\frac{\theta}{10}\right)}-1}$$

This katabatic coefficient slowly and smoothly increases with slope angle until the angle reaches zero degree (Figure 38).
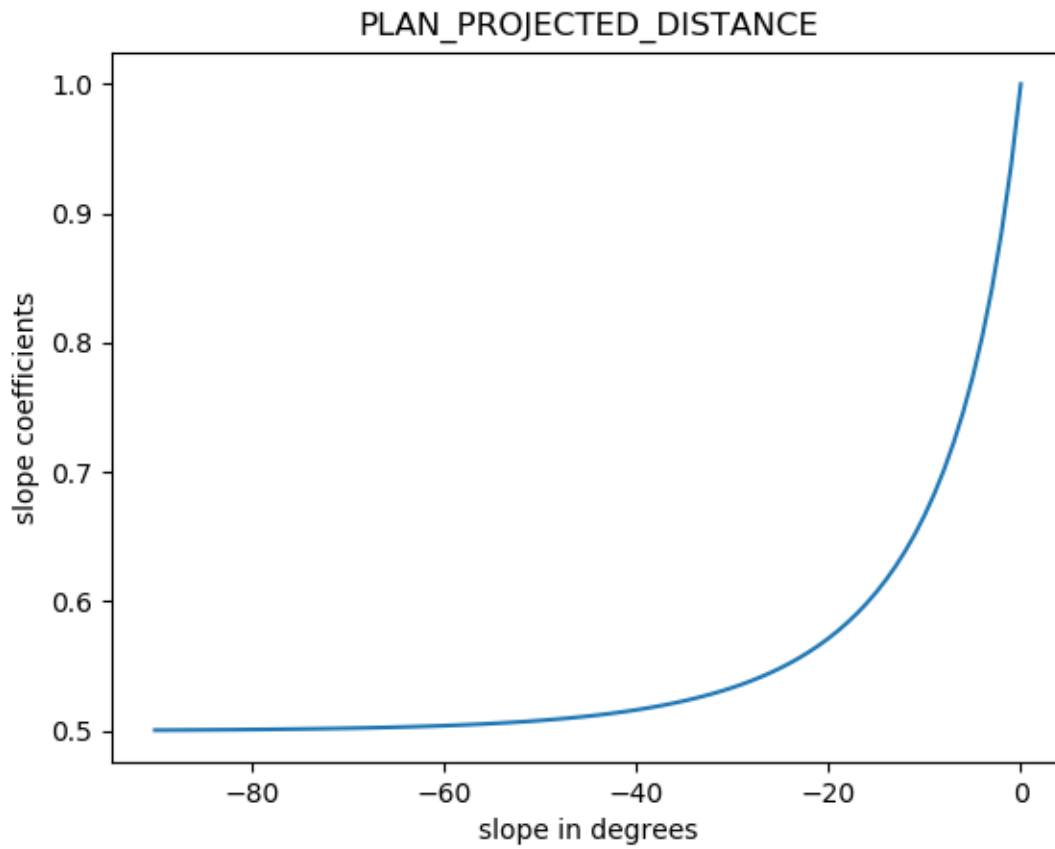
Figure 38: ROS coefficient's trend of anabatic and katabatic slope of plan/projected distance

(2) Equation of $slope_{katabatic}$ along ground/linear distance is following.

$$slope_{katabatic} = \frac{2^{-\frac{\theta}{10}}}{2^{\left(1-\frac{\theta}{10}\right)} \cdot COS(-\theta) - 1}$$

The slope coefficient shows slow increase with fluctuation in accordance with angle (Figure 39). This fluctuation appears erroneous. For instance, a blip around -58 ° does not have any reason for surge of fire spreading at this angle.
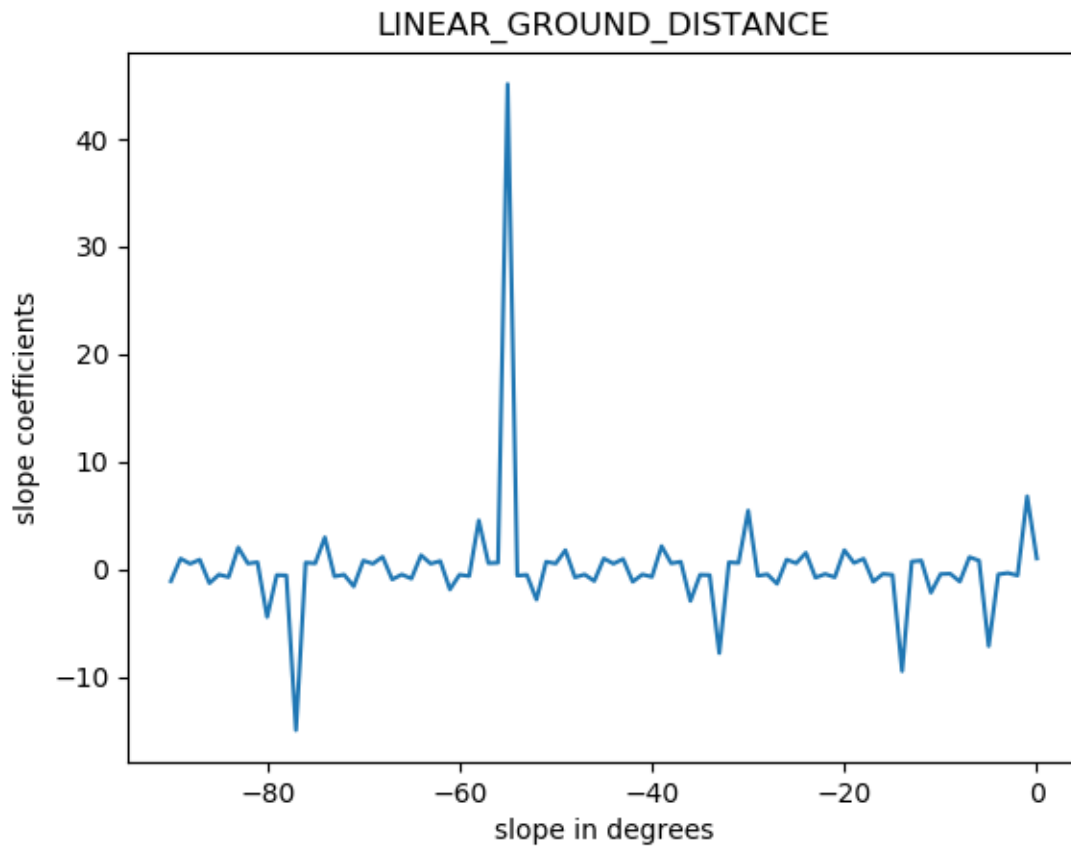
Figure 39: ROS coefficient's trend of anabatic and katabatic slope of linear/ground distance

In Prototype 2, (1) plan/projected distance is selected as default because the trend of slope coefficient is more stable than linear/ground distance (Figure 38 and Figure 39). However, these can be switched by the configuration, which has an impact on distance as well mentioned in the section 5.11.

Table 87: Notation of variables of uphill ROS ($ROS_{katabatic}$)

Notation	Description
$ROS_{anabatic}$	Anabatic fire rate of spread in (m h^{-1})
ROS	Fire rate of spread in the plane in (m h^{-1})
θ	Slope of ground surface in (°)

5.10 ROS coefficient to adjust date and time for fire propagation

ROS coefficient adjusts date and time so that fire can propagation on right time. Elapse is calculated by diving distance from one to another location by ROS. Therefore, the total elapse is inversely proportional to the number of adjacent grids and differs among geometries (3.1.1.7). In other words, it is necessary to place a bias or friction to tune ROS up so that the total shape of fire propagation is similar to each other among geometries after these elapses become closer to the reality. There are three ways of adjustment, static adjustment, dynamic adjustment, and rate by geometry.

Table 88: Comparison of bias types

Types	Advantages	Drawbacks
Static	- Multi-ignitions are possible - Bias is evenly applied	- Time consuming - Observed duration is required
Dynamic	- Only one experiment is necessary - Multi-ignitions are possible	- Bias is unevenly applied - Observed duration is required
By Geometry	- Observed duration is not required	- Only single ignition is assumed - Bias rate is required from other experiments

5.10.1 Static ROS adjustment

Static ROS is useful in case there are multi-ignitions. The burning duration is adjusted fairly since this bias is evenly applied. On the other hand, it is time-consuming because it is necessary to calculate a bias in the first experiment. Once bias is calculated, this bias can be applied to the next simulation run.

The ROS for the first round with the bias coefficient is simply calculated as following,

$$ROS = ROS_{org} \cdot bias$$

$$bias = \prod_{i=1}^{n} \left(\frac{elapse_{(i-1)}}{elapse_{truth}} \right)$$

Where ROS_{org} indicates ROS without bias; $bias$ is a product of biases; $elapse_{(i-1)}$ is elapse in the previous round with the same conditions such as slope distance type; and $elapse_{truth}$ is the one in ground truth. The bias affects evenly to ROS.

5.10.2 Dynamic ROS adjustment

Dynamic ROS is useful in case there are multi-ignitions. It can save time for simulation because it is not necessary to calculate bias beforehand. However, the bias is not evenly applied. For instance, there is no bias is applied at the initial ignition since there is no data.

ROS bias is calculated with the comparison of duration per distance between ground truth and on-going simulation.

$$Bias = \frac{duration_{sim}}{duration_{obs}}$$

Where $duration_{sim}$ is duration per burnt distance and $duration_{obs}$ is for a ground truth with notice that each duration is reciprocal of speed. Namely, $duration_x = \frac{period_x}{\sqrt{(area_{burnt_x})}}$ with x as on-going simulation or ground truth. Therefore, this equation is the same as:

$$Bias = \frac{period_{sim} \cdot \sqrt{area_{burnt_{obs}}}}{period_{obj} \cdot \sqrt{area_{burnt_{sim}}}}$$

The bias affects ROS unevenly since the period per burnt area is dynamically changing.

5.10.3 ROS adjustment by geometry

ROS bias is calculated from the past data by geometry and registered in the configuration. Advantage of ROS adjustment by geometry is that no observed duration for burning is required. Limitation is that this bias is only for single ignition.

5.11 Distance

Spatial distance is a variable to estimate elapse with fire rate of spreading (ROS). There are two methods to calculate distance from one to another in accordance with the configuration of Katabatic ROS in section 5.9.2. In either case, the distance is calculated based on Euclidean distance (Figure 40). If the plan/projected distance is selected, then two-dimensional distance is calculated. If the linear/ground distance is chosen, three-dimensional distance is computed (Table 89). As above mentioned, the former is suitable for large scale landscape and the latter is for small scale.

$$\sqrt{((P1.x - P2.x)^2 + (P1.y - P2.y)^2)} \qquad \sqrt{((P1.x - P2.x)^2 + (P1.y - P2.y)^2 + (P1.z - P2.z)^2)}$$
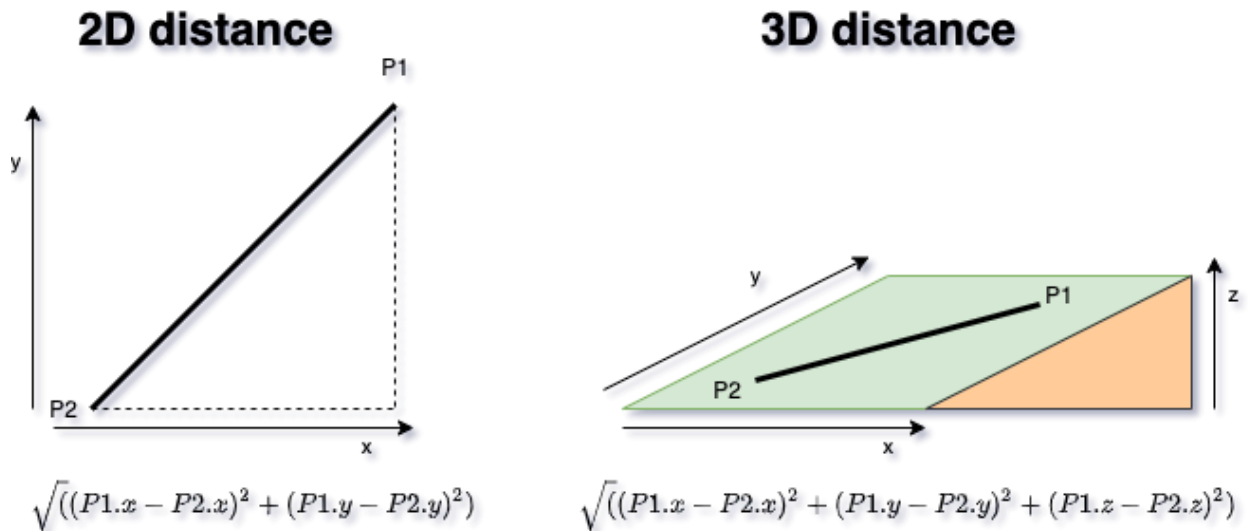
Figure 40: 2D and 3D Euclidean Distances

Table 89: Katabatic slope distance

#	Katabatic slope	Distance	Suitable scale of landscape
(1)	Plan/project	Two-dimensional	Large
(2)	Linear/ground	Three-dimensional	Small

Generally speaking, distance is not explicitly specified either plan/projected or linear/ground (Sullivan *et al.*, 2014). Therefore, the system chooses the same distance for anabatic slope as the one for katabatic slope for consistency.

5.12 Alignment of fire propagation and wind direction

Surface wind plays one of the significant roles for fire propagation (Sharples, McRae and Weber, 2010). Although the Research Prototype takes into account wind magnitude, it does not account for wind direction. In previous prototype, Prototype 1, direction bias has been placed so that degree of alignment between fire and wind is considered (Ozaki, Aryal and Fox-Hughes, 2019). This concept is also employed in Prototype 2.
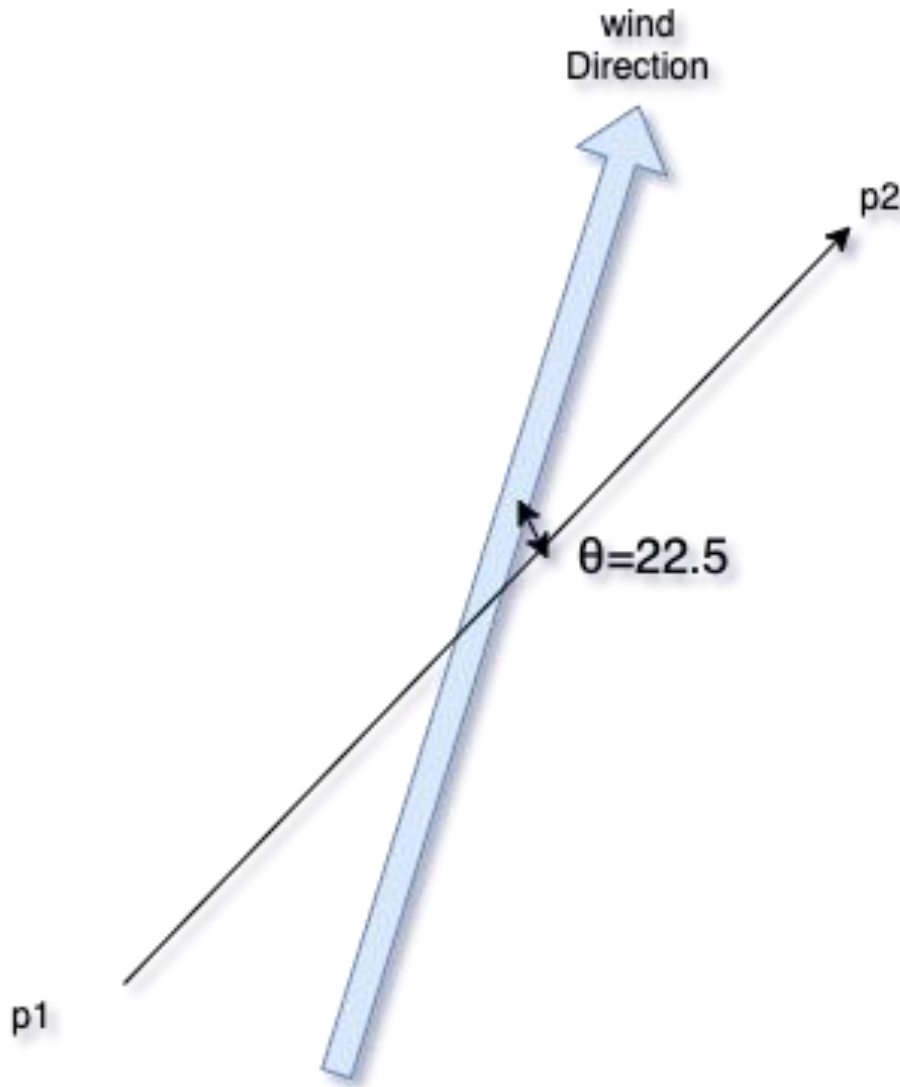
Figure 41: Wind-Fire alignment. Fire heads from p1 to p2 while wind blow slightly in different angle. The difference between two events are then divided by 180 degrees to compute degree of agreement cited from (Ozaki, Aryal and Fox-Hughes, 2019).

Range of bias can be configured by following the predecessor prototype. Equation of the wind direction rate is as following:

$$agreement = closeness \cdot (threshold_{max} - threshold_{min}) + threshold_{min}$$

where the closeness is computed below.

$$closeness =| (π- | (orientation_{wind} - orientation_{fire}) |))/π |$$

Note that the closeness is computed based on radian. π is replaced with 180 ° if its unit is degrees. Both orientations must be between 0 and 2π or 0 ° and 180 °.

Table 90: Notation of variables of wind direction rate

Notation	Description
$agreement$	Rate of orientation agreement between fire and wind
$threshold_{max}$	The maximum value of the range. Default value is 1.
$threshold_{min}$	The minimum value of the range. Default value is 0.
$orientation_{wind}$	Orientation of wind which north indicates 0.
$orientation_{fire}$	Orientation of fire which north indicates 0.

Note that this function is optional for research purpose and configurable in this prototype.

5.13 Sigmoid function

Sigmoid function is employed in some fire models, such as Spinifex (5.3), Button grass (5.4) and Malleeheath (5.6) to calculate the probability of flaming. Sigmoid function is commonly used in the neural network (NN), a type of Machine Learning, and normalise value within appropriate range (Han and Moraga, 1995). The sigmoid function in Research Prototype is the logistic sigmoid, which is non-linear and normalised between 0 and 1 as below.
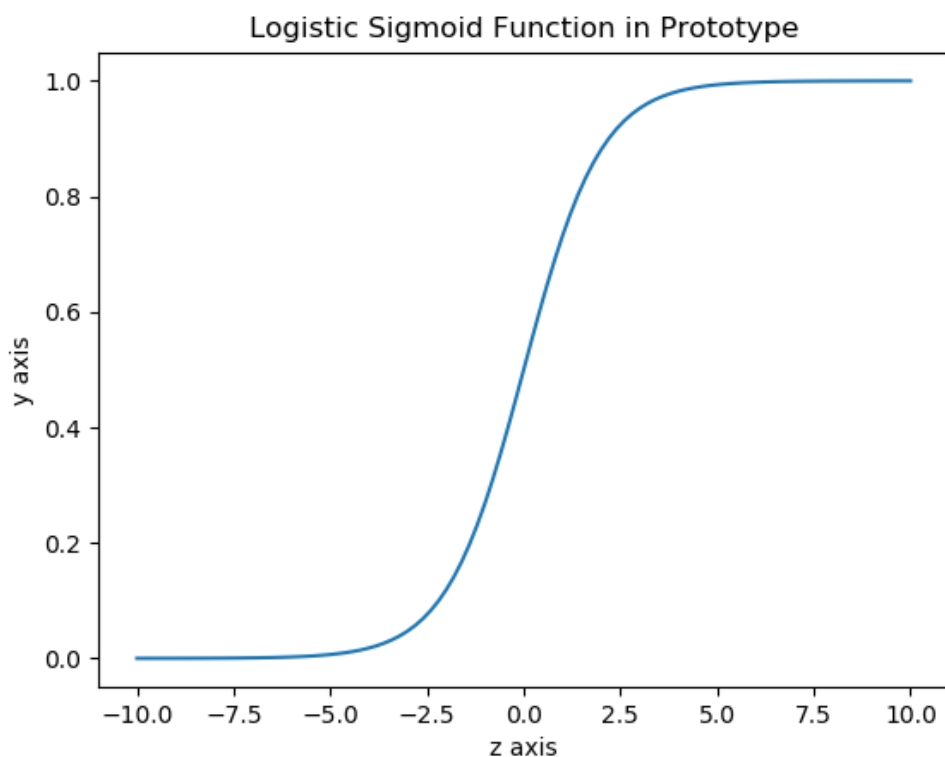
Figure 42: Logistic sigmoid function

Its common usage is as following:

$$Probability = \frac{1}{1 + exp(-z)}$$

Where z is an arbitrary equation in each model.

5.14 Comparison of fire danger indices with previous study

Fire models between Prototype 1 and 2 are compared in this section. In previous prototype, there were three fire indices, McArthur's Forest Fire Danger Index (FFDI), McAuthur's Grassland Fire Danger Index (GFDI) and Butongrass Moorland Fire Index (Noble, Gill and Bary, 1980; Marsden-Smedley and Catchpole, 1995b). GFDI and FFDI are superseded by new fire models while the Buttongrass Moorland Fire Index model keeps being employed by modifying minorly as below.

Table 91: Comparison of Prototype 1 and 2. FFDI and GFDI are replaced while Buttongrass Moorlands model remains

Old	New
GFDI	CSIRO Grassland fire spread meter
GFDI	CSIRO Grassland for northern Australia
GFDI	Desert spinifex model

Buttongrass moorlands model	Buttongrass moorlands model
FFDI	Dry Eucalypt Forest Fire Model (DEFFM or "Vesta")
GFDI	Mallee heath model
GFDI	Heathland model
FFDI	Adjusted Pine model

6 Verification

There are some verification measures such as confusion matrix, Cohen's Kappa score and fractions skill score, in Prototype 2. Two common events are observed and predicted fire propagation to verify quality of simulation. These events are distributed as binary figures on each grid. In terms of the observed event, the grid within fire area are substitute 1 as true and others are 0 as false (Figure 43).
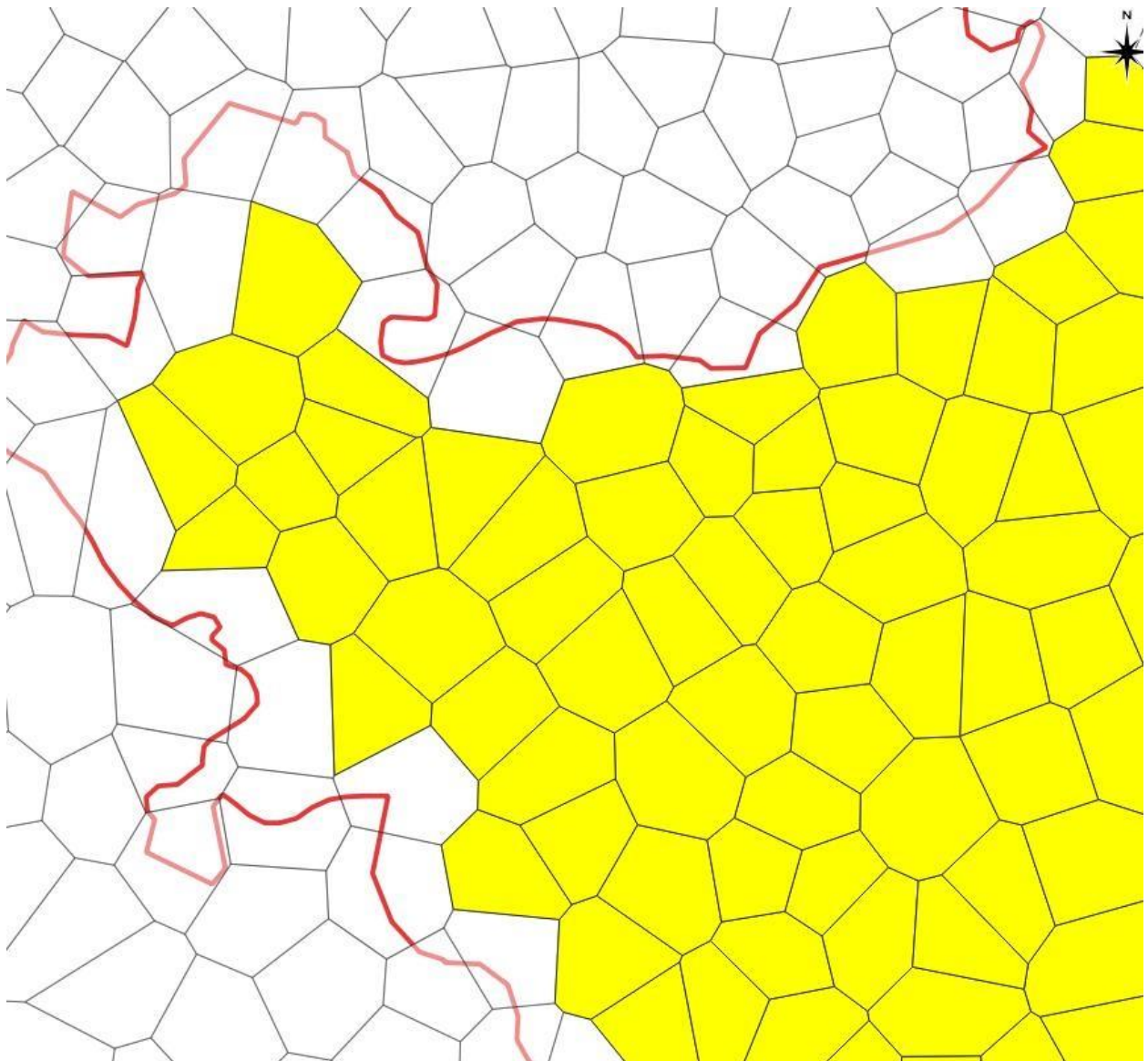
Figure 43: Grids in yellow are attributed to burnt area with 1 (true) within the fire isochrone for ground truth.

On the other hand, the grids with assess status, "Done (DN)", are counted as 1 (true) and others are 0 (false) for the predicted events (Figure 44).
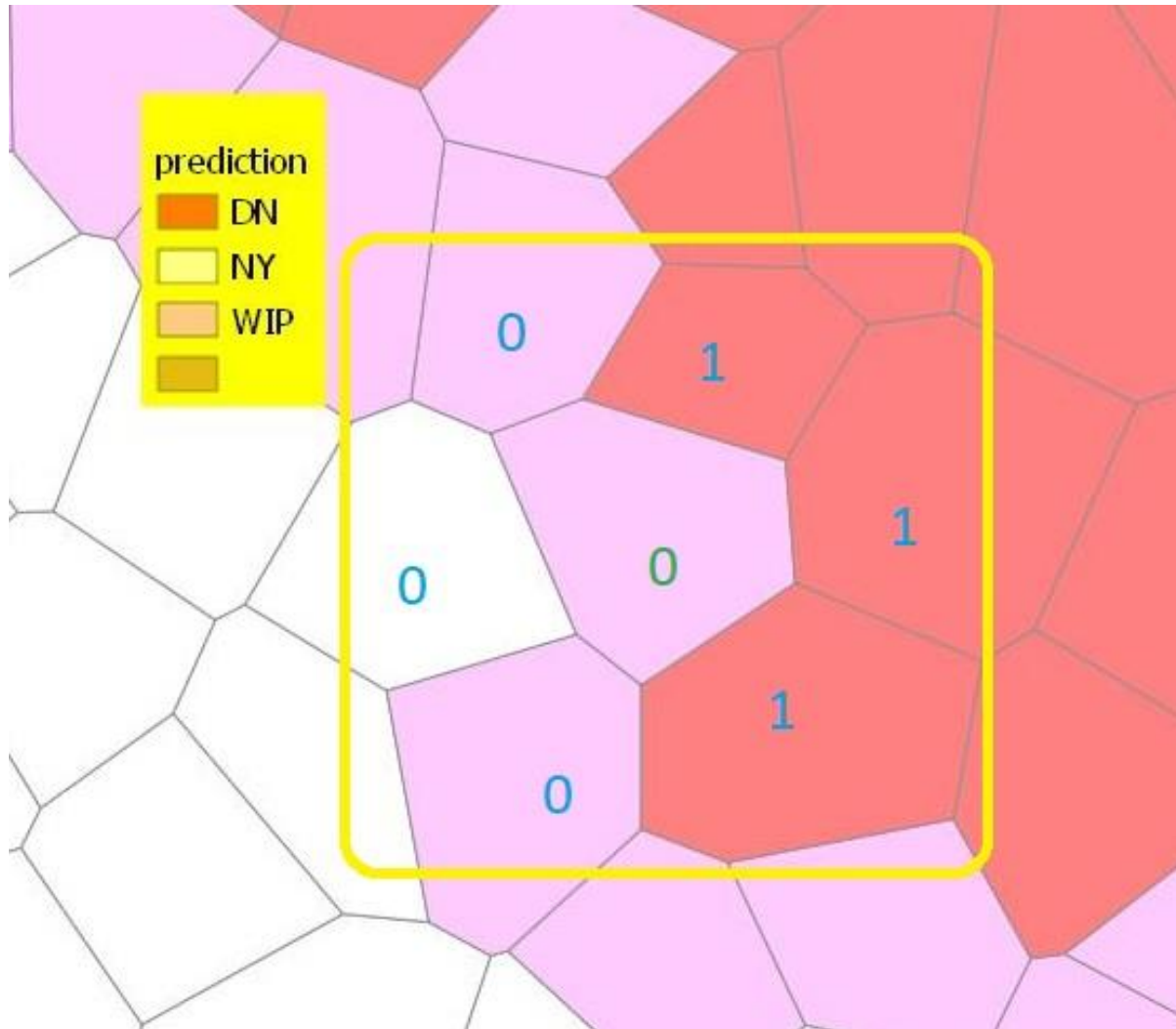
Figure 44: Prediction grids with DN are substituted 1 as true while others are 0 as false for predicted events.

6.1   Confusion Matrix

Confusion matrix is employed to verify quality of simulation by comparing with historical fire as ground truth in this prototype. The concept of the confusion matrix is originated from the classification, one of machine learning techniques, and is designed to classify the frequency of various statuses against certain behaviour as well as summarise accuracy and precision by comparison of simulations with observed results (Markham, 2014). In this study, the binary confusion matrix is employed, in which there are four categories, true positive (TP), true negative (TN), false positive (FP) and false negative (FN). The observed event is fire history data as a true class while the simulated result is an inferred class (Figure 45).
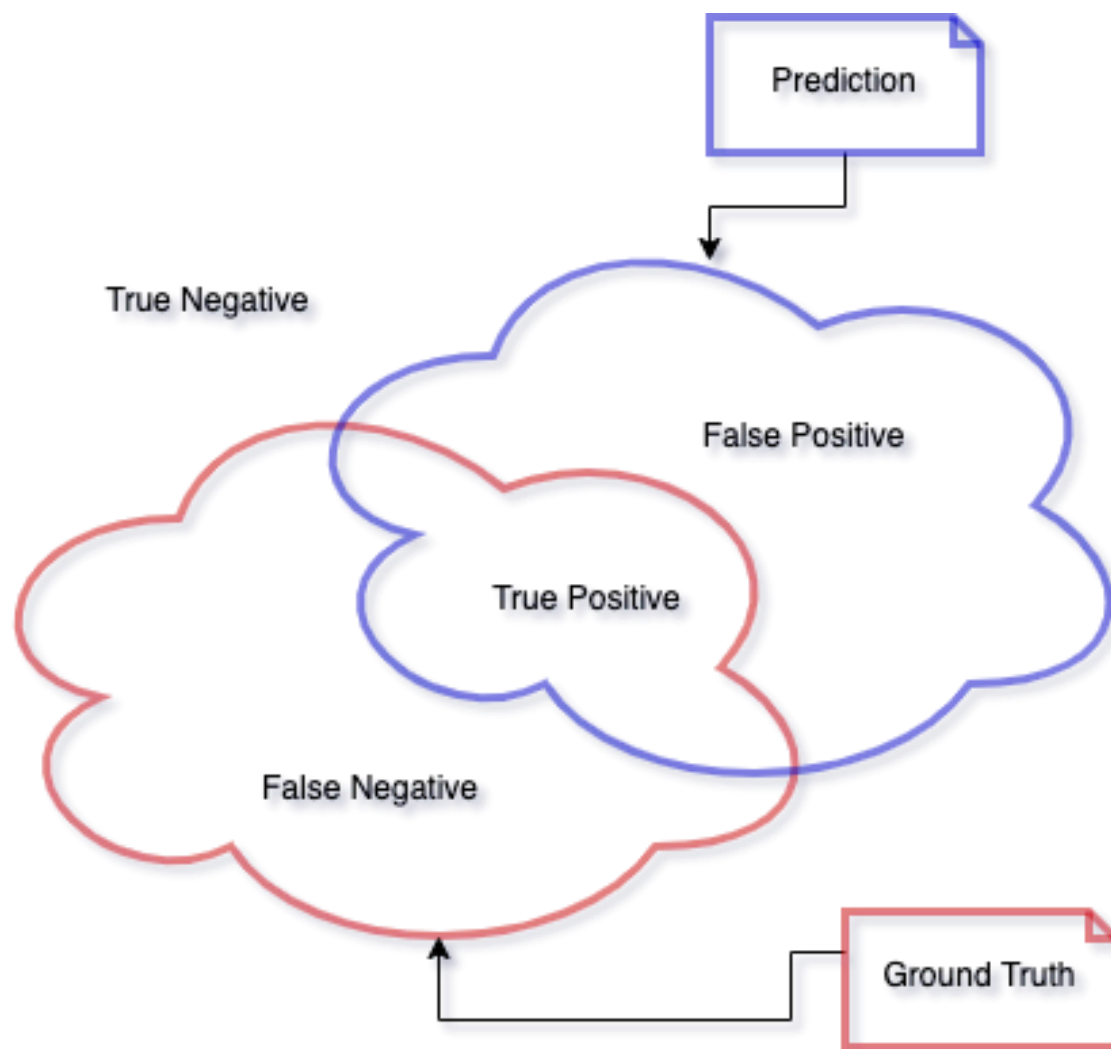
Figure 45: Confusion matrix parameter adapted to fire simulation. True negative is the parameter which both prediction and observation agree to be positive. True negative is the parameter which both agree to be negative. On the one hand, false negative is the parameter that value is predicted as positive but it is negative according to the ground truth. On the other hand, false positive is the parameter that the value is predicted as negative but the observed data assesses it as positive.

These statuses are represented in two dimensions and contain the number of TN, FN, FP and TP (Table 92). In addition to general confusion matrix, threat score is anew employed in this prototype. This score indicates how well the simulated area is overlapped with the observed area and is widely used in meteorology. If the threat score is close to one, it indicates good. If the score is close to zero, the quality is poor (Faggian *et al.*, 2017a; Sharples *et al.*, 2017).

Table 92: Confusion Matrix for classification of performance cited in (Markham, 2014)

		Inferred class	
		Predicted No	Predicted Yes
True class	Actual No	TN	FP
	Actual Yes	FN	TP

TP indicates the number of cases in which both the simulated and the observed have true. There are several indicators in common by combining these statuses of confusion matrix seen below.

Table 93: Confusion matrix indicators for interpretation of performance

Indicator	Equation	Description
Accuracy	$\dfrac{TP + TN}{TP + TN + FP + FN}$	Frequency of correct classifier
Misclassification Rate (aka, Error Rate)	$\dfrac{FP + FN}{TP + TN + FP + FN}$	Frequency of incorrect classifier = (1-accuracy)
True Positive Rate (aka, Sensitivity or Recall)	$\dfrac{TP}{TP + FN}$	Rate of observed true over both classifiers indicating true
False Positive Rate	$\dfrac{FP}{TN + FP}$	Rate of observed false over both classifiers representing true
Specificity	$\dfrac{TN}{TN + FP}$	Rate of observed false over both classifiers representing no = (1- False Positive Rate)
Precision	$\dfrac{TP}{TP + FP}$	Rate of correct prediction yes
Prevalence	$\dfrac{FN + TP}{TP + TN + FP + FN}$	Rate of "Actual Yes"
Threat Score	$\dfrac{TP}{TP + FP + FN}$	Rate of how well the simulated area overlap with the observed area (Faggian *et al.*, 2017b)
Goodness-of-fit (GoF)	$\sum \dfrac{TP}{(TP + FN)} \cdot \dfrac{TP}{(TP + FP)}$	Degree of spatial concordance (Hargrove, Hoffman and Hessburg, 2006)

Details are described in the previous study (Ozaki, Aryal and Fox-Hughes, 2019).

6.2   Cohen's Kappa score

Cohen's kappa statistic is the statistic score, which measures precision; so-called interrater reliability or interobserver agreement. Because the Kappa statistic allows for probability of occurrence agreement, this statistic is considered to be more robust than simple rating calculation (Glen, 2014; tutorialspoint, 2020). The formula to computer Cohen's kappa coefficient is defined as following:

$$\kappa = \frac{p_0 - p_e}{1 - p_e} = 1 - \frac{1 - p_0}{1 - p_e}$$

Where p_0 indicates the relative observed agreement among raters and p_e does the hypothetical probability of agreement of chance.

The below shows the example of kappa statistic normalised to range from 0 to 1.

Table 94: Example of kappa indicator showing magnitude of agreement cited in (Glen, 2014; tutorialspoint, 2020)

κ	Description of agreement
0	None
0.1 - 0 .20	Slight
0.21 – 0.40	Far
0.41 – 0.60	Moderate
0.61 – 0.80	Substantial
0.81 – 0.99	Nearly perfect
1	Perfect

6.3   Fractions Skill Score (FSS)

Fractions skill score (FSS) is the probabilistic approach in which credit is provided by neighbourhood. FSS was invented to spatially measure how skilful a prediction of accumulated precipitation is (Roberts and Lean, 2008; Mittermaier and Roberts, 2010; Skok and Roberts, 2016). This metric is useful to find likelihood of frequency between observation and prediction. The equation below is proposed (Ebert, 2008, 2009; Faggian *et al.*, 2015),

$$FSS = 1 - \frac{FBS}{N^{-1} \cdot \sum_{i=1}^{N} P^2 + N^{-1} \cdot \sum_{i=1}^{N} P_0^2}$$

Where N represents the number of neighbours and FBS indicates Fractions Brier Score (FBS) as defined below,

$$FBS = N^{-1} \cdot \sum_{i=1}^{N} (P - P_0)^2$$

$$P = n^{-1} \cdot \sum_{i=1}^{n} p_i$$

$$P_0 = n^{-1} \cdot \sum_{i=1}^{n} p_{0_i}$$

Where P is the average of the neighbours of prediction p and p itself and P_0 is the average of the neighbours of the observation p_0 and p_0 itself. For instance, if a cursor is on the grid in the centre of yellow rectangle as shown in Figure 44, p is the average, 3/7, because there are three one and four zero out of seven grids in neighbourhood for the predicted event. Similarly, the observed events are computed with neighbourhood by identifying their location against the fire area. Note that definition of neighbour in this prototype follows the section 4.2.3.

Now, FSS is simplified as

$$FSS = 1 - \frac{N^{-1} \cdot \sum_{i=1}^{N}(P - P_0)^2}{N^{-1} \cdot \left(\sum_{i=1}^{N} P^2 + \sum_{i=1}^{N} P_0^2\right)} = 1 - \frac{\sum_{i=1}^{N}(P - P_0)^2}{\sum_{i=1}^{N} P^2 + \sum_{i=1}^{N} P_0^2}$$

Where P is prediction and P_0 is ground truth. The value of FSS is 1 for complete match and 0 for complete mismatch.

Threshold of usefulness is

$$FSS_{useful} = 0.5 + \frac{f_{obs}}{2}$$

Where f_{obs} is coverage of fire propagation in ground truth over domain, i.e. rate of burnt area. Namely, FSS_{useful} indicates the minimum limit of useful scale. The scale can be attributed to skilful scale if FSS is greater than FSS_{useful} (Ebert, 2009).

7   Configuration

There are pairs of key-value in configuration such as raster_types and others (Table 95 and Table 96).

Table 95: Configuration for raster types

Configuration Key	Description	Default Value	BARRA ID	Note (BARRA id)
RAS_TYPE_ASPECT	degrees	1		Aspect which indicates the direction of downhill as degrees
RAS_TYPE_DEM	metres	2		Digital Elevation Model
RAS_TYPE_SLOPE	degrees	3		slope
RAS_TYPE_AWAP_UF	fraction	4		relative soil moisture in upper layer (Raupach *et al.*, 2009, 2012; CSIRO AWAP Team, 2014)
RAS_TYPE_CURING	%	5		Dryness of fuel
RAS_TYPE_EVP		6	accum_evap	Evaporation
RAS_TYPE_PRCP	$kg \cdot m^{-2} \cdot ts^{-1}$	7	accum_ls_prcp	Amount of rain as kilogram per squared meters per timespan. See 4.7.2
RAS_TYPE_MSLP	Pascal	8	av_mslp	Air pressure at mean sea level
RAS_TYPE_DEWPT	Kelvin	9	dewpt_scrn	Dew point at 1.5 m

RAS_TYPE_DFH		10	dfh	Drought Factor calculated from SDI and precipitation in the last 20 days
RAS_TYPE_FFDI		11	ffdi	McArthur Forest Fire Danger Index
RAS_TYPE_MSDI		12	msdih	Mount's Soil Dryness Index
RAS_TYPE_RH	%	13	rh2m_1	Relative humidity
RAS_TYPE_TEMP	Kelvin	14	temp_scrn	Temperature. See 4.7.1
RAS_TYPE_CLD	%	15	ttl_cld	Total cloud cover
RAS_TYPE_UWND	$m \cdot s^{-1}$	16	uwnd10m	U wind component at 10 m
RAS_TYPE_VWND	$m \cdot s^{-1}$	17	vwnd10m	V wind component at 10 m
RAS_TYPE_WND_MAG_NINJA	$m \cdot s^{-1}$	18		Wind magnitude resampled by WindNinja
RAS_TYPE_WND_DIR_NINJA	Degrees	19		Wind direction resampled by WindNinja. N is 0 °.
RAS_TYPE_MSLP_DIR	Degrees	20		Degree of mean sea level pressure from high to low. N is 0 °. (time, latitude, longitude)
RAS_TYPE_VAXIS	Degrees	21		Direction of higher elevation on the valley axis. N is 0 °.
RAS_TYPE_DIURNAL_VALLEY	Degrees	22		Expected direction of forced channelling in the valley. N is 0 °. (time, latitude, longitude)
RAS_TYPE_FORCED_VALLEY	Degrees	23		Expected direction of forced channelling in the valley. N is 0 °. (time, latitude, longitude)
RAS_TYPE_PRESSURE_VALLEY	Degrees	24		Expected direction of pressure driven channelling in the valley. N is 0 °. (time, latitude, longitude)

Table 96: Other configurations

Configuration Key	Description	Default Value	Note
MAX_NUMBER_OF_THREADING	The number of threads for concurrent prediction	20	
SRID	SRID for a study area		
WNDNINJA_ON	Binary option for Windninja	True	True: use of Windninja, False: crude wind
MAX_YEARS_SINCE_LAST_FIRE	Maximum years to descend for buttongrass model	5	
IGNITION_PROBABILIY	Probability of ignition between 0 and 1	1	Can be overridden by regional data
LAST_PRECIPITATION	Last precipitation (hours) for grassland moorland	$(24 \cdot 30)$	

8 References

Aguado, I. *et al.* (2007) 'Estimation of dead fuel moisture content from meteorological data in Mediterranean areas. Applications in fire danger assessment', *International Journal of Wildland Fire*, 16(4), pp. 390–397.

Allan, G. *et al.* (2003) 'Application of NDVI for predicting fuel curing at landscape scales in northern Australia: can remotely sensed data help schedule fire management operations?', *International Journal of Wildland Fire*, 12(4), pp. 299–308.

American Meteorological Society (2020) *Meteorology Glossary*. Available at: http://glossary.ametsoc.org/wiki (Accessed: 4 May 2020).

Anderson, W.R. *et al.* (2015) 'A generic, empirical-based model for predicting rate of fire spread in shrublands', *International Journal of Wildland Fire*, 24(4), pp. 443–460.

Andrews, P.L., Anderson, S.A. and Anderson, W.R. (2006) 'Evaluation of a dynamic load transfer function using grassland curing data', in. *In: Andrews, Patricia L.; Butler, Bret W., comps. 2006. Fuels Management-How to Measure Success: Conference Proceedings. 28-30 March 2006; Portland, OR. Proceedings RMRS-P-41. Fort Collins, CO: US Department of Agriculture, Forest Service, Rocky Mountain Research Station. p. 381-394*.

Boldstad, P. (2012) *GIS Funfamentals, A First Text on Geographic Information Systems*. White Bear Lake, Minn. : Eider Press, 2012.

Burrough, P.A. *et al.* (2015) *Principles of geographical information systems*. Oxford University Press.

Burrows, N., Gill, M. and Sharples, J. (2018) 'Development and validation of a model for predicting fire behaviour in spinifex grasslands of arid Australia', *International journal of wildland fire*, 27(4), pp. 271–279.

Burrows, N.D., Liddlelow, G.L. and Ward, B. (2014) *A guide to estimating fire rate of spread in spinifex grasslands of Western Australia*. Department of Environment and Conservation, Kensington, WA: Science and Conservation Division (Mk2v3).

Bushfire CRC (2011) *Predicting fires from dry lightning*. Available at: https://www.bushfirecrc.com/sites/default/files/managed/resource/predicting_fires_from_dry_lightning_0.pdf (Accessed: 20 July 2019).

Centre for Australian Weather and Climate Research - List of THREDDS catalogs (2017). Available at: http://opendap.bom.gov.au:8080/thredds/catalog/curing_modis_500m_8-day/aust_regions/nsw/tiff/mapvictoria/catalog.html (Accessed: 29 April 2018).

Cheney, N.P. *et al.* (2012) 'Predicting fire behaviour in dry eucalypt forest in southern Australia', *Forest Ecology and Management*, 280, pp. 120–131.

Cheney, N.P., Gould, J.S. and Catchpole, W.R. (1998) 'Prediction of fire spread in grasslands', *International Journal of Wildland Fire*, 8(1), pp. 1–13.

Cruz, M. *et al.* (2018) 'A Hierarchical Classification of Wildland Fire Fuels for Australian Vegetation Types', *Fire*, 1(1), p. 13. Available at: https://doi.org/10.3390/fire1010013.

Cruz, M.G. *et al.* (2012) 'Anatomy of a catastrophic wildfire: The Black Saturday Kilmore East fire in Victoria, Australia', *Forest Ecology and Management*, 284, pp. 269–285.

Cruz, M.G. *et al.* (2013) 'Fire behaviour modelling in semi-arid mallee-heath shrublands of southern Australia', *Environmental Modelling & Software*, 40, pp. 21–34.

Cruz, Miguel G *et al.* (2015) 'Effects of curing on grassfires: II. Effect of grass senescence on the rate of fire spread', *International Journal of Wildland Fire*, 24(6), pp. 838–848.

Cruz, Miguel G. *et al.* (2015) 'Empirical-based models for predicting head-fire rate of spread in Australian fuel types', *Australian Forestry*, 78(3), pp. 118–158.

Cruz, M.G., Alexander, M.E. and Fernandes, P.A. (2008) 'Development of a model system to predict wildfire behaviour in pine plantations', *Australian Forestry*, 71(2), pp. 113–121.

Cruz, M.G., Alexander, M.E. and Wakimoto, R.H. (2005) 'Development and testing of models for predicting crown fire rate of spread in conifer forest stands', *Canadian Journal of Forest Research*, 35(7), pp. 1626–1639.

CSIRO AWAP Team (2014) *Australian Water Availability Project*. Available at: http://www.csiro.au/awap/ (Accessed: 1 July 2020).

Dowdy, A.J. and Mills, G.A. (2009) *Atmospheric states associated with the ignition of lightning-attributed fires*. Centre for Australian Weather and Climate Research.

Ebert, E.E. (2008) 'Fuzzy verification of high-resolution gridded forecasts: a review and proposed framework', *Meteorological Applications*, 15(1), pp. 51–64.

Ebert, E.E. (2009) 'Neighborhood verification: A strategy for rewarding close forecasts', *Weather and Forecasting*, 24(6), pp. 1498–1510.

Faggian, N. *et al.* (2015) 'Fast calculation of the fractions skill score', *Mausam*, 66(3), pp. 457–466.

Faggian, N. *et al.* (2017a) 'An evaluation of fire spread simulators used in Australia', *Bushfire Predictive Services Final report* [Preprint].

Faggian, N. *et al.* (2017b) 'Final Report: An evaluation of fire spread simulators used in Australia', *Bureau of Meteorology* [Preprint].

Firelab (2020) *WindNinja Tutorials version 3.6.0*, *WindNinja Tutorials version 3.6.0*. Available at: https://weather.firelab.org/windninja/tutorials/ (Accessed: 1 April 2022).

Geoscience Australia (2020) *Geoscience Australia*. Available at: https://www.ga.gov.au/ (Accessed: 23 May 2020).

Glen, S. (2014) *Cohen's Kappa Statistic*, *Cohen's Kappa Statistic*. Available at: https://www.statisticshowto.datasciencecentral.com/cohens-kappa-statistic/ (Accessed: 30 March 2020).

Gould, J.S., McCaw, W.L. and Cheney, N.P. (2011) 'Quantifying fine fuel dynamics and structure in dry eucalypt forest (Eucalyptus marginata) in Western Australia for fire management', *Forest Ecology and Management*, 262(3), pp. 531–546.

Hall, J. *et al.* (2015) 'Long-distance spotting potential of bark strips of a ribbon gum (Eucalyptus viminalis)', *International Journal of Wildland Fire*, 24(8), pp. 1109–1117.

Han, J. and Moraga, C. (1995) 'The influence of the sigmoid function parameters on the speed of backpropagation learning', in. *International Workshop on Artificial Neural Networks*, Springer, pp. 195–201.

Hargrove, W.W., Hoffman, F.M. and Hessburg, P.F. (2006) 'Mapcurves: a quantitative method for comparing categorical maps', *Journal of Geographical Systems*, 8(2), pp. 187–208. Available at: https://doi.org/10.1007/s10109-006-0025-x.

Heywood, D.I., Cornelius, S. and Carver, S. (2011) *An introduction to geographical information systems*. Harlow : Prentice Hall, 2011. 4th ed.

Holloway, J. (1967) 'Numerical integration of a ninelevel global primitive equations model formulated by the box method', *Mon. Wea. Rev*, 95, pp. 509–530.

JAXA (2022) *Earth-graphy*. Available at: https://earth.jaxa.jp/en/index.html (Accessed: 30 August 2022).

Lee, S.-C., KwofuAU-Xiong, XiaoxiongAU-Sun, ChengboAU-Anderson, SamuelTI-The S.-NPP VIIRS Day-Night Band On-Orbit Calibration/Characterization and Current State of SDR Products (2014) 'The S-NPP VIIRS Day-Night Band On-Orbit Calibration/Characterization and Current State of SDR Products', *Remote Sensing*, 6(12), pp. 12427–12446. Available at: https://doi.org/10.3390/rs61212427.

Listi, H. *et al.* (2018) 'SPECTRAL ANALYSIS OF THE HIMAWARI-8 DATA FOR HOTSPOT DETECTION FROM LAND/FOREST FIRES IN SUMATRA', *International Journal of Remote Sensing and Earth Sciences (IJReSES)*, 15, p. 15. Available at: https://doi.org/10.30536/j.ijreses.2018.v15.a2836.

Liu, W. and Fang, J. (2019) 'Iterative Framework of Machine-Learning Based Turbulence Modeling for Reynolds-Averaged Navier-Stokes Simulations', *arXiv preprint arXiv:1910.01232* [Preprint].

Markham, K. (2014) *Simple guide to confusion matrix terminology*. Available at: http://www.dataschool.io/simple-guide-to-confusion-matrix-terminology/ (Accessed: 8 April 2018).

Marsden-Smedley, J. (2009) 'Planned burning in Tasmania: operational guidelines and review of current knowledge'.

Marsden-Smedley, J.B. and Catchpole, W.R. (1995a) 'Fire behaviour modelling in tasmanian buttongrass moorlands i. Fuel characteristics', *International Journal of Wildland Fire*, 5(4), pp. 203–214.

Marsden-Smedley, J.B. and Catchpole, W.R. (1995b) 'Fire Behaviour Modelling in Tasmanian Buttongrass Moorlands .II. Fire Behaviour', *International Journal of Wildland Fire*, 5(4), pp. 215–228.

Marsden-Smedley, J.B., Catchpole, W.R. and Pyrke, A. (2001) 'Fire modelling in Tasmanian buttongrass moorlands. IV. Sustaining versus non-sustaining fires', *International Journal of Wildland Fire*, 10(2), pp. 255–262.

Miller, C. *et al.* (2015) 'SPARK – A Bushfire Spread Prediction Tool', *Environmental software systems: infrastructures, services and applications*, 448, pp. 262–271. Available at: https://doi.org/10.1007/978-3-319-15994-2_26.

Mittermaier, M. and Roberts, N. (2010) 'Intercomparison of spatial forecast verification methods: Identifying skillful spatial scales using the fractions skill score', *Weather and Forecasting*, 25(1), pp. 343–354.

Ndalila, M.N., Williamson, G.J. and Bowman, D.M.J.S. (2018) 'Geographic Patterns of Fire Severity Following an Extreme Eucalyptus Forest Fire in Southern Australia: 2013 Forcett-Dunalley Fire', *Fire*, 1(3). Available at: https://doi.org/10.3390/fire1030040.

Noble, I.R., Gill, A.M. and Bary, G.A.V. (1980) 'McArthur's fire-danger meters expressed as equations', *Australian Journal of Ecology*, 5(2), pp. 201–203.

ORNL DAAC (2018) *MODIS and VIIRS Land Products Global Subsetting and Visualization Tool*. Available at: https://www.earthdata.nasa.gov/learn/find-data/near-real-time/viirs (Accessed: 13 November 2020).

Ozaki, M., Aryal, J. and Fox-Hughes, P. (2019) 'Dynamic wildfire navigation system', *ISPRS International Journal of Geo-Information*, 8(4), p. 194.

Plekhanova, J. (2009) 'Evaluating web development frameworks: Django, Ruby on Rails and CakePHP', *Institute for Business and Information Technology* [Preprint].

Python Software Foundation (2020a) *combination*. Available at: https://docs.python.org/3.1/library/itertools.html (Accessed: 22 July 2020).

Python Software Foundation (2020b) *random — Generate pseudo-random numbers*. Available at: https://docs.python.org/3/library/random.html#random.random (Accessed: 19 June 2020).

Raupach, M. *et al.* (2009) 'Australian water availability project (AWAP): CSIRO marine and atmospheric research component: final report for phase 3', *Melbourne: Centre for Australian weather and climate research (bureau of meteorology and CSIRO)*, 67.

Raupach, M. *et al.* (2012) 'Australian water availability project', *Canberra: CSIRO Marine and Atmospheric Research* [Preprint].

Roberts, N.M. and Lean, H.W. (2008) 'Scale-selective verification of rainfall accumulations from high-resolution forecasts of convective events', *Monthly Weather Review*, 136(1), pp. 78–97.

Schroeder, W. (2017) *Visible Infrared Imaging Radiometer Suite (VIIRS) 375 m & 750 m Active Fire Detection Data Sets Based on NASA VIIRS Land Science Investigator Processing System (SIPS) Reprocessed Data - Version 1*, *Visible Infrared Imaging Radiometer Suite (VIIRS) 375 m & 750 m Active Fire Detection Data Sets Based on NASA VIIRS Land Science Investigator Processing System (SIPS) Reprocessed Data - Version 1*. Available at: https://lpdaac.usgs.gov/documents/132/VNP14_User_Guide_v1.3.pdf (Accessed: 22 September 2022).

Sharples, J. *et al.* (2011) 'Lateral bushfire propagation driven by the interaction of wind, terrain and fire', in. *MODSIM2011, 19 th International Congress on Modelling and Simulation. Modelling and Simulation Society of Australia and New Zealand*, pp. 235–241.

Sharples, J. *et al.* (2017) 'Dynamic simulation of the Cape Barren Island fire using the Spark framework', in. *MODSIM2017, 22nd International Congress on Modelling and Simulation, eds G. Syme, D. Hatton MacDonald, B. Fulton, and J. Piantadosi (Hobart, TAS: Modelling and Simulation Society of Australia and New Zealand)*, pp. 1111–1117.

Sharples, J.J., McRae, R.H.D. and Weber, R.O. (2010) 'Wind characteristics over complex terrain with implications for bushfire risk management', *Environmental Modelling & Software*, 25(10), pp. 1099–1120. Available at: https://doi.org/10.1016/j.envsoft.2010.03.016.

Sharples, J.J., McRae, R.H.D. and Wilkes, S.R. (2012) 'Wind–terrain effects on the propagation of wildfires in rugged terrain: fire channelling', *International Journal of Wildland Fire*, 21(3), pp. 282–296.

Skok, G. and Roberts, N. (2016) 'Analysis of fractions skill score properties for random precipitation fields and ECMWF forecasts', *Quarterly Journal of the Royal Meteorological Society*, 142(700), pp. 2599–2610.

Snyder, A. (1986) 'Encapsulation and inheritance in object-oriented programming languages', in. *Conference proceedings on Object-oriented programming systems, languages and applications*, pp. 38–45.

Su, C.-H. *et al.* (2019) 'BARRA v1. 0: the bureau of meteorology atmospheric high-resolution regional reanalysis for Australia', *Geoscientific Model Development*, 12(5), pp. 2049–2068.

Sullivan, A.L. *et al.* (2014) 'A downslope fire spread correction factor based on landscape-scale fire behaviour', *Environmental Modelling and Software*, 62, pp. 153–163.

The Australasian Fire and Emergency Service Authorities Council (AFAC) (2020) *Australian Fire Danger Rating System - Research Prototype*, *Australian Fire Danger Rating System*. Available at: https://www.afac.com.au/initiative/afdrs/afdrs-publications-and-reports (Accessed: 19 May 2020).

The Australasian Fire and Emergency Service Authorities Council (AFAC) (2022) *Australian Fire Danger Rating System Technical Guide*. Available at: https://www.afac.com.au/initiative/afdrs/technical-resources (Accessed: 27 September 2022).

tutorialspoint (2020) *Statistics - Cohen's kappa coefficient*, *Statistics - Cohen's kappa coefficient*. Available at: https://www.tutorialspoint.com/statistics/cohen_kappa_coefficient.htm (Accessed: 2 May 2020).

United State Geological Survey (USGS) (2020) *Earth Explorer*. Available at: https://earthexplorer.usgs.gov/ (Accessed: 15 June 2020).

USGS EROS Archive - Digital Elevation - Shuttle Radar Topography Mission (SRTM) 1 Arc-Second Global (2020). Available at: https://www.usgs.gov/centers/eros/science/usgs-eros-archive-digital-elevation-shuttle-radar-topography-mission-srtm-1-arc?qt-science_center_objects=0#qt-science_center_objects (Accessed: 15 June 2020).

Wagenbrenner, N.S. *et al.* (2019) 'Development and Evaluation of a Reynolds-Averaged Navier-Stokes Solver in WindNinja for Operational Wildland Fire Applications', *Atmosphere*, 10(11), p. 672.

Wang, W.-C., ChangyongTI-NOAA-20 and S.-NPP VIIRS Thermal Emissive Bands On-Orbit Calibration Algorithm Update and Long-Term Performance Inter-Comparison (2021) 'NOAA-20 and S-NPP VIIRS Thermal Emissive Bands On-Orbit Calibration Algorithm Update and Long-Term Performance Inter-Comparison', *Remote Sensing*, 13(3). Available at: https://doi.org/10.3390/rs13030448.

Wegner, P. (1990) 'Concepts and paradigms of object-oriented programming', *ACM Sigplan Oops Messenger*, 1(1), pp. 7–87.

Wentao, H. and Yu, C. (2020) 'Fire Severity', in S.L. Manzello (ed.) *Encyclopedia of Wildfires and Wildland-Urban Interface (WUI) Fires*. Cham: Springer International Publishing, pp. 409–414. Available at: https://doi.org/10.1007/978-3-319-52090-2_226.

Yumimoto, K. *et al.* (2016) 'Aerosol data assimilation using data from Himawari-8, a next-generation geostationary meteorological satellite', *Geophysical Research Letters*, 43(11), pp. 5886–5894. Available at: https://doi.org/10.1002/2016GL069298.